Effects of variable viscosity on non-Newtonian fluids

By

Azad Hussain

Department of Mathematics
Quaid-i-Azam University
Islamabad, Pakistan
2013

Effects of variable viscosity on non-Newtonian fluids

By

Azad Hussain

Supervised By

Dr. Malik Muhammad Yousaf

Department of Mathematics
Quaid-i-Azam University
Islamabad, Pakistan
2013

Effects of variable viscosity on non-Newtonian fluids

By

Azad Hussain

DOCTOR OF PHILOSOPHY

IN

MATHEMATICS

Supervised By

Dr. Malik Muhammad Yousaf

Department of Mathematics
Quaid-i-Azam University
Islamabad, Pakistan
2013

Effects of variable viscosity on non-Newtonian fluids

By

Azad Hussain

CERTIFICATE

A DISSERTATION SUBMITTED IN THE PARTIAL FULFILLMENT OF THE REQUIREMENTS FOR THE DEGREE OF THE DOCTOR OF PHILOSOPHY

We accept this dissertation as conforming to the required standard

1. _____
Prof. Dr. Muhammad Ayub
(Chairman)

2. _____
Dr. Malik M. Yousaf
(Supervisor)

3. _____
Prof. Dr. M. Ozair Ahmad
(External Examiner)

4. _____
Dr. Tasneem Shah
(External Examiner)

Department of Mathematics
Quaid-i-Azam University
Islamabad, Pakistan
2013

ACKNOWLEDGEMENT

I humbly thanks Allah the Most Gracious, Most Merciful, Who bestowed me the blessing of shaping and polishing my thinking. My gratitude is to the Holy Prophet Hazrat Muhammad (PBUH) whose guidance always inspired me.

I am extremely grateful to my supervisor Dr. Malik Muhammad Yousaf for his valuable advice and inestimable guidance. His moral support, suggestions and valuable comments enabled me to enhance and improve my research capabilities. Without his generous help and guidance, it was not possible for me to complete this uphill task.

I am also heartily thankful to Dr. Sohail Nadeem whose encouragement, guidance and support throughout my studies enabled me to develop a deep understanding about the subject.

I offer my regards and blessings to Prof. Dr. Muhammad Ayub, Chairman Department of Mathematics and the other faculty members for supporting me during the completion of the thesis. I can't imagine my current position without constant source of love and support from my family. They gave me freedom to explore my own and at the same time the guidance to recover when my steps faltered.

My friends Abdul Rehman, Muhammad Naseer, Aziz ur Rehman, Sharafat Ali Awan, Tayyab, Salman, Rizwan, Rashid, Sajjad, Anwar Hussain, Ashfaq, Muhammad Bilal, Taimoor Salahuddin, Majid Hussain, Zahid Iqbal and Azeem Shehzad are really assets for me. Without their company it was very difficult to complete this task.

I can't ignore Higher Education Commission of Pakistan whose financial support enabled me to complete PhD studies successfully.

I am also thankful to the managerial staff of the Department of Mathematics for their cooperation throughout this period.

Azad Hussain

Contents

0 Introduction **4**

1 Flow of a Jeffery-six constant fluid in cylinders **13**

1.1 Introduction 13

1.2 Mathematical model 13

1.3 Couette flow 15

1.4 Solution of the problem 17

1.5 Generalized Couette flow 19

1.6 Graphical results and discussion 21

1.7 Conclusions 22

2 Analytical treatment of Generalized Couette flow of an Oldroyd 8-constant fluid bounded by two concentric cylinders with variable viscosity **28**

2.1 Introduction 28

2.2 Mathematical equations 29

2.3 Physical model 30

2.4 Series Solutions for Reynolds' model 32

2.5 Series solutions for Vogel's model 34

2.6 Graphical results and discussion 35

2.7 Conclusions 37

3 Analytical and numerical treatments of Generalized Couette flow through cylinders with variable viscous properties **43**

3.1 Introduction . . . 43
3.2 Modeling of the problem . . . 44
3.2.1 Case 1: Motion of an inner cylinder . . . 45
3.2.2 Case 2: Movement of outer cylinder . . . 45
3.3 Solution of the problem . . . 46
3.4 Numerical solution . . . 48
3.5 Graphical results and discussion . . . 48
3.6 Conclusions . . . 50

4 An analytical treatment of Generalized Couette non-Newtonian nanofluid flow with variable viscosity 59
4.1 Introduction . . . 59
4.2 Problem statement . . . 59
4.3 Solution of the problem . . . 61
4.4 Graphical results and discussion . . . 63
4.5 Conclusions . . . 64

5 Boundary layer flow of an Eyring-Powell model fluid due to a stretching cylinder with variable viscosity 73
5.1 Introduction . . . 73
5.2 Description of the problem . . . 73
5.3 Series Solutions for Reynolds model . . . 76
5.4 Series solutions for Vogel's model . . . 79
5.5 Graphical results and discussion . . . 79
5.6 Conclusions . . . 80

6 Boundary layer flow of a Walter's B fluid due to a stretching cylinder with temperature dependent viscosity 87
6.1 Introduction . . . 87
6.2 Description of the problem . . . 88
6.3 Solution of the problem . . . 89

6.4 Graphical results and discussion 90
6.5 Conclusions 91

7 Boundary layer flow of a hyperbolic tangent fluid due to a stretching cylinder with temperature dependent viscosity 100

7.1 Introduction 100
7.2 Description of the problem 101
7.3 Solution of the problem 102
7.4 Graphical results and discussion 103
7.5 Conclusions 103

8 Conclusions 110

Chapter 0

Introduction

The non-Newtonian fluids flow has earned significant grandness due to its applications in industry like polymers, plastic, petroleum, printing materials, soap, pharmaceuticals and rubber [1]. The flow behavior of non-Newtonian fluid in microchannels is of mellow interest in pragmatic applications such as sample collection, detection, reaction, dispensing, mixing, and separation of various chemical and biological species in microchips incorporated with fluidic pumps, sensors, and valves, as well as in capillary viscometer to evaluate the non-Newtonian viscosity of biological and chemical polymeric solutions [2]. In hydraulic fracturing, fluids are used that consist of chemical additives exhibiting properties of non-Newtonian fluids that might drastically influence hydraulic behavior of these fluids. Equally forceful alteration in injection rate, wellhead pressure and hydraulic horse power requirement might result from these fluid properties [3]. The flow of non-Newtonian fluids through inflatable as well as collapsible tubes plays a vital role in biofluid mechanics. Esophagus may be regarded as a tube connecting the stomach and throat. The movement of liquids or food through human throat may be considered as an example of non-Newtonian fluid flow through a tube. The knowledge of the mechanisms like esophageal and pharyngeal makes us able to the better treatment of such systems with malfunctioning. Biological science of these systems is very complicated. The food and liquids could have viscous non-Newtonian or viscous Newtonian or viscous and elastic non-Newtonian flow behavior; the latter possibly due to the presence of viscoelastic biopolymers [4]. Damir Dominko and Matija Culo are of the view that one application of non-Newtonian fluid could be a flexible military suit (Wikipedia). Inside the suit there would be some kind of non-Newtonian

fluid which would remain in liquid state while the soldier stands still, moves or runs, but would immediately go into the solid state when the bullet hits, acting as a sort of flexible bulletproof armor. Non-Newtonian fluids could also be used in shoe manufacturing. The inside layer of the shoes would be filled with a non-Newtonian fluid. During standing, walking, or easy running, when pressures which act on the shoe are weak, the non-Newtonian fluid would remain in a liquid state and therefore the shoe interior would adapt the position and shape of the foot. This would make non-Newtonian fluid sport shoes very comfortable. During fast running or other activities which apply strong pressures on the foot, the non-Newtonian fluid would solidify at places and prevent possible injuries. Again, the main hurdle in making such a shoe is finding a non-Newtonian fluid whose viscosity vs. stress dependence satisfies the above requirements. In four-wheel drive vehicles the driving and non-driving shafts are connected by a mechanical device called viscous coupling. The device consists of many circular plates with perforations. Those plates are placed in a drum and fitted very close to each other. Inside the drum there is a non-Newtonian fluid whose viscosity increases with shear stress. Plates are alternately connected to the driving shaft at one end and non-driving shaft at the other. When a vehicle moves without skidding, both shafts together with their connected plates rotate with the same rotational speed. The non-Newtonian fluid remains in liquid state due to the absence of shear between adjacent plates. But, in a situation in which the vehicle is skidding the difference in rotational speed of adjacent plates produces shear stress: the fluid abruptly increases its viscosity (it responds much like a solid) and therefore transfers motion between plates. The end effect is a transfer of torque from driving to the non-driving shaft in other words, we switch from a two-wheel to a four-wheel drive.

The flow of non-Newtonian fluids in open channels is of great importance to the mining industry. Fixed-shape open channels can transport ore slurries and tailings streams as a more economic alternative to pumping, when the terrain allows. Currently the design of these flumes is often done using crude estimates based on the conditions established for water with a limited set of field observations. In the context of a tailings storage facility, self-formed channels at sufficient gradient or slope will generate enough turbulence to maintain particles in suspension. Also, a shallower gradient will reduce the turbulence intensity, which allows more solids to settle in the channel bed. The study of non-Newtonian suspensions in open channels will provide the

fundamental information about the design and operation of industrial channels for the transport of mineral suspensions.

Due to extensive use of non-Newtonian fluid flows in several technical and industrial processes, scientists paid their attention towards different non-Newtonian fluid model flows through different geometries. As for as literature survey is concerned, Rajagopal and Gupta [5] studied an exact solution for the flow of a non-Newtonian fluid past an infinite plate. Rajagopal et al. [6] discussed an existence theorem for the flow of a non-Newtonian fluid past an infinite porous plate. Fetecau et al. [7] considered unsteady flow of a second grade fluid between two side walls perpendicular to a plate. Vieru et al. [8] found exact solutions corresponding to the first problem of Stokes for Oldroyd-B fluids. The first problem of Stokes for Burgers' fluids was discussed by Vieru et al. [9]. Tan and Masuoka [10] examined Stokes first problem for an Oldroyd-B fluid in a porous half space. Chen et al. [11] analyzed unsteady unidirectional flow of an Oldroyd-B fluid in a circular duct with different given volume flow rate conditions. Ariel et al. [12] probed flow of a third grade fluid through a porous flat channel. Siddiqui et al. [13] talked about some unsteady unidirectional flows of a non-Newtonian fluid. Moving boundary in a non-Newtonian fluid was viewed by Asghar et al. [14]. Hayat et al. [15] dissected an oscillating hydromagnetic non-Newtonian flow in a rotating system. Hayat et al. [16] studied into Hall effects on unsteady duct flow of a non-Newtonian fluid in a porous medium. Nadeem et al. [17] obtained numerical solutions of peristaltic flow of a Jeffrey-six constant fluid with variable MHD.

Viscosity is another physical property of fluids. "Viscosity is a measure of the resistance of a fluid which is being deformed by either shear or tensile stress. In everyday terms (and for fluids only), viscosity is thickness or internal friction" (Wikipedia). A large number of papers have been discussed in which fluid viscosity is considered to be constant. In certain situations, it is not necessary that the fluid viscosity is constant it may vary with distance, temperature or pressure. For example in coal slurries the viscosity of the fluid vary with temperature. In general the coefficient of viscosity for real fluids are functions of temperature. In many thermal transport processes, the temperature distribution with in the flow field is not uniform, i.e., the fluid viscosity may be changed noticeably if a large temperature difference exists in the system. Therefore, it is highly desirable to take into account the temperature dependent

viscosity in momentum as well as in energy equation. Literature survey indicates that very less attention has been given to the flow of non-Newtonian fluids with variable viscosity. The works of Massoudi and Christie [18], Pakdermirli and Yilbas [19]and Pantokratoras [20] may be mentioned in this direction. One of non-Newtonian fluids models is Jeffery-six constant fluid. Aristov and Skul'skii [21], discussed this model of fluid in a plane channel. Nadeem et al. [22] discussed effects of partial slip on a fourth grade fluid with variable viscosity. Further, Akbar et al. [23] discussed simulation of heat transfer on the peristaltic flow of a Jeffrey-six constant fluid in a diverging tube. Oldroyd 8-constant model is an important non-Newtonian fluid model. Baris et al. [24] considered an Oldroyd 8-constant model to discuss the steady flow in a convergent channel. The couette, poiseuile and generalized couette flows of an Oldroyd 8-constant magnetohydrodynamic fluid are discussed by Hayat et al. [25]. The problem dealing with the steady flow of an Oldroyd 8-constant fluid over a suddenly moved plate is considered by Ellahi et al. [26]. In continuation, Ellahi et al. [27] discussed Oldroyd 8-constant fluid with non-linear slip condition. A complex mathematical model known as Eyring-Powell fluid model was developed by Powell and Eyring in 1944. Powell and Eyring [28] studied mechanism for the relaxation theory of viscosity. This model is another addition to the regime of non-Newtonian fluids.

Stretching is another important phenomena which plays a vital role in our daily life. The flow of a stretching plate is observed in a large number of industrial processes. Examples of fabrication of adhesive tapes, the extrusion of plastic sheets and application of coating layers onto rigid substrates may be mentioned in this regard. Polymer sheets are manufactured by continuous extrusion of the polymer from a die to a windup roller [29]. A continuously moving surface with a non-uniform velocity through the ambient fluid is constituted by the thin polymer sheet. Flows caused by a continuously moving surface are encountered in many processes of thermal and moisture treatment of materials, predominantly in processes involving continuous pulling of a sheet through a reaction zone; as in crystalline materials, paper industries, in textiles, in the manufacture of glass sheets and metallurgy. It is worth mentioning that many metallurgical processes involve the cooling of continuous stripes or filaments by drawing them through a quiescent fluid, and in the process of drawing, these strips are stretched [30-34]. In view of these applications, stretching flows with various geometries for both Newtonian and non-

Newtonian fluids have been discussed analytically, numerically and experimentally by number of researchers.

The flow of a Newtonian fluid over a linear stretching surface was first studied by Crane [35]. Subsequently, various aspects of the flow and/or heat transfer problems for stretching surfaces moving in the infinite fluid medium have been explored in many investigations [36-44]. In the manufacture of metal and polymer solid cylinders, the material is usually in a molten phase when thrust through an extrusion die and then cools and solidifies some distance away from the die. Experiments by Vleggaar [45] show that the velocity of the material is approximately proportional to the distance, so these systems are often modeled as linearly stretching rods or cylinders. Wang [46] has studied the steady flow of a viscous and incompressible fluid outside of a stretching hollow cylinder in an ambient fluid at rest. However, very less attention has been given to the flows of a non-Newtonian fluid due to a stretching cylinder with variable viscosity. The fluids are necessary for heat transfer in engineering equipment.

Low thermal conductivity of conventional heat transfer fluids like water, oil, and ethylene glycol mixture is a limitation in enhancing the performance and compactness of such engineering equipment. To overcome this difficulty, there is need to find advanced heat transfer fluids with higher conductivity. Recent simulations of the cooling system of a large truck engine predicts that replacement of the conventional engine coolant (ethylene glycol-water mixture) by a nanofluid would provide remarkable advantages by removing more heat from the engine. Hence, there is strong motivation in the use of nanofluids for any process that uses process heat that needs cooling, i.e., engines, heat treating, rubber manufacturing, etc. Processing time could be minimized using nanoparticles in water compared to using water to cool from processing temperatures. Recently, a special attention has been given to the nanofluids. The term nanofluid was introduced by Choi 1995; means a liquid containing a suspension of submicron solid particles (nano particles). The major advantage of nanofluids is thermal conductivity enhancement (see Masuda et. al 1993;). The major use of nanofluids technology is in advance nuclear systems. A comprehensive study about natural convection of nanofluids have been examined by Putra et. al [47]. They [47] experimentally discussed the natural convection of nanofluids inside horizontal cylinder heated from one end and cooled from the other end. Kuznetsov and Nield [48] have examined the natural convective boundary layer flow of a nanofluid past a vertical

plate. In another study, Kuznetsorv and Nield [49] have reported the thermal instability in a porous medium layer saturated by a nanofluid. A numerical study about boundary layer flow of a nanofluid past a stretching sheet have been presented by Khan and Pop [50]. However, non-Newtonian nanofluid flows with variable viscosity are very rare. Keeping in mind the above highlights the purpose of present thesis is to discuss the effects of variable viscosity for different non-Newtonian fluid models in different physical geometries. Motivated from the above important studies the present thesis is arranged as follow: In chapter zero brief literature survey is highlighted.

In chapter one, we discuss the flow of a Jeffrey-six constant incompressible fluid between two infinite coaxial cylinders in the presence of heat transfer analysis. The governing equations of Jeffrey-six constant fluid along with energy equation have been derived in cylindrical coordinates. The highly nonlinear equations are simplified with the help of nondimensional parameters and then solved analytically with the help of homotopy analysis method (HAM)[51] for two fundamental flows namely Couette and Generalized Couette flow. The content of this chapter is published in **Communications in Theoretical Physics. 56(2011)345 – 351**.

Chapter two is devoted to the study of flow of an Oldroyd 8-constant fluid with variable temperature dependent viscosity between coaxial cylinders. The analytic solutions are obtained by using homotopy analysis method (HAM). The content of this chapter is published in **Communications in Theoretical Physics 56(2011)933 – 938..**

The flow of a third grade fluid between two coaxial cylinders with temperature dependent viscosity has been examined in chapter three. The medium is considered to be porous. Two types of geometrical problems with Reynolds' and Vogel's viscosity models are taken into account. In first case the motion of the fluid is due to a constant pressure gradient and a movement of inner cylinder while the outer cylinder is kept fixed. In second case we considered that the inner cylinder is fixed while the disturbance in the fluid comes due to the constant pressure gradient and the movement of outer cylinder. Analytical solutions have been calculated using homotopy analysis method (HAM) for temperature and velocity equations. The numerical solution of the problem has also been computed by shooting method.

In chapter 4, we have focused our attention to highlight the study of non-Newtonian nanofluid between coaxial cylinders with variable viscosity. Analytical solutions are com-

puted with the help of HAM technique. The content of this chapter is published in **ZNA. 67a(2011)255 – 261**.

In chapter 5, an analytical treatment of a steady boundary layer flow of an Eyring-Powell model fluid due to a stretching cylinder with temperature dependent variable viscosity is discussed. This work is accepted in Scientia Iranica.

Chapter 6 is devoted to describe the study of boundary layer flow of a Walter's B fluid due to a stretching cylinder with temperature dependent variable viscosity. The content of this chapter is submitted for publication in communication in mathematical physics.

Chapter 7 is developed to study the flow of a hyperbolic tangent fluid due to a stretching cylinder with temperature dependent variable viscosity. This work is submitted for possible publication in computer physics communication.

Nomenclature	
$\mathbf{V}$	Velocity
$\mathbf{S}$	Extra stress tensor
$\boldsymbol{\tau}$	Cauchy stress tensor
ρ	Density of the fluid
μ	Viscosity
Υ	Transpose
a	Radius of tube
c	A constant with positive value
a_m, b_m, c_m	Material constants of Jeffrey-six constant fluid
ζ_3, ζ_4	Oldroyd 8-constant parameters
ζ_6	Jeffrey fluid parameter
Re	Reynold number
D_T	Thermophoretic diffusion coefficient
κ	Thermal conductivity
N_b	Brownian motion parameter
N_t	Thermophoresis parameter
β_1, c_1	Material constant of Eyring Powell fluid
D_B	Brownian diffusion coefficient
E, F, G, J	Material constant of Jeffrey six-constant fluid model
G_r	Grashof number
C_p	Specific heat
w	Velocity component in z-direction
E_1, E_2	Eyring Powell fluid parameters
E_c	Eckert number
λ_2	The delay time
μ, η	Viscosities
A	Vogel's model parameter
ρ_p	Density of particle

$\mathbf{I}$	The identity tensor
$\mathbf{A}_1$	The first Rivlin-Ericksen tensor
$\frac{D}{Dt}$	The contravarient convected derivative
β	Volumetric expansion coefficient of the fluid
β_3	Dimensional third grade parameter
Λ	The dimensionless non-Newtonian parameter
λ_1	The ratio of relaxation to retardation times
λ_2	The retardation time
R_0	Inward cylinder radius
R_1	Outward cylinder radius
λ_{11}	Relaxation time
t	Time
p	Pressure
ζ_5	Walters' B fluid parameter
v_0	Constant velocity of the inner cylinder
q	Embedding parameter
Pr	Prandtl number
M	Reynolds' model viscosity parameter
C, C^*, B	Constants of Vogel's model
b	A constant
σ	Temperature in dimensional form
P	Porous medium parameter
g	Gravitational force
α_3	Thermal diffusivity
ϕ_1	Porosity
W	Antisymmetric part of velocity gradient
ϕ	Nanoparticle fraction
$(\rho c)p$	The heat capacity of the nanoparticle material

Chapter 1

Flow of a Jeffery-six constant fluid in cylinders

1.1 Introduction

The current chapter handles flow of a Jeffery-six constant fluid through annulus region of two concentric cylinders in the presence of heat transfer analysis. The arising non linear partial differential equations are simplified by using nondimensional parameters. Two fundamental flows namely Couette and Generalized Couette flow are studied. The effects of emerging parameters are discussed through graphs. To see the series solution's convergence we portrait h-curves.

1.2 Mathematical model

We consider flow of a Jeffrey-six constant fluid through annulus region of two concentric cylinders. The equations which govern the problem are given by

$$\boldsymbol{\nabla}.\mathbf{V} = 0, \tag{1.1}$$

$$\rho\frac{d\mathbf{V}}{dt} = \operatorname{div}\boldsymbol{\tau}, \tag{1.2}$$

$$\rho C_p \frac{dT}{dt} = \boldsymbol{\tau}.\mathbf{L} + k\boldsymbol{\nabla}^2 T, \tag{1.3}$$

where ρ is density, $\mathbf{V}$ is velocity vector, C_p denotes specific heat, T is temperature and $\boldsymbol{\tau}$ is the Cauchy stress tensor, which is different for different fluid models.

The stress tensor for Jeffrey-six constant fluid is defined as [21]

$$\boldsymbol{\tau} + \lambda_{11} F_{a^\star b^\star c^\star} \boldsymbol{\tau} = \mu(\mathbf{D} + \lambda_2 F_{a^\star b^\star c^\star} \mathbf{D}), \tag{1.4}$$

or is written in an expanded from as

$$\begin{aligned} \boldsymbol{\tau} + \lambda_{11}[\frac{d\boldsymbol{\tau}}{dt} - \mathbf{W}.\boldsymbol{\tau} + \boldsymbol{\tau}.\mathbf{W} + a^\star(\boldsymbol{\tau}.\mathbf{D} + \mathbf{D}.\boldsymbol{\tau}) + b^\star \boldsymbol{\tau} \quad &: \quad \mathbf{D}I + c^\star \mathbf{D}\ tr\boldsymbol{\tau}] = 2\mu[\mathbf{D} \\ +\lambda_2(\frac{d\mathbf{D}}{dt} - \mathbf{W}.\mathbf{D} + \mathbf{D}.\mathbf{W} + 2a^\star \boldsymbol{D}.\mathbf{D} + b^\star \mathbf{D} \quad &: \quad \mathbf{D}I)]. \end{aligned} \tag{1.5}$$

In the above equation, $\boldsymbol{\nabla}\mathbf{V} = \mathbf{D} + \mathbf{W}$ is the velocity gradient, $\mathbf{D} = (\boldsymbol{\nabla}\mathbf{V}^\Upsilon + \boldsymbol{\nabla}\mathbf{V})/2$ is the symmetric part of velocity gradient, $\mathbf{W} = (\boldsymbol{\nabla}\mathbf{V}^\Upsilon - \boldsymbol{\nabla}\mathbf{V})/2$ is the antisymmetric part of velocity gradient.

For the problem under consideration we take the velocity and temperature distribution of the form

$$\mathbf{V} = [0,\ 0,\ v(r)],\ T = T(r). \tag{1.6}$$

In the light of Eqs. (1.5) and (1.6), continuity equation (1.1) is identically satisfied, momentum and energy equations become

$$\begin{aligned} &\mu\frac{d^2v}{dr^2} + 2A_3^*\frac{\partial p}{\partial z}\left(\frac{dv}{dr}\right)^2 + (2HA_3^* + A_2^* + A_4^*)\,\frac{\mu}{r}\left(\frac{dv}{dr}\right)^3 (2HA_3^* + A_2^* + A_4^*) \\ &+ \left(HA_3^{*2} + A_1^*\right)\frac{\mu}{r}\left(\frac{dv}{dr}\right)^5 + (2HA_3^* + 3A_2^* + 3A_4^*)\,\mu\frac{d^2v}{dr^2}\left(\frac{dv}{dr}\right)^2 + \frac{\mu}{r}\frac{dv}{dr} \\ &-A_3^{*2}\frac{\partial p}{\partial z}\left(\frac{dv}{dr}\right)^4 + \left(\frac{dv}{dr}\right)^4\left(\left(HA_3^{*2} + 5A_1^*\right)\mu\frac{d^2v}{dr^2} + \left(HA_3^{*2} + A_1^*\right)\mu\frac{d\mu}{dr}\frac{dv}{dr}\right) = 0, \end{aligned} \tag{1.7}$$

$$\mu H\left(\frac{dv}{dr}\right)^2+\frac{\mu[(1-H)\left(\frac{dv}{dr}\right)^2+A_4^*\left(\frac{dv}{dr}\right)^4]}{1+A_3^*\left(\frac{dv}{dr}\right)^2}-\kappa[\frac{1}{r}\frac{dT}{dr}+\frac{d^2T}{dr^2}]=0, \tag{1.8}$$

where

$$\begin{aligned}
H &= \frac{\lambda_2}{\lambda_{11}},\ A_4^*=\frac{\lambda_2}{2}\left(a^\star+b^\star-1\right)\left(1+a^\star+c^\star\right)\left(\lambda_2-\lambda_{11}\right),\\
A_3^* &= \frac{\lambda_{11}}{2}\left\{\lambda_{11}\left(1-a^\star-c^\star\right)\left(1+a^\star+b^\star\right)-b^\star c^\star\lambda_{11}-\lambda_2\left(1+a^\star+c^\star\right)\left(a^\star+b^\star-1\right)\right\},\\
A_2^* &= \frac{1}{2}(\lambda_{11}-\lambda_2)\left\{\lambda_1\left(1-a^\star-c^\star\right)\left(1+a^\star+b^\star\right)-b^\star c^\star\lambda_{11}-\lambda_2\left(1+a^\star+c^\star\right)\left(a^\star+b^\star-1\right)\right\},\\
A_1^* &= \frac{\lambda_{11}\lambda_2}{4}\left(a^\star+b^\star-1\right)\left(1+a^\star+c^\star\right)\left(\lambda_2-\lambda_{11}\right)(\lambda_{11}\left(1-a^\star-c^\star\right)\left(1+a^\star+b^\star\right)-b^\star c^\star\lambda_{11}\\
&\quad -\lambda_2\left(1+a^\star+c^\star\right)\left(a^\star+b^\star-1\right)).
\end{aligned} \tag{1.9}$$

Moreover, $a^\star$, $b^\star$ and $c^\star$ are constants.

1.3 Couette flow

Consider the flow which is bounded by two infinite cylinders. Only the inner cylinder's motion is responsible for the flow. The walls of both the cylinders are heated with temperatures T_o and T_1 respectively.

The associated boundary conditions are

$$v\left(R_0\right)=v_0,\ T\left(R_0\right)=\ T_0,\ v\left(R_1\right)=0,\ T\left(R_1\right)=T_1 \tag{1.10}$$

where R_0 is the radius of the inner cylinder, R_1 is the radius of outer cylinder and v_0 is the constant velocity of inner cylinder.

Introducing the following nondimensional variables

$$\bar{r}=\frac{r}{R_0},\ F=\frac{A_1^*v_0^4}{R_0^4},\ G=\frac{A_2^*v_0^2}{R_0^2},\ \theta=\frac{T-T_1}{T_o-T_1},\ b=\frac{R_1}{R_0},\ C_1=\frac{\partial p}{\partial z},\ E=\frac{A_3^*v_0^2}{R_0^2}, \tag{1.11}$$

$$C=\frac{C_1R_0^2}{\mu_*v_0},\Gamma=\frac{\mu_*^2\mathbf{v}_0}{\kappa(T_o-T_1)},\bar{v}=\frac{v}{v_0},\bar{\mu}=\frac{\mu}{\mu_*},J=\frac{A_4^*v_0^2}{R_0^2}, \tag{1.12}$$

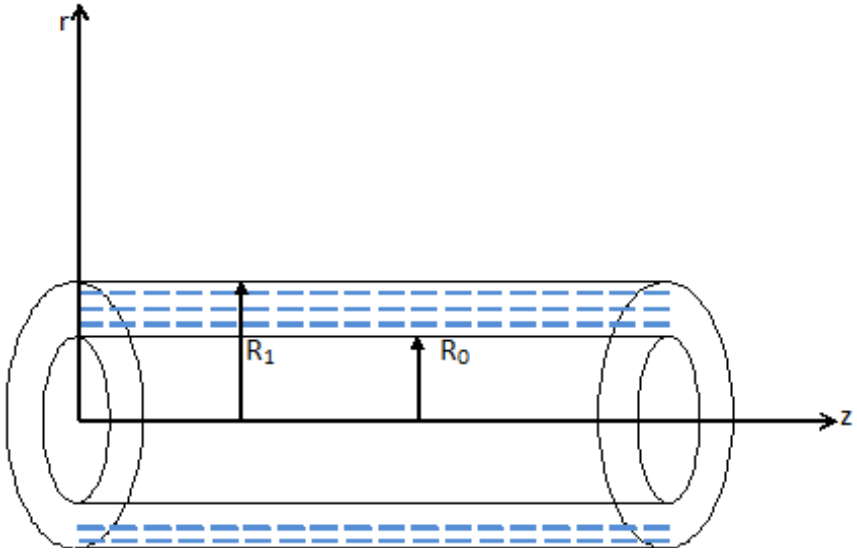

Fig. 1*a*: Geometry of the problem.

Substituting Eq. (1.11) into Eqs. (1.7), (1.8) and boundary conditions (1.10), we obtain the following equations after dropping bars,

$$\left(\frac{\mu}{r}\left(J+G+2EH\right)\frac{dv}{dr}+\mu\left(3J+3G+2EH\right)\right)\left(\frac{dv}{dr}\right)^{2}$$
$$+\mu\frac{d^{2}v}{dr^{2}}+\frac{\mu}{r}\left(E^{2}H+F\right)\left(\frac{dv}{dr}\right)^{5}+\mu\left(E^{2}H+5F\right)\frac{d^{2}v}{dr^{2}}\left(\frac{dv}{dr}\right)^{4}+\frac{\mu}{r}\frac{dv}{dr}=0, \quad (1.12)$$

$$\mu\Gamma\left(\frac{dv}{dr}\right)^{2}+\mu\left(J+EH\right)\Gamma\left(\frac{dv}{dr}\right)^{4}+\frac{1}{r}\frac{d\theta}{dr}+\frac{d^{2}\theta}{d^{2}r}-\left(\frac{E}{r}+E\frac{d^{2}\theta}{d^{2}r}\right)\left(\frac{dv}{dr}\right)^{2}=0, \quad (1.13)$$

$$v(1)=\theta(1)=1. \quad (1.14)$$

$$v(b)=\ \theta(b)=0. \quad (1.15)$$

1.4 Solution of the problem

The solution of above boundary value problem have been computed analytically adopting homotopy analysis method. For series solution we take the initial estimate

$$v_0(r) = \frac{(b-r)}{(b-1)}, \tag{1.16}$$

$$\theta_0(r) = \frac{(b-r)}{(b-1)}. \tag{1.17}$$

The auxiliary linear operators are defined as

$$\pounds_{vel}(v) = v'', \tag{1.18}$$

$$\pounds_{temp}(\theta) = \theta'', \tag{1.19}$$

possessing

$$\mathcal{L}_{vel}(A_{11} + B_1 r) = 0, \tag{1.20}$$

$$\mathcal{L}_{temp}(A_{12} + B_2 r) = 0, \tag{1.21}$$

where A_{11}, A_{12} , B_1 and B_2 are constants and $\pounds_{vel}$ and $\mathcal{L}_{temp}$ stands for linear operators for velocity and temperature.

If $q \in [0,1]$ is an embedding parameter then the problems at the zero and mth order are respectively given by

$$(1-q)\mathcal{L}_{vel}[\bar{v}(r,q) - v_0(r)] = q\hbar N_v[\bar{v}(r,q), \bar{\theta}(r,q)], \tag{1.22}$$

$$(1-q)\mathcal{L}_{temp}[\bar{\theta}(r,q) - \theta_0(r)] = q\hbar N_\theta[\bar{v}(r,q), \bar{\theta}(r,q)], \tag{1.23}$$

$$\mathcal{L}_{vel}[v_m(r) - \chi_m v_{m-1}(r)] = \hbar R_v(r), \tag{1.24}$$

$$\mathcal{L}_{temp}[\theta_m(r) - \chi_m \theta_{m-1}(r)] = \hbar R_\theta(r), \tag{1.25}$$

$$\bar{v}(1,q) = \bar{\theta}(1,q) = 1, \tag{1.26}$$

$$\bar{v}(b,q) = \bar{\theta}(b,q) = 0. \tag{1.27}$$

$$\bar{v}_m(1,q) = \bar{\theta}_m(1,q) = 0, \tag{1.28}$$

$$\bar{v}_m(b,q) = \bar{\theta}_m(b,q) = 0, \tag{1.29}$$

where

$$\begin{aligned} N_v[\bar{v}(r,q)] &= \tfrac{\mu}{r}\tfrac{dv}{dr} + \tfrac{\mu}{r}\left(J+G+2EH\right)\left(\tfrac{dv}{dr}\right)^3 + \tfrac{\mu}{r}\left(E^2H+F\right)\left(\tfrac{dv}{dr}\right)^5 \\ &+\mu\frac{d^2v}{dr^2} + \left(\mu\left(E^2H+5F\right)\frac{d^2v}{dr^2}\left(\frac{dv}{dr}\right)^2 + \mu\left(3J+3G+2EH\right)\frac{d^2v}{dr^2}\right)\left(\frac{dv}{dr}\right)^2, \end{aligned} \tag{1.30}$$

$$\begin{aligned} N_\theta[\bar{v}(r,q),\bar{\theta}(r,q)] &= \mu\Gamma\left(\tfrac{dv}{dr}\right)^2 + \mu\left(J+EH\right)\Gamma\left(\tfrac{dv}{dr}\right)^4 \\ &-\frac{1}{r}\frac{d\theta}{dr} - \frac{d^2\theta}{dr^2} - \frac{E}{r}\left(\frac{dv}{dr}\right)^2 - E\frac{d^2\theta}{dr^2}\left(\frac{dv}{dr}\right)^2, \end{aligned} \tag{1.31}$$

$$\begin{aligned} R_v &= \tfrac{\mu}{r}v_{m-1}^{'} + \tfrac{\mu}{r}\left(J+G+2EH\right)\sum_{k=0}^{m-1}\sum_{l=0}^{k} v_{m-1-k}^{'}v_{k-l}^{'}v_l^{'} \\ &+\frac{\mu}{r}\left(E^2H+F\right)\sum_{k=0}^{m-1}\sum_{l=0}^{k}\sum_{s=0}^{l}\sum_{j=0}^{s} v_{m-1-k}^{'}v_{k-l}^{'}v_{l-s}^{'}v_{s-j}^{'}v_j^{'} \\ &+\mu\left(E^2H+5F\right)\sum_{k=0}^{m-1}\sum_{l=0}^{k}\sum_{s=0}^{l}\sum_{j=0}^{s} v_{m-1-k}^{'}v_{k-l}^{'}v_{l-s}^{'}v_{s-j}^{'}v_j^{''} \\ &+\mu\left(3J+3G+2EH\right)\sum_{k=0}^{m-1}\sum_{l=0}^{k} v_{m-1-k}^{'}v_{k-l}^{'}v_l^{''} + \mu v_{m-1}^{''}, \end{aligned} \tag{1.32}$$

$$\begin{aligned} R_\theta &= \mu\Gamma\sum_{k=0}^{m-1} v_{m-1-k}^{'}v_k^{'} + \mu\left(J+EH\right)\Gamma\sum_{k=0}^{m-1}\sum_{l=0}^{k}\sum_{s=0}^{l} v_{m-1-k}^{'}v_{k-l}^{'}v_{l-s}^{'}v_s^{'} \\ &-\frac{1}{r}\theta_{m-1}^{'} - \theta_{m-1}^{''} - \frac{E}{r}\sum_{k=0}^{m-1} v_{m-1-k}^{'}v_k^{'} - E\sum_{k=0}^{m-1}\sum_{l=0}^{k} v_{m-1-k}^{'}v_{k-l}^{'}\theta_l^{''}. \end{aligned} \tag{1.33}$$

The solution of Eqs.(1.32) and (1.33) using Mathematica are obtained in the form

$$v_m(r) = \sum_{n=0}^{m+1} a_{m,n}r^n,\ \theta_m(r) = \sum_{n=0}^{m+2} d_{m,n}r^n, m \geq 0. \tag{1.34}$$

1.5 Generalized Couette flow

Let us consider the flow of a Jeffrey-six constant fluid with constant viscosity bounded by two infinite coaxial cylinders. The movement of inner cylinder and constant pressure gradient are responsible for the occurrence of disturbance in the fluid. The nondimensional momentum and energy equations in the presence of pressure are defined as

$$\frac{\mu}{r}\left(J+G+2EH\right)\left(\frac{dv}{dr}\right)^{3}+\left(\mu\left(E^{2}H+5F\right)\frac{d^{2}v}{dr^{2}}+\frac{\mu}{r}\left(E^{2}H+F\right)\left(\frac{dv}{dr}\right)\right)\left(\frac{dv}{dr}\right)^{4}-C$$
$$+\mu\frac{d^{2}v}{dr^{2}}+\frac{\mu dv}{rdr}+\left(\mu\left(3J+3G+2EH\right)\frac{d^{2}v}{dr^{2}}-CE^{2}\left(\frac{dv}{dr}\right)^{2}-2C\right)\left(\frac{dv}{dr}\right)^{2}=0. \tag{1.35}$$

$$\mu\Gamma\left(\frac{dv}{dr}\right)^{2}+\mu\left(J+EH\right)\Gamma\left(\frac{dv}{dr}\right)^{4}+\frac{1}{r}\frac{d\theta}{dr}+\frac{d^{2}\theta}{dr^{2}}-E\left(\frac{1}{r}+\frac{d^{2}\theta}{dr^{2}}\right)\left(\frac{dv}{dr}\right)^{2}=0. \tag{1.36}$$

The corresponding boundary conditions are defined in Eqs. (1.14) and (1.15) . Initial guesses and auxiliary linear operators are defined in Eqs. (1.16) to (1.19) for HAM solution.

If $q\in[0,1]$ is an embedding parameter and $\hbar$ is auxiliary parameter then the problems at the zero and mth order are respectively given by

$$(1-q)\mathcal{L}_{vel}[\bar{v}(r,q)-v_{0}(r)]=q\hbar N_{vel}[\bar{v}(r,q),\bar{\theta}(r,q)], \tag{1.37}$$

$$(1-q)\mathcal{L}_{temp}[\bar{\theta}(r,q)-\theta_{0}(r)]=q\hbar N_{temp}[\bar{v}(r,q),\bar{\theta}(r,q)], \tag{1.38}$$

$$\mathcal{L}_{vel}[v_{m}(r)-\chi_{m}v_{m-1}(r)]=\hbar R_{vel}(r), \tag{1.39}$$

$$\mathcal{L}_{temp}[\theta_{m}(r)-\chi_{m}\theta_{m-1}(r)]=\hbar R_{temp}(r), \tag{1.40}$$

$$\bar{v}(1,q)=\bar{\theta}(1,q)=1, \tag{1.41}$$

$$\bar{v}(b,q)=\bar{\theta}(b,q)=0, \tag{1.42}$$

$$\bar{v}_{m}(1,q)=\ \bar{\theta}_{m}(1,q)=0, \tag{1.43}$$

$$\bar{v}_{m}(b,q)=\ \bar{\theta}_{m}(b,q)=0, \tag{1.44}$$

where

$$
\begin{aligned}
N_{vel}[\bar{v}(r,q)] &= \left(\tfrac{\mu}{r}\left(J+G+2EH\right)\tfrac{dv}{dr}+\mu\left(3J+3G+2EH\right)\tfrac{d^2v}{dr^2}\right)\left(\tfrac{dv}{dr}\right)^2 \\
&-\left(CE^2\left(\frac{dv}{dr}\right)^2+2C-\mu\left(E^2H+5F\right)\frac{d^2v}{dr^2}\left(\frac{dv}{dr}\right)^2\right)\left(\frac{dv}{dr}\right)^2-C \\
&+\mu\frac{d^2v}{dr^2}+\frac{\mu^2}{r^2}\left(E^2H+F\right)\left(\frac{dv}{dr}\right)^5\frac{dv}{dr}, \qquad (1.45)
\end{aligned}
$$

$$
\begin{aligned}
N_{temp}[\bar{v}(r,q),\bar{\theta}(r,q)] &= \mu\Gamma\left(\tfrac{dv}{dr}\right)^2+\mu\left(J+EH\right)\Gamma\left(\tfrac{dv}{dr}\right)^4-\tfrac{1}{r}\tfrac{d\theta}{dr} \\
&-\frac{d^2\theta}{dr^2}-\left(\frac{E}{r}+E\frac{d^2\theta}{dr^2}\right)\left(\frac{dv}{dr}\right)^2, \qquad (1.46)
\end{aligned}
$$

$$
\begin{aligned}
R_{vel} &= \tfrac{\mu}{r}v_{m-1}^{'}+\tfrac{\mu}{r}\left(J+G+2EH\right)\sum_{k=0}^{m-1}\sum_{l=0}^{k}v_{m-1-k}^{'}v_{k-l}^{'}v_{l}^{'}-C \\
&+\frac{\mu}{r}\left(E^2H+F\right)\sum_{k=0}^{m-1}\sum_{l=0}^{k}\sum_{s=0}^{l}\sum_{j=0}^{s}v_{m-1-k}^{'}v_{k-l}^{'}v_{l-s}^{'}v_{s-j}^{'}v_{j}^{'}-2C\sum_{k=0}^{m-1}v_{m-1-k}^{'}v_{k}^{'} \\
&+\mu\left(3J+3G+2EH\right)\sum_{k=0}^{m-1}\sum_{l=0}^{k}v_{m-1-k}^{'}v_{k-l}^{'}v_{l}^{''}-CE^2\sum_{k=0}^{m-1}\sum_{l=0}^{k}\sum_{s=0}^{l}v_{m-1-k}^{'}v_{k-l}^{'}v_{l-s}^{'}v_{s}^{'} \\
&+\mu\left(E^2H+5F\right)\sum_{k=0}^{m-1}\sum_{l=0}^{k}\sum_{s=0}^{l}\sum_{j=0}^{s}v_{m-1-k}^{'}v_{k-l}^{'}v_{l-s}^{'}v_{s-j}^{'}v_{j}^{''}+\mu v_{m-1}^{''}, \qquad (1.47)
\end{aligned}
$$

$$
\begin{aligned}
R_{\theta} &= \left(\mu\Gamma-\tfrac{E}{r}\right)\sum_{k=0}^{m-1}v_{m-1-k}^{'}v_{k}^{'}+\mu\left(J+EH\right)\Gamma\sum_{k=0}^{m-1}\sum_{l=0}^{k}\sum_{s=0}^{l}v_{m-1-k}^{'}v_{k-l}^{'}v_{l-s}^{'}v_{s}^{'} \\
&-\frac{1}{r}\theta_{m-1}^{'}-\theta_{m-1}^{''}-E\sum_{k=0}^{m-1}\sum_{l=0}^{k}v_{m-1-k}^{'}v_{k-l}^{'}\theta_{l}^{''}. \qquad (1.48)
\end{aligned}
$$

By Mathematica the solutions of Eqs. (1.47) and (1.48) can be written as

$$
v_m\left(r\right)=\sum_{n=0}^{2m+1}a_{m,n}^{\prime}r^n,\ \theta_m\left(r\right)=\sum_{n=0}^{2m+1}d_{m,n}^{\prime}r^n,\ m\geq 0, \qquad (1.49)
$$

where $a_{m,n}^{\prime}$ and $d_{m,n}^{\prime}$ are constants to be determined by substituting (1.49) into (1.37) -(1.38).

1.6 Graphical results and discussion

To report the convergence of the obtained series solutions and the effects of sundry parameters in the present investigation, we have plotted Figs. 1.1 to 1.10. Figs. 1.1 to 1.3 are prepared to see the convergence region. Figs. 1.1 and 1.2 correspond to Couette flow, where as Fig. 1.3 relates to Generalized Couette flow. Fig. 1.4 depicts the temperature profile for Generalized Couette flow for different values of J. The increment in J means increasment in velocity of inner cylinder. Since inner cylinder is moving in the direction parallel to motion of the fluid. The velocity of fluid particles increases. The kinetic energy depends upon the velocity. The rise in velocity would rise the average kinetic energy of the system. As temperature depends upon kinetic energy i.e. temperature is directly proportional to kinetic energy. Consequently, temperature of the fluid rises up. This is what we are observing in Fig. 1.4.

Fig. 1.5 shows influence of variation of E on temperature distribution for Generalized Couette flow. Since E is directly proportional to square of velocity of inner cylinder. When E is increasing, it indicates that velocity of inner cylinder enhancing the velocity of fluid particles. The kinetic energy of system is directly proportional to the square of average velocity of fluid particles. Thus, we come across the conclusion that kinetic energy of the system as a whole is increasing. This enhancement in kinetic energy influences temperature in such a way that it rises up. Fig. 1.6 is plotted in order to see the velocity variation for Generalized Couette flow for C. It is depicted that velocity field decreases as C increases. Since pressure is in a direction opposite to the flow. So as the pressure opposes the motion. The fluid velocity decreases due to rise in pressure.

Fig. 1.7 shows velocity field for Generalized Couette flow for F. It is seen that velocity decreases as F increases. Fig. 1.8 shows the velocity variation for Couette flow for J. It is depicted that velocity increases as J increases. When J is increasing , it is evident that it is because of enhancement in velocity of inner cylinder i.e. the average velocity of the fluid particles increases. As a result, velocity of the fluid rises. Fig. 1.9 is prepared to observe the velocity variation for Generalized Couette flow for different values of J. Observation reveals that velocity increases as J increases. Increase in J means, inner cylinder is moving with greater speed i.e. disturbance in the fluid is increased. Since the motion of the fluid and movement of the cylinder are along the same direction. So as a result velocity of fluid increases. This is

what we are observing in Fig. 1.9. Fig. 1.10 is plotted to see velocity distribution for various values of G.

1.7 Conclusions

In this chapter, we have investigated analytically the flow of a Jeffrey-six constant incompressible fluid between two infinite coaxial cylinders. The highly non-linear problem is solved analytically by powerful technique homotopy analysis method. Effects of emerging parameters on the flow and temperature profiles are examined. The following conclusions are drawn.

1. Temperature profiles increase with the increase of J and E for Generalized Couette flow.
2. Velocity increases with the increase of J for Generalized Couette flow.
3. An increment in parameters C, F and G reduces velocity for Generalized Couette flow.
4. The increase of parameter J leads to the decrease of temperature profile for Couette flow.
5. Velocity increases with the increase of J for Couette flow.

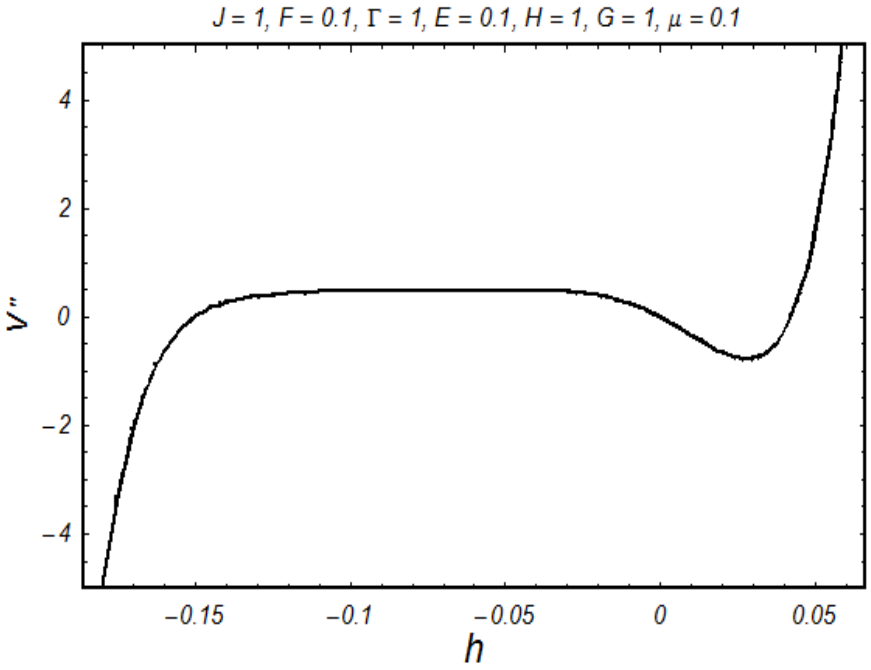

Fig. 1.1. h-curve for velocity for Couette flow.

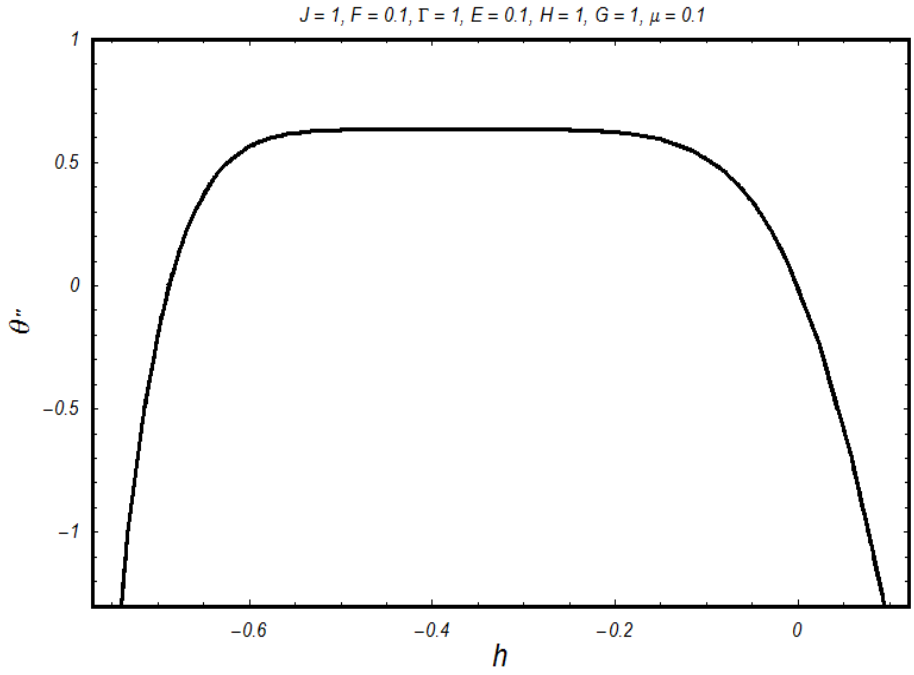

Fig. 1.2. h-curve for temperature for Couette flow.

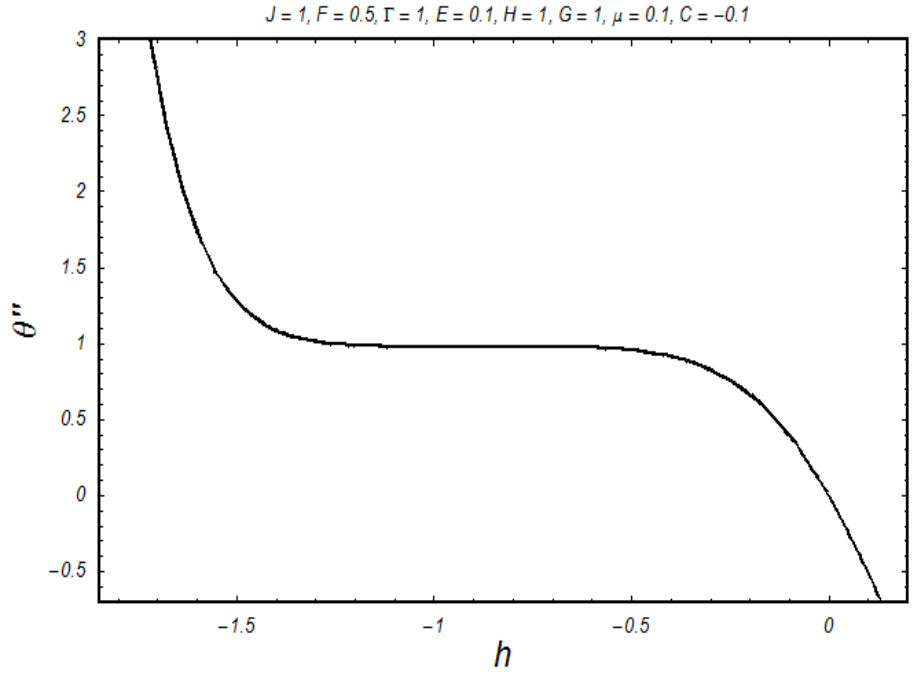

Fig. 1.3. h-curve for temperature for Generalized Couette flow.

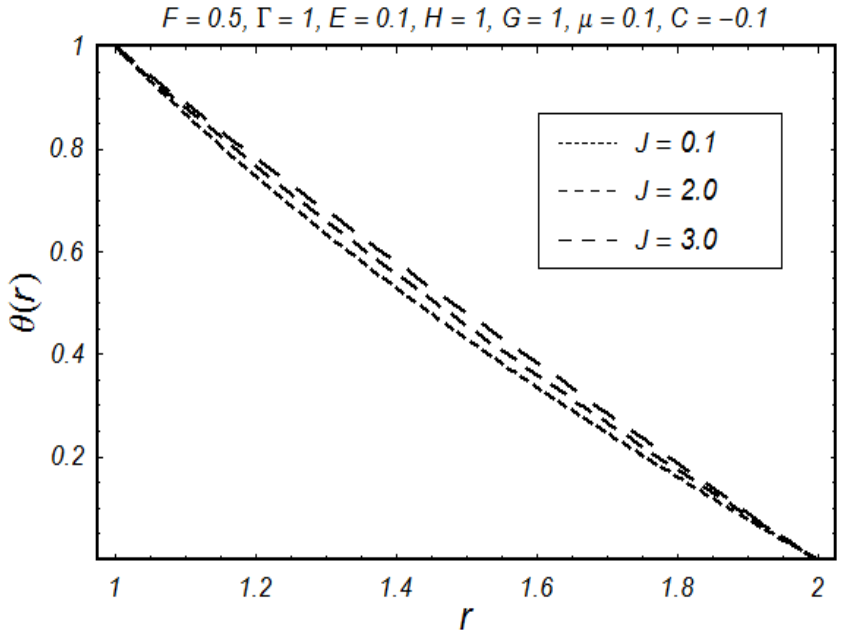

Fig. 1.4. Temperature distribution for Generalized Couette flow for J.

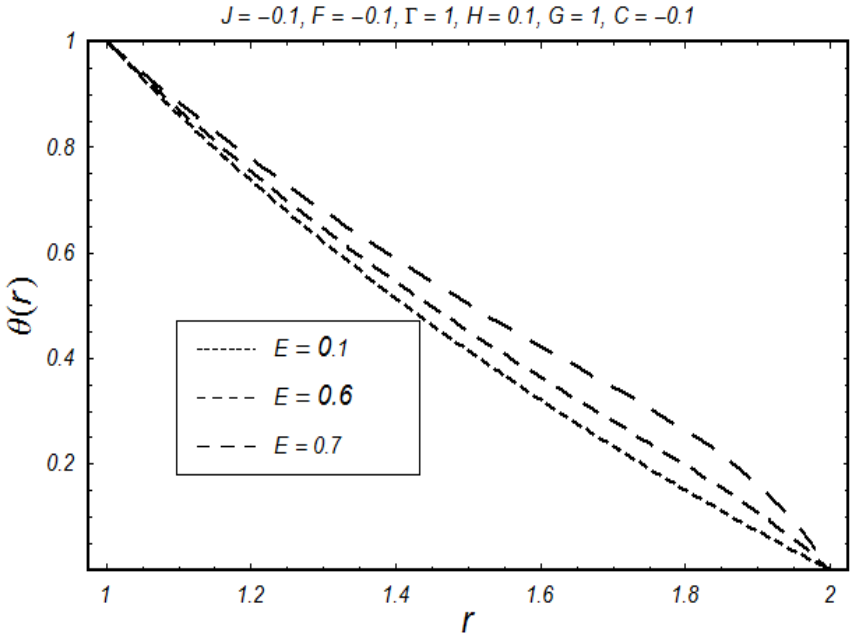

Fig. 1.5. Temperature distribution for Generalized Couette flow for E.

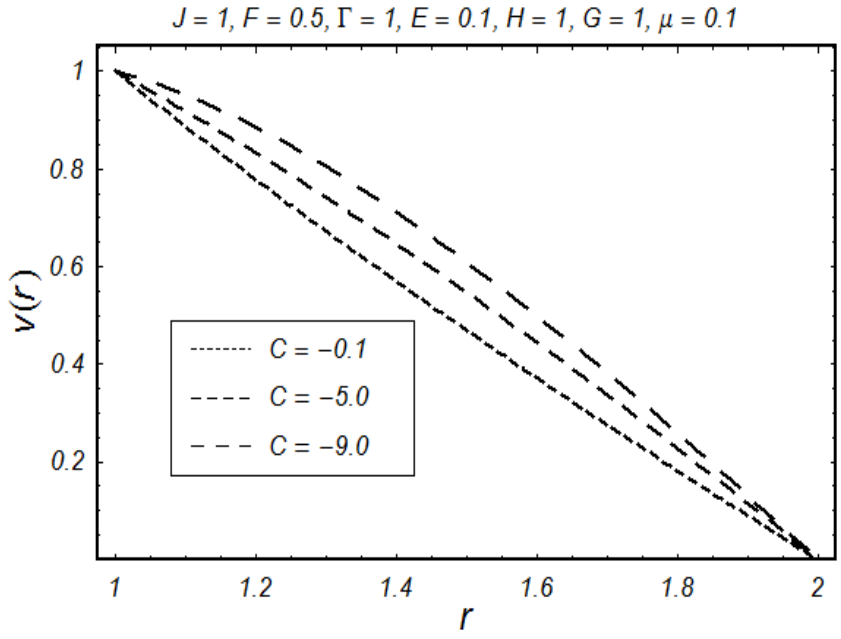

Fig. 1.6. Velocity distribution for Generalized Couette flow for C.

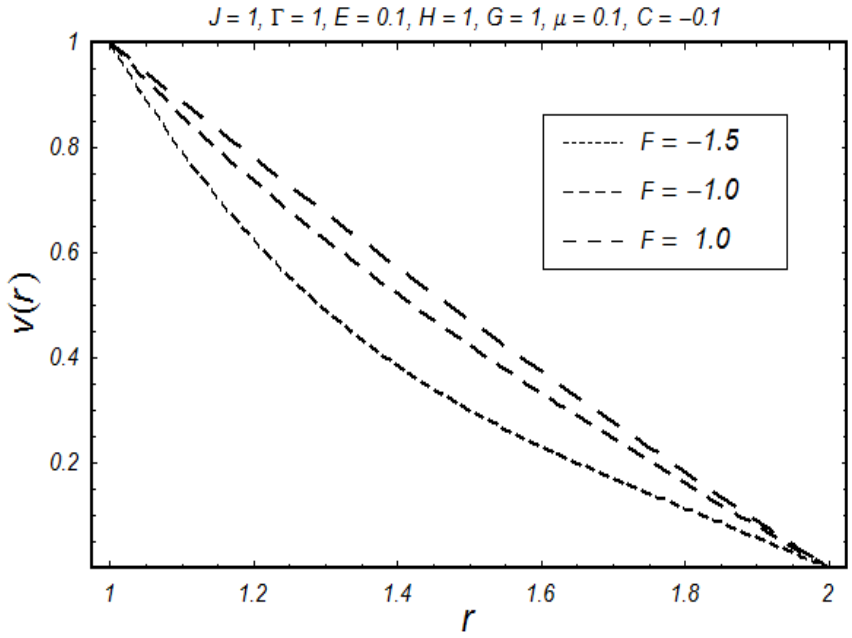

Fig. 1.7. Velocity distribution for Generalized Couette flow for F.

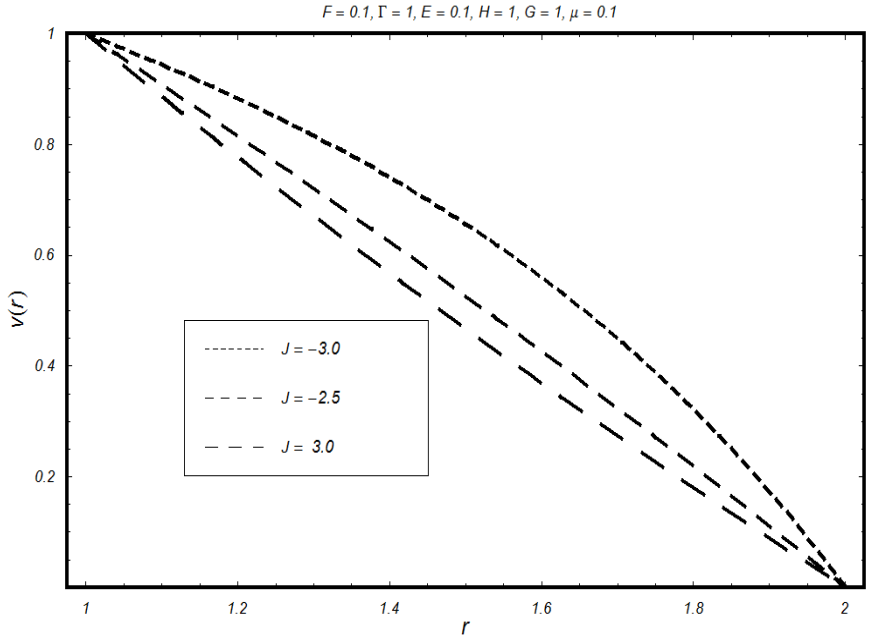

Fig. 1.8. Velocity distribution for Couette flow for J.

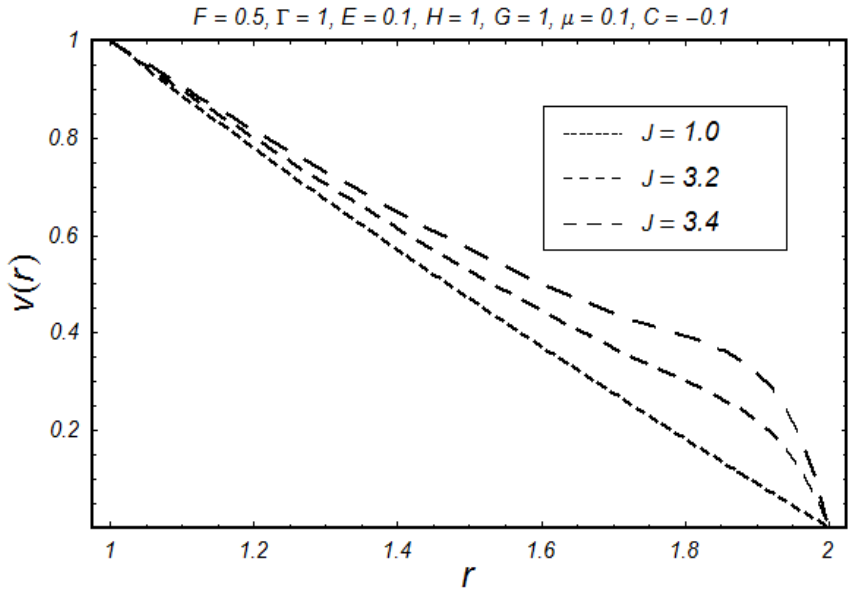

Fig. 1.9. Velocity distribution for Generalized Couette flow for J.

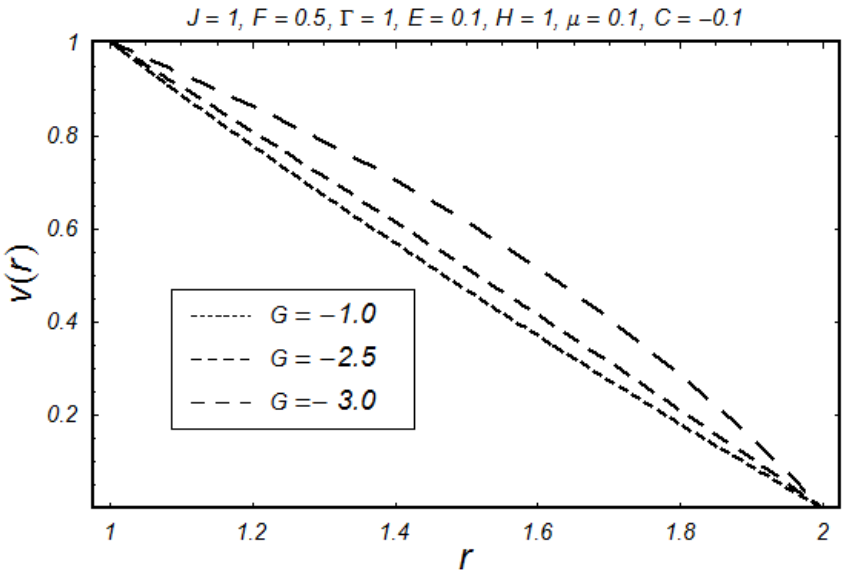

Fig. 1.10. Velocity distribution for Generalized Couette flow for different values of G.

Chapter 2

Analytical treatment of Generalized Couette flow of an Oldroyd 8-constant fluid bounded by two concentric cylinders with variable viscosity

2.1 Introduction

The present chapter investigates the study of the steady flow of an Oldroyd 8-constant fluid model with temperature dependent viscosity lying between concentric cylinders. The movement of inner cylinder is prescribed in the axial direction and pressure gradient cause the fluid flow where as the outward cylinder remains at rest. Besides this, the heat transfer effects are also taken into account. Two models of temperature dependent viscosity are studied in order to comprehend variable viscosity effects. The governing equations are simplified by a suitable similarity transformation. An analytical solution of non linear problem is obtained by using HAM. Graphical results for various parameters are presented and discussed.

2.2 Mathematical equations

The constitutive equation for Oldroyd 8-constant fluid is given by

$$\boldsymbol{\tau} = \mathbf{S} - \mathbf{pI}, \tag{2.1}$$

in which p is pressure, $\mathbf{I}$ is identity tensor and extra stress tensor $\mathbf{S}$ is stated as

$$\mathbf{S}+\lambda_1\frac{D\mathbf{S}}{Dt}+\frac{\lambda 3}{2}(\mathbf{S}\mathbf{A}_1+\mathbf{A}_1\mathbf{S})+\frac{\lambda_5}{2}(tr\mathbf{S})\mathbf{A}_1+\frac{\lambda_6}{2}[(tr\mathbf{S})\mathbf{A}_1]I=\mu\left[\mathbf{A}_1+\lambda_2\frac{D\mathbf{A}_1}{Dt}+\lambda_4\mathbf{A}_1^2+\frac{\lambda_7}{2}[(tr\mathbf{A}_1^2)\mathbf{A}_1]\mathbf{I}\right], \tag{2.2}$$

where

$$\mathbf{A}_1 = \mathbf{L}_1 + \mathbf{L}^{\Upsilon}, \mathbf{L} = \operatorname{grad}\mathbf{V}, \tag{2.3}$$

in which $\mathbf{A}_1$ is first Rivlin-Ericksen tensor and λ_i $(i = 1 - 7)$ are material parameters of fluid which are assumed to be constant. The contravarient convected derivative D / Dt for steady flow is defined as

$$\frac{D\mathbf{S}}{Dt} = (\mathbf{V}.\nabla)\mathbf{S} - \mathbf{LS} - \mathbf{SL}^{\Upsilon}. \tag{2.4}$$

We take the velocity and stress as

$$\mathbf{V}(r) = \begin{pmatrix} 0 \\ 0 \\ v \end{pmatrix}, \ \mathbf{S}(r) = \begin{bmatrix} S_{rr} & S_{r\theta} & S_{rz} \\ S_{\theta r} & S_{\theta\theta} & S_{\theta z} \\ S_{zr} & S_{z\theta} & S_{zz} \end{bmatrix}. \tag{2.5}$$

In the light of Eq.(2.5), the equation of continuity is satisfied identically and Eqs. (2.1 to 2.5) take following form

$$\frac{\partial p}{\partial r} = \frac{1}{r}\frac{d}{dr}(rS_{rr}) - \frac{S_{\theta\theta}}{r} \tag{2.6}$$

$$\frac{1}{r}\frac{\partial p}{\partial \theta} = \frac{1}{r^2}\frac{d}{dr}\left(r^2 S_{r\theta}\right), \tag{2.7}$$

$$\frac{\partial p}{\partial z} = \frac{1}{r}\frac{d}{dr}(rS_{rz}), \tag{2.8}$$

$$S_{rr} + (\lambda_3 + \lambda_6)S_{rz}\frac{dv}{dr} = \mu(\lambda_4 + \lambda_7)(\frac{dv}{dr})^2, \tag{2.9}$$

$$S_{r\theta} + \frac{\lambda 3}{2} S_{z\theta} \frac{dv}{dr} = 0, \tag{2.10}$$

$$S_{rz} + \frac{(\lambda_3 + \lambda_5)}{2}(S_{rr} + S_{zz})\frac{dv}{dr} + \frac{\lambda_5}{2} S_{\theta\theta}\frac{dv}{dr} - \lambda_1 S_{rr}\frac{dv}{dr} = \mu\frac{dv}{dr}, \tag{2.11}$$

$$S_{\theta\theta} + \lambda_6 S_{rz}\frac{dv}{dr} = \mu\lambda_7(\frac{dv}{dr})^2, \tag{2.12}$$

$$S_{\theta z} + \frac{(\lambda_3 - 2\lambda_1)}{2} S_{\theta r}\frac{dv}{dr} = 0, \tag{2.13}$$

$$S_{zz} + (\lambda_3 + \lambda_5 - 2\lambda_1) S_{rz}\frac{dv}{dr} = \mu(\lambda_4 + \lambda_7 - 2\lambda_2)(\frac{dv}{dr})^2. \tag{2.14}$$

Eqs. $(2.9) - (2.14)$ yield

$$S_{r\theta} = S_{\theta z} = 0, \tag{2.15}$$

$$S_{rr} = \frac{\mu(\lambda_4 + \lambda_7 - \lambda_3 - \lambda_6)\left(\frac{dv}{dr}\right)^2}{1 + \zeta_2\left(\frac{dv}{dr}\right)^2} + \frac{\mu\{(\lambda_4 + \lambda_7)\zeta_2 - (\lambda_3 + \lambda_6)\zeta_1\}\left(\frac{dv}{dr}\right)^4}{1 + \zeta_2\left(\frac{dv}{dr}\right)^2}, \tag{2.16}$$

$$S_{rz} = \frac{\mu\frac{dv}{dr} + \mu\zeta_1\left(\frac{dv}{dr}\right)^3}{1 + \zeta_2\left(\frac{dv}{dr}\right)^2}, \tag{2.17}$$

$$S_{\theta\theta} = \frac{\mu(\lambda_7 - \lambda_6)\left(\frac{dv}{dr}\right)^2 - \mu(\lambda_7\zeta_2 - \lambda_6\zeta_1)\left(\frac{dv}{dr}\right)^4}{1 + \zeta_2\left(\frac{dv}{dr}\right)^2}, \tag{2.18}$$

in which

$$\zeta_1 = \lambda_1(\lambda_4 + \lambda_7) - (\lambda_3 + \lambda_5)(\lambda_4 + \lambda_7 - \lambda_2) - \frac{\lambda_5\lambda_7}{2},$$

$$\zeta_2 = \lambda_1(\lambda_3 + \lambda_6) - (\lambda_3 + \lambda_5)(\lambda_3 + \lambda_6 - \lambda_1) - \frac{\lambda_5\lambda_6}{2}.$$

2.3 Physical model

Considering the same geometry (see Fig. $1\,(a)$), the steady flow of an Oldroyd 8-constant fluid with variable temperature dependent viscosity is focused. From Eqs. (2.5) to (2.7) and (2.15), imply

$$\frac{\partial p}{\partial r} = \frac{1}{r}\frac{d}{dr}(rS_{rr}) - \frac{S_{\theta\theta}}{r}, \tag{2.19}$$

$$\frac{1}{r}\frac{\partial p}{\partial \theta} = 0, \tag{2.20}$$

$$\frac{\partial p}{\partial z} = \frac{1}{r}\frac{d}{dr}(rS_{rz}). \tag{2.21}$$

The z differential of pressure is constant since the flow is due to a constant pressure gradient and the motion of the inward cylinder. From Eq. (2.21), the velocity field is determined. The pressure field is determined from Eq. (2.19). The momentum and energy equations are given by

$$\frac{1}{r}\frac{d}{dr}\left[\frac{1}{r}\left(\frac{\mu\frac{dv}{dr}+\mu\zeta_1\left(\frac{dv}{dr}\right)^3}{1+\zeta_2\left(\frac{dv}{dr}\right)^2}\right)\right]=\frac{\partial p}{\partial z}, \tag{2.22}$$

$$\frac{\mu\left(\frac{dv}{dr}\right)^2+\mu\zeta_1\left(\frac{dv}{dr}\right)^4}{1+\zeta_2\left(\frac{dv}{dr}\right)^2}+k[\frac{1}{r}\frac{dT}{dr}+\frac{d^2T}{dr^2}]=0. \tag{2.22a}$$

The corresponding boundary conditions are

$$\begin{aligned} v(R_0) &= v_0,\ T\ (R_0)\ =\ T_0, \\ v(R_1) &= 0,\ T\ (R_1)\ =\ T_1. \end{aligned} \tag{2.23}$$

Using dimensionless parameters

$$v^*=\frac{v}{v_0},\ \mu^*=\frac{\bar{\mu}}{\mu},\ r^*=\frac{r}{R_0},\ z^*=\frac{z}{R_0},\ \zeta_1^*=\frac{\zeta_1}{(R_0/v_0)^2},\ \zeta_2^*=\frac{\zeta_2}{(R_0/v_0)^2}. \tag{2.24}$$

Eqs. (2.22) to (2.24), after dropping asterisks, take the form

$$\begin{aligned} &\mu\frac{dv}{dr}+r\left(3\mu(\zeta_3+\zeta_4)\frac{d^2v}{dr^2}-2C\zeta_4\right)\left(\frac{dv}{dr}\right)^2+r\left(\zeta_4+\zeta_3\right)\left(\frac{\mu}{r}+\frac{d\mu}{dr}\right)\left(\frac{dv}{dr}\right)^3-Cr \\ &+r\left((5\mu\zeta_3\zeta_4\frac{d^2v}{dr^2}-C\zeta_4^2)+r\mu\frac{d^2v}{dr^2}+\zeta_3\zeta_4(\frac{\mu}{r}+\frac{d\mu}{dr})\frac{dv}{dr}\right)\left(\frac{dv}{dr}\right)^4+r\frac{d\mu}{dr}\frac{dv}{dr}\ =\ 0, \end{aligned} \tag{2.25}$$

$$r\mu\Gamma\left(\frac{dv}{dr}\right)^2+r\mu\Gamma\zeta_3\left(\frac{dv}{dr}\right)^4+\frac{d\theta}{dr}\left(1+\zeta_4\frac{dv}{dr}\right)+r\frac{d^2\theta}{dr^2}+\zeta_4 r\frac{dv}{dr}\frac{d^2\theta}{dr^2}=0, \tag{2.26}$$

$$v(1)=\theta(1)=1,\ v(b)=\theta(b)=0, \tag{2.27}$$

in which

$$\zeta_3=\frac{\zeta_1 v_0^2}{R_0^2},\ \zeta_4=\frac{\zeta_2 v_0^2}{R_0^2},\ C=\frac{R_0^2C_1}{u^*v_0},\ b=\frac{R_1}{R_0},\ C_1=\frac{\partial p}{\partial z},\ \Gamma=\frac{v_0\mu_*^2}{\kappa(T_1-T_o)}. \tag{2.28}$$

2.4 Series Solutions for Reynolds' model

In this case, temperature dependent viscosity is given as[18]

$$\mu = e^{-M\theta}. \tag{2.28a}$$

Using Maclaurin's series Eq. (2.28a) takes the form

$$\mu = 1 - M\theta + O(\theta^2). \tag{2.28b}$$

Invoking Eq. (2.28b) into Eqs. (2.25) to (2.27), one has

$$\begin{aligned}
&\frac{\zeta_3}{r}\left(\frac{dv}{dr}\right)^3 - \frac{M\theta\zeta_3}{r}\left(\frac{dv}{dr}\right)^3 - M\zeta_3\frac{d\theta}{dr}\left(\frac{dv}{dr}\right)^3 - M\theta\frac{d^2v}{dr^2}\\
&-2C\zeta_4\left(\frac{dv}{dr}\right)^2 - C + \frac{d^2v}{dr^2} + 5\zeta_3\zeta_4\left(\frac{dv}{dr}\right)^4\frac{d^2v}{dr^2} + \frac{1}{r}\frac{dv}{dr}\\
&+\frac{\zeta_3\zeta_4}{r}\left(\frac{dv}{dr}\right)^5 - \frac{M\theta\zeta_3\zeta_4}{r}\left(\frac{d\theta}{dr}\right)^5 - M\theta\frac{d^2v}{dr^2} - M\frac{d\theta}{dr}\frac{dv}{dr}\\
&-\frac{M\theta}{r}\frac{dv}{dr} - C\zeta_4^2\left(\frac{dv}{dr}\right)^4 - M\zeta_4\frac{d\theta}{dr}\left(\frac{dv}{dr}\right)^3 - \frac{M\theta\zeta_4}{r}\left(\frac{dv}{dr}\right)^3\\
&+\left(\frac{dv}{dr}\right)^2\left(3\left(\zeta_3+\zeta_4\right)\frac{d^2v}{dr^2} + \frac{\zeta_4}{r}\frac{dv}{dr} - 3M\theta\left(\zeta_3+\zeta_4\right)\frac{d^2v}{dr^2}\right)\\
&-M\zeta_3\zeta_4\frac{d\theta}{dr}\left(\frac{dv}{dr}\right)^5 - 5\zeta_3\zeta_4\left(\frac{dv}{dr}\right)^4\frac{d^2v}{dr^2}\left(M\theta-1\right)\\
&-3M\theta\left(\zeta_3\left(\tfrac{dv}{dr}\right)^2\tfrac{d^2v}{dr^2} + \zeta_4\left(\tfrac{dv}{dr}\right)^2\tfrac{d^2v}{dr^2}\right) \;=\; 0,
\end{aligned} \tag{2.29}$$

$$\begin{aligned}
&\Gamma\left(\frac{dv}{dr}\right)^2 - \Gamma M\left(\frac{dv}{dr}\right)^2 + \Gamma\zeta_3\left(\frac{dv}{dr}\right)^4 - M\Gamma\zeta_3\left(\frac{dv}{dr}\right)^4\\
&+\frac{d\theta}{dr}\left(\frac{1}{r} + \frac{\zeta_4}{r}\frac{dv}{dr}\right) + \frac{d^2\theta}{dr^2}\left(1 + \zeta_4\frac{dv}{dr}\right) = 0.
\end{aligned} \tag{2.30}$$

For HAM solution, we choose the following initial guesses

$$v_0\left(r\right) = \frac{\left(b-r\right)}{\left(b-1\right)}, \tag{2.31}$$

$$\theta_0\left(r\right) = \frac{(b-r)}{(b-1)}. \tag{2.32}$$

The auxiliary linear operators are in the form

$$\pounds_{vel}\left(v\right) = v'', \tag{2.33}$$

$$\pounds_{temp}\left(\theta\right) = \theta'', \tag{2.34}$$

which satisfy

$$\mathcal{L}_{vel}(A_{31} + B_{33}r) = 0, \tag{2.35}$$

$$\mathcal{L}_{temp}(A_{32} + B_{34}r) = 0, \tag{2.36}$$

where $A_{31}, A_{32}, B_{33}, B_{34}$ are the constants.

The zeroth and mth order deformation equations for the present flow problem are stated as

$$(1-q)\mathcal{L}_{vel}[\ \bar{v}(r,q) - \ v_0\ (r)] = q\hbar N_{vel}[\ \bar{v}\ (r,q), \bar{\theta}(r,q)], \tag{2.37}$$

$$(1-q)\mathcal{L}_{temp}[\ \bar{\theta}(r,q) - \ \theta_0\ (r)] = q\hbar N_{temp}[\ \bar{v}\ (r,q), \bar{\theta}(r,q)], \tag{2.38}$$

$$\mathcal{L}_{vel}[v_m(r) - \chi_m v_{m-1}(r)] = \hbar R_{vel}(r), \tag{2.39}$$

$$\mathcal{L}_{temp}[\theta_m(r) - \chi_m \theta_{m-1}(r)] = \hbar R_{temp}(r), \tag{2.40}$$

$$\bar{v}(1,q) = \bar{\theta}(1,q) = 1, \tag{2.41}$$

$$\bar{v}(b,q) = \bar{\theta}(b,q) = 0, \tag{2.42}$$

$$\bar{v}_m(1,q) = \bar{\theta}_m(1,q) = 0, \tag{2.43}$$

$$\bar{v}_m(b,q) = \bar{\theta}_m(b,q) = 0, \tag{2.44}$$

where

$$
\begin{aligned}
N_v[\bar{v}(r,q),\bar{\theta}(r,q)] &= \left(\tfrac{\zeta_3}{r}\left(\tfrac{dv}{dr}\right)^3 - M\zeta_4\tfrac{d\theta}{dr}\tfrac{dv}{dr} - C\zeta_4^2\left(\tfrac{dv}{dr}\right)^2 + 3\left(\zeta_3+\zeta_4\right)\tfrac{d^2v}{dr^2}\right)\left(\tfrac{dv}{dr}\right)^2 \\
&- \left(\frac{dv}{dr}\right)^2\left(\frac{M\theta\zeta_3}{r}\frac{dv}{dr} - \frac{\zeta_4}{r}\frac{dv}{dr} + 2C\zeta_4 + M\theta\frac{d^2v}{dr^2} - \frac{\zeta_3\zeta_4}{r}\left(\frac{dv}{dr}\right)^3 + \frac{M\theta\zeta_3\zeta_4}{r}\left(\frac{d\theta}{dr}\right)^3\right) \\
&+ \left(5\zeta_3\zeta_4\left(\frac{dv}{dr}\right)^2\frac{d^2v}{dr^2} - M\zeta_3\frac{d\theta}{dr}\frac{dv}{dr} - 3M\theta\left(\zeta_3+\zeta_4\right)\frac{d^2v}{dr^2}\right)\left(\frac{dv}{dr}\right)^2 - M\zeta_3\zeta_4\frac{d\theta}{dr}\left(\frac{dv}{dr}\right)^5 \\
&-5M\theta\zeta_3\zeta_4\left(\frac{dv}{dr}\right)^4\frac{d^2v}{dr^2} - \frac{M\theta\zeta_4}{r}\left(\frac{dv}{dr}\right)^3 - C + \frac{1}{r}\frac{dv}{dr} + \frac{d^2v}{dr^2} - M\frac{d\theta}{dr}\frac{dv}{dr} - \frac{M\theta}{r}\frac{dv}{dr}, \quad (2.45)
\end{aligned}
$$

$$
\begin{aligned}
N_{temp}[\,\bar{v}\,(r,q),\bar{\theta}(r,q)] &= \Gamma\left(\tfrac{dv}{dr}\right)^2 - \Gamma M\left(\tfrac{dv}{dr}\right)^2 + \Gamma\zeta_3\left(\tfrac{dv}{dr}\right)^4 \\
&-M\Gamma\zeta_3\left(\frac{dv}{dr}\right)^4 + \frac{1}{r}\frac{d\theta}{dr} + \frac{\zeta_4}{r}\frac{d\theta}{dr}\frac{dv}{dr} + \frac{d^2\theta}{dr^2} + \zeta_4\frac{dv}{dr}\frac{d^2\theta}{dr^2}, \quad (2.46)
\end{aligned}
$$

By Mathematica the solutions of Eqs. (2.45) and (2.46) can be written as

$$
v_m(r) = \sum_{n=0}^{3m}\epsilon_{m,n}r^n,\ m\geq 0,\ \theta_m(r) = \sum_{n=0}^{3m+1}T_{m,n}r^n,\ m\geq 0. \quad (2.47)
$$

2.5 Series solutions for Vogel's model

The non-dimensional form of viscosity is given by[18]

$$
\mu = \zeta\exp\left[\frac{A}{(B+\theta)} - T_1\right], \quad (2.48)
$$

which by Maclaurin's series reduces to

$$
\mu = \frac{C}{C^*}(1-\frac{A\theta}{B^2}), \quad (2.49)
$$

$$
\text{where } C^* = \frac{C}{\exp\left[\frac{A}{B}-T_1\right]},\ \zeta = \exp(_{T_1}) \quad (2.50)
$$

With the help of Eq. (2.48), Eqs. (2.25) and (2.27) become

$$
\begin{aligned}
&-\frac{3A\zeta_3 C\theta}{B^2C^*}\left(\frac{dv}{dr}\right)^2\frac{d^2v}{dr^2}-\frac{AC\theta}{rB^2C^*}\frac{dv}{dr}+\frac{C}{C^*}\frac{d^2v}{dr^2}-\frac{AC\zeta_3\theta}{rB^2C^*}\left(\frac{dv}{dr}\right)^3-\frac{AC\theta}{B^2C^*}\frac{d^2v}{dr^2}\\
&+\frac{C\zeta_3\zeta_4}{rC^*}\left(\frac{dv}{dr}\right)^5-\frac{AC\zeta_3\zeta_4\theta}{rB^2C^*}\left(\frac{dv}{dr}\right)^5-\frac{AC\zeta_3}{B^2C^*}\frac{d\theta}{dr}\left(\frac{dv}{dr}\right)^3-\frac{AC}{B^2C^*}\frac{d\theta}{dr}\frac{dv}{dr}-C\\
&+\frac{3\zeta_3 C}{C^*}\left(\frac{dv}{dr}\right)^2\frac{d^2v}{dr^2}+\frac{3\zeta_4 C}{C^*}\left(\frac{dv}{dr}\right)^2\frac{d^2v}{dr^2}-\frac{5AC\zeta_3\zeta_4\theta}{rB^2C^*}\left(\frac{dv}{dr}\right)^4\frac{d^2v}{dr^2}+\frac{C}{rC^*}\frac{dv}{dr}\\
&-\frac{AC\zeta_4\theta}{rB^2C^*}\left(\frac{dv}{dr}\right)^3+\frac{3A\zeta_4 C\theta}{B^2C^*}\left(\frac{dv}{dr}\right)^2\frac{d^2v}{dr^2}-2C\zeta_4\left(\frac{dv}{dr}\right)^2-\frac{AC\zeta_3\zeta_4}{B^2C^*}\frac{d\theta}{dr}\left(\frac{dv}{dr}\right)^5\\
&+\left(\frac{C\zeta_4}{rC^*}+5\zeta_3\zeta_4\frac{C}{C^*}\frac{dv}{dr}\frac{d^2v}{dr^2}-\frac{AC\zeta_4}{B^2C^*}\frac{d\theta}{dr}-C\zeta_4^2\frac{dv}{dr}+\frac{C\zeta_3}{C^*}\right)\left(\frac{dv}{dr}\right)^3 \;=\; 0, \qquad (2.51)
\end{aligned}
$$

$$
\begin{aligned}
&\frac{C\Gamma}{C^*}\left(\frac{dv}{dr}\right)^2-\frac{AC\Gamma}{B^2C^*}\left(\frac{dv}{dr}\right)^2+\frac{C\Gamma\zeta_3}{C^*}\left(\frac{dv}{dr}\right)^4+\frac{1}{r}\frac{d\theta}{dr}\\
&-\left(\frac{AC\Gamma\zeta_3}{B^2C^*}\left(\frac{dv}{dr}\right)^3-\frac{\zeta_4}{r}\frac{d\theta}{dr}\right)\frac{dv}{dr}+\frac{d^2\theta}{dr^2}\left(1+\zeta_4\frac{dv}{dr}\right) \;=\; 0. \qquad (2.52)
\end{aligned}
$$

By adopting the similar procedure as discussed earlier the solution of this case is straightforward written as.

$$
\begin{aligned}
v &= \sum v_m(r)=\sum_{n=0}^{3m}\epsilon'_{m,n}r^n,\ m\geq 0,\\
\theta &= \sum \theta_m(r)=\sum_{n=0}^{3m+1}\sigma'_{m,n}r^n,\ m\geq 0, \qquad (2.53)
\end{aligned}
$$

where $\epsilon'_{m,n}$ and $\sigma'_{m,n}$are constants.

2.6 Graphical results and discussion

We plotted Figs. 2.1 to 2.11 to check the convergence and influence of various parameters The convergence regions of these series are strongly dependent upon the non-zero auxiliary parameters $\hbar$ which can be adjusted and controlled by means of a proper value of $\hbar$. To see the range of admissible value of $\hbar$, $\hbar-$curves are plotted. Fig. 2.1 corresponds to Reynolds' model where as Fig. 2.2 relates to Vogel's model. Fig. 2.3 depicts the velocity variation for Reynolds' model for M. It is noted that velocity increases as M increases. The relation (2.28b)

explains that by increasing M, viscosity of fluid decreases i.e. opposing forces are reduced. As a consequence, the fluid moves with greater velocity. That is what we are observing in Fig. 2.3.

Fig. 2.4 shows the temperature variation for ζ_4 for Reynolds' model. It can be seen that temperature increases as ζ_4 increases. Since ζ_4 depends upon speed of cylinder. When ζ_4 is increased, it means that cylinder is moving fast. Since the movement of the cylinder is along the motion of the fluid. So velocity of fluid particles increases. As a result the kinetic energy of the fluid rises. Hence as a consequence, temperature of the fluid increases. This is the case, we are observing in Fig. 2.4.

Fig. 2.5 is plotted in order to see the velocity variation for Reynolds' model for ζ_4, it is observed that velocity decreases as ζ_4 increases. Figs. 2.6 to 2.11 correspond to Vogel's model. Fig. 2.6 studies the velocity variation for Vogel's model for C. It is seen that velocity decreases as C increases. Fig. 2.7 reveals the temperature variation for Vogel's model for C. It is studied that temperature increases as C increases. Since the pressure gradient is taken negative here, it means it opposes the motion of the fluid particles. The motion of the fluid experiences opposition. As a result the kinetic energy of the system decrease with rise of C. Fig. 2.8 is prepared to observe the velocity variation for Vogel's model for B. It is obvious from relation (2.49) that viscosity increases with rise of B i.e. the viscous forces become stronger. The fluid particles experience more opposing forces. The velocity of fluid reduces.

Fig. 2.9 is plotted to see the temperature variation for Vogel's model for B. The relation for velocity given by Vogel's model shows that viscosity increases as B increases. The viscous forces slow down the motion of the fluid particles i.e. the average speed of fluid particles reduces. This factor is responsible for reduction of the velocity of fluid. As kinetic energy of a system is directly proportional to the square of velocity. The average kinetic energy of the system decreases. Since temperature of the system is dependent upon kinetic energy. Consequently, temperature of the system reduces. Fig. 2.10 presents the velocity variation for Vogel's model for A. Fig. 2.11 gives the temperature variation for Vogel's model for A.

2.7 Conclusions

This chapter investigates analytically the flow of an Oldroyd 8-constant fluid with variable temperature dependent viscosity between coaxial cylinders. The highly non-linear problem is solved analytically by powerful technique homotopy analysis method. Effects of the various emerging parameters on velocity and temperature distribution are examined. The following conclusions are drawn.

1. Temperature distribution increases with the increase of ζ_4 for Reynolds' model.

2. Velocity increases with the increase of viscosity parameter M for Reynolds' model for an Oldroyd 8-constant fluid.

3. Velocity field decreases with rise of viscosity parameter C and B for Vogel's model and increases with the increase of A.

4. Increase of viscosity parameter A and C leads to the increase of temperature profile for Vogel's model and the profile decreases with rise of viscosity parameter B.

5. Velocity decreases with the increase of ζ_4 for Reynolds' model.

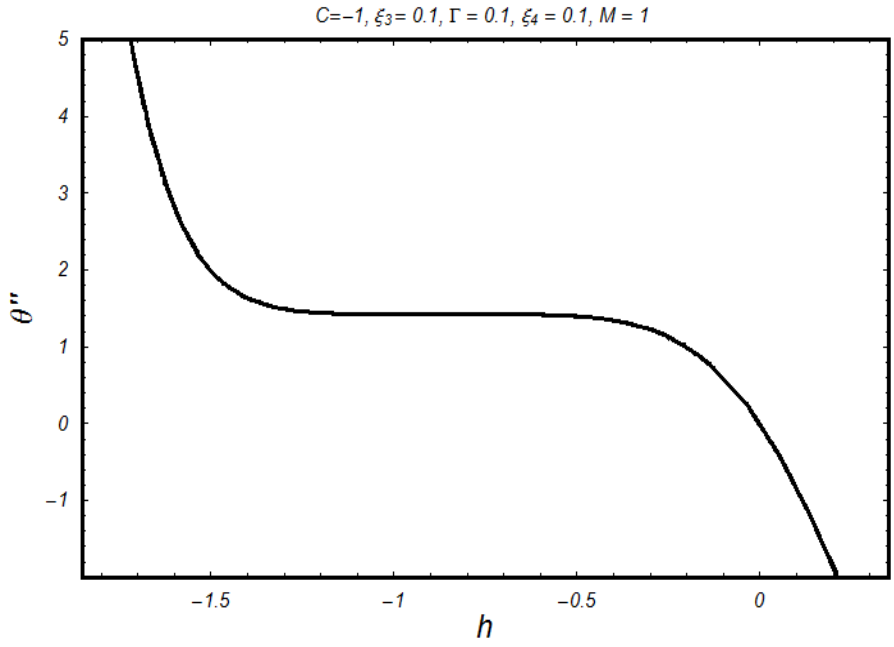

Fig. 2.1. h-curve for Reynolds' model for temperature distribution.

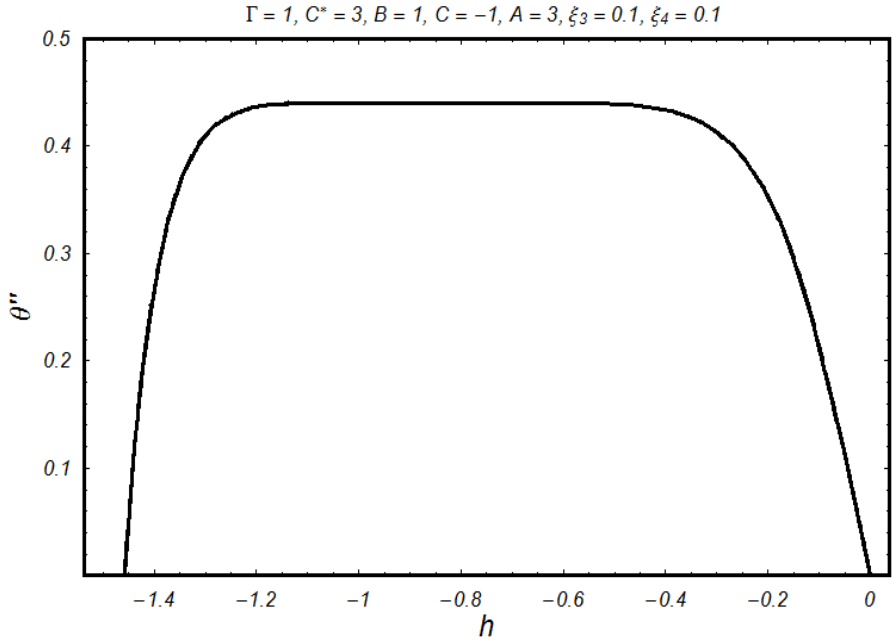

Fig. 2.2. h-curve for Vogel's model for temperature distribution.

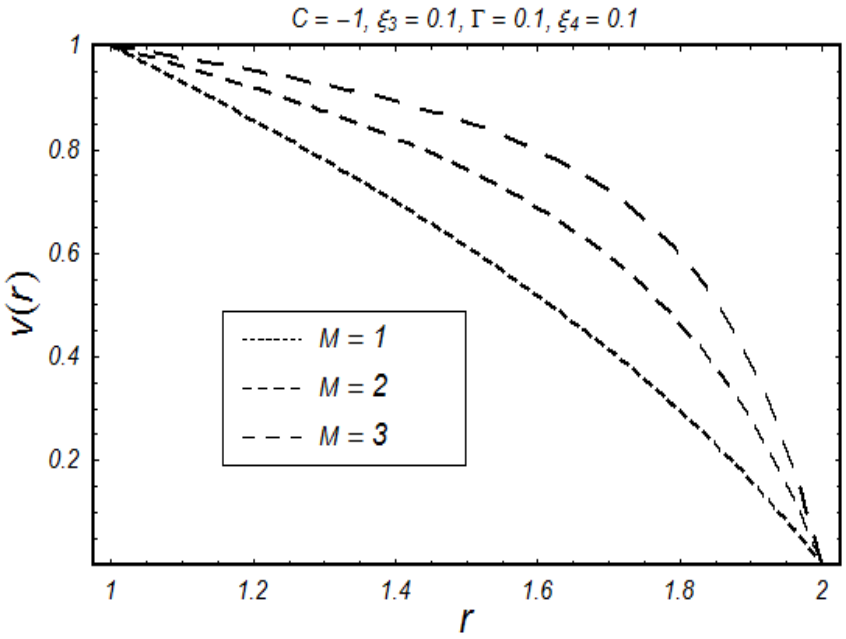

Fig. 2.3. Velocity distribution for M for Reynolds' model

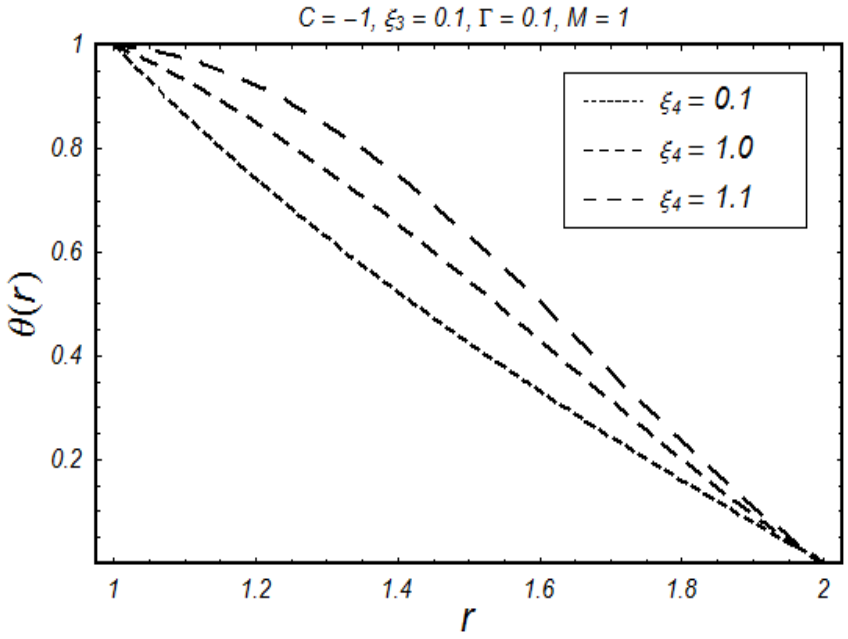

Fig. 2.4. Temperature field for ζ_4 for Reynolds' model.

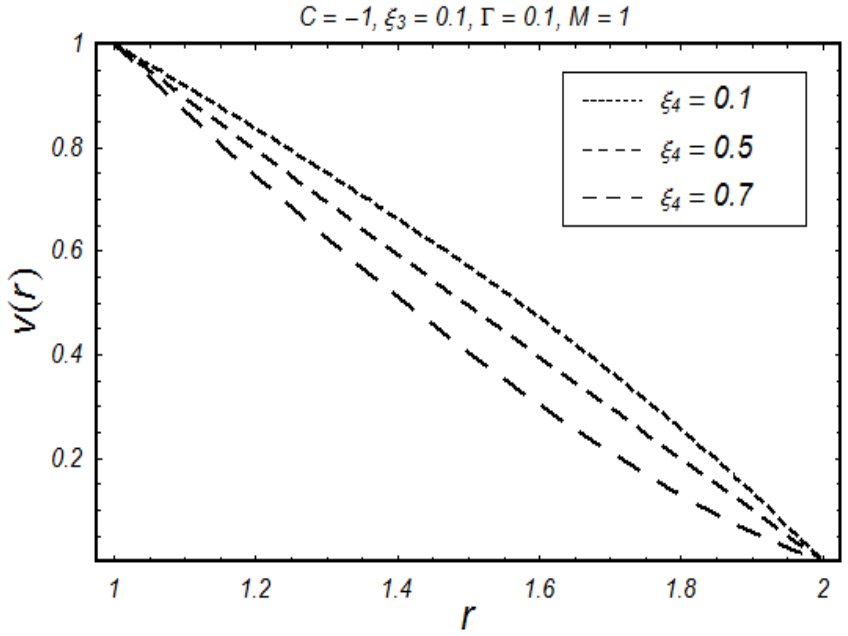

Fig. 2.5. Velocity field for ζ_4 for Reynolds' model

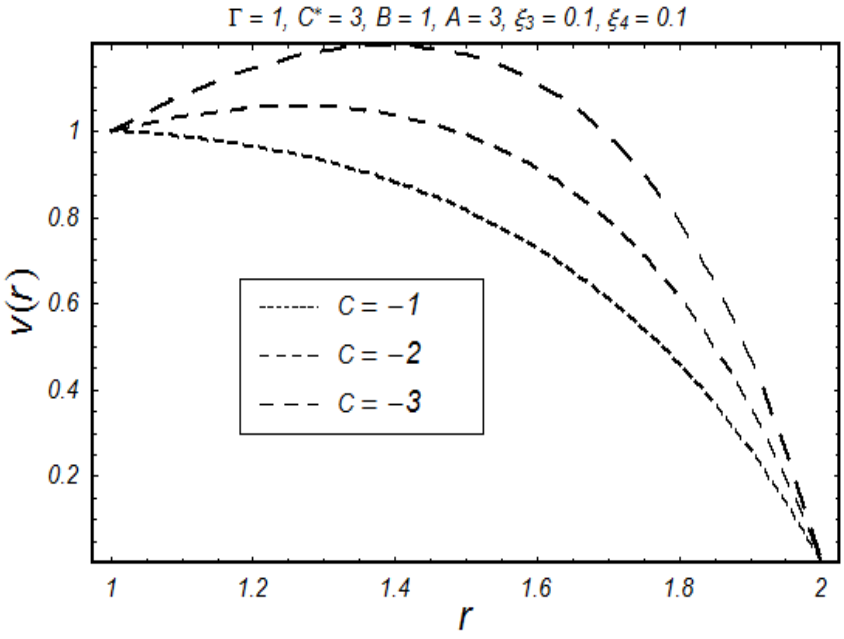

Fig. 2.6. Velocity field for C for Vogel's model.

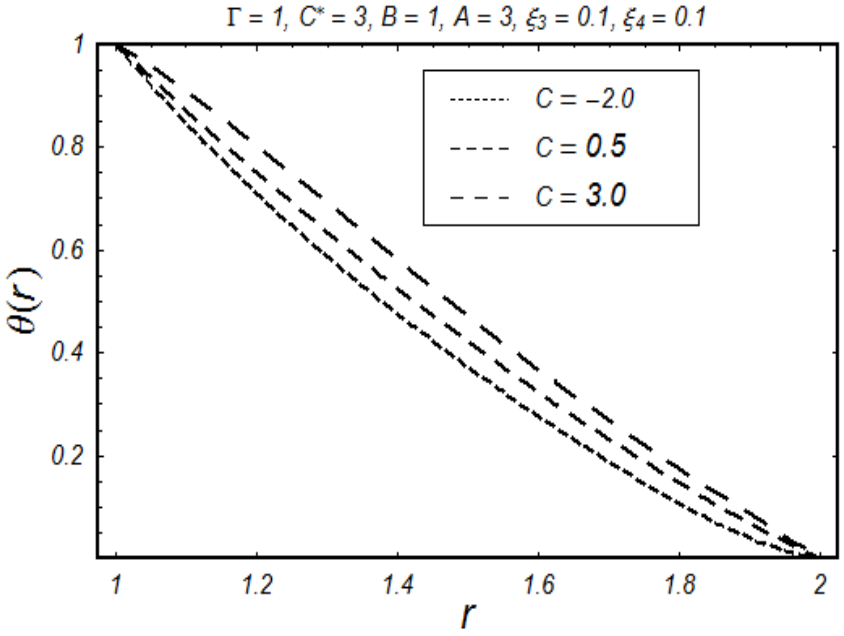

Fig. 2.7. Temperature field for C for Vogel's model.

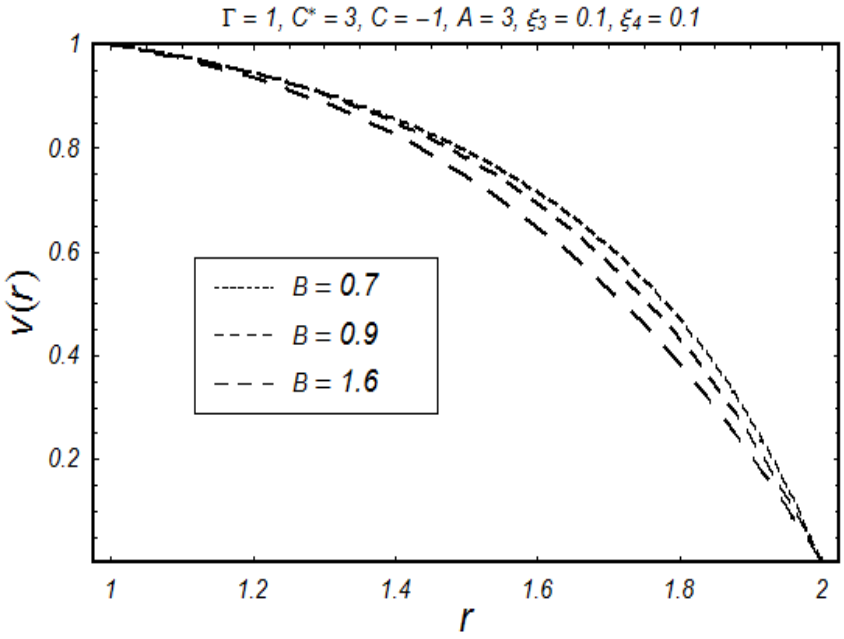

Fig. 2.8. Velocity field for B for Vogel's model.

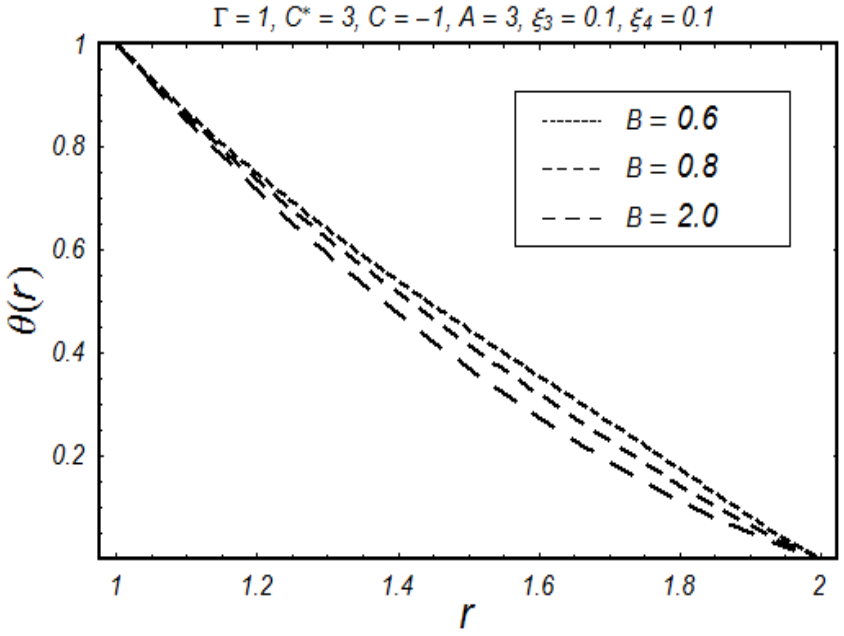

Fig. 2.9. Temperature field for B for Vogel's model.

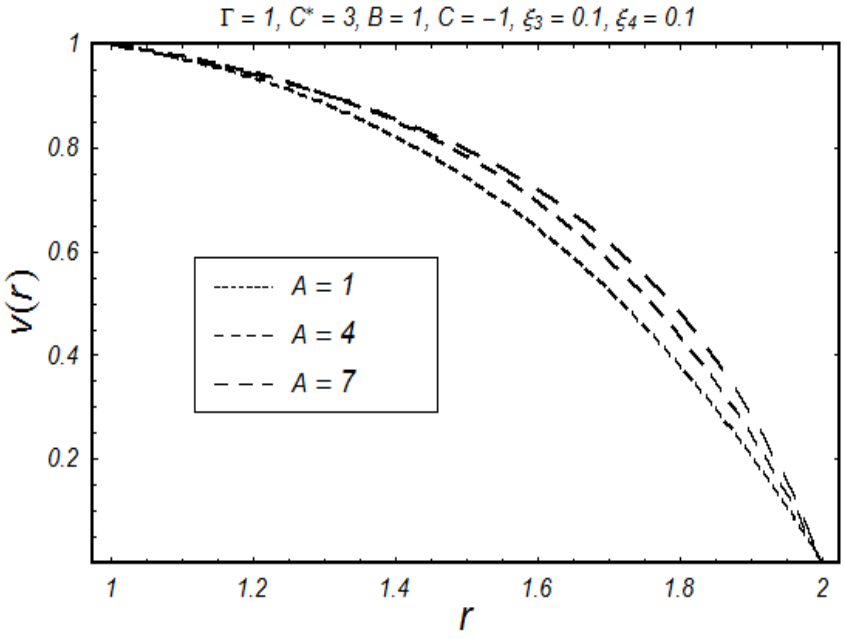

Fig. 2.10. Velocity profile for A for Vogel's model.

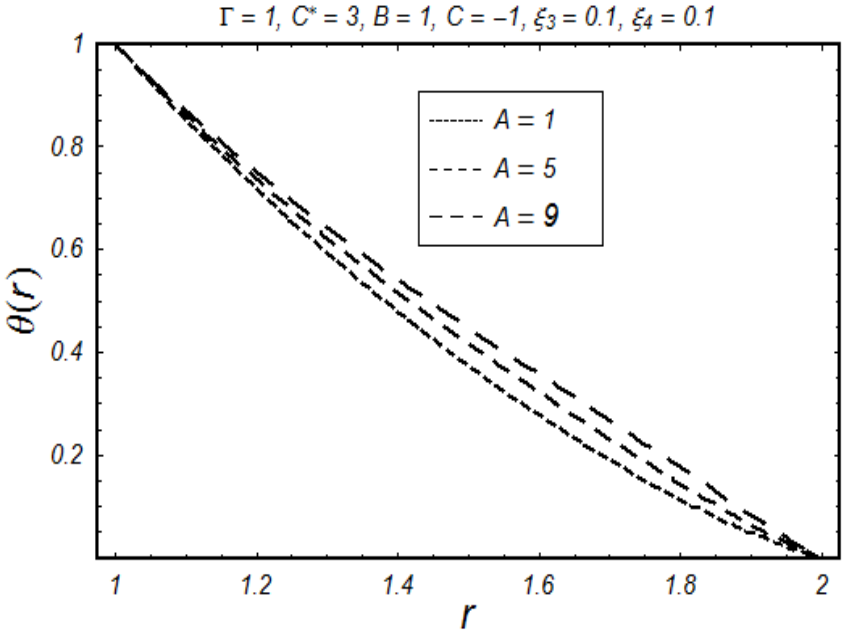

Fig. 2.11. Temperature distribution for A for Vogel's model.

Chapter 3

Analytical and numerical treatments of Generalized Couette flow through cylinders with variable viscous properties

3.1 Introduction

In this chapter, we have presented the flow with temperature dependent viscosity. The medium is assumed to be porous. Two types of geometrical problems with Reynolds' and Vogel's viscosity models are taken into account. In first case the motion of the fluid is because of a constant pressure gradient and a movement of inward cylinder while the outward cylinder is in the state of rest. In second problem we considered that the inward cylinder is fixed while the disturbance in the fluid comes because of the constant pressure gradient and the movement of outward cylinder. The governing equations are first simplified and then solved numerically and analytically. The numerical treatments are found by adopting shooting technique and analytical solutions are calculated by adopting homotopy analysis method. The comparison of both solutions are also presented. It is concluded that by taking $\mu = 1$ and $\mu = r$, the results for the constant as well as space viscosity may be achieved. By assuming $\Phi = 0$ or $\kappa \to \infty$

results for non porous medium may be attained. Results obtained by shooting method and homotopy analysis method are in good agreement.

3.2 Modeling of the problem

We consider an incompressible flow of a third grade fluid between two coaxial cylinders. The fluid saturates the porous medium. The viscosity of the fluid is considered to be temperature dependent. The equations which govern the flow of the fluid in the presence of Darcy resistance along with heat transfer take the form

$$\rho\frac{d\mathbf{V}}{dt} = \operatorname{div}\boldsymbol{\tau} + \mathbf{R}, \tag{3.1}$$

$$\rho C_p\frac{dT}{dt} = \boldsymbol{\tau}.\mathbf{L} + k\boldsymbol{\nabla}^2 T, \tag{3.2}$$

where ρ is the specific heat. The Cauchy stress tensor $\boldsymbol{\tau}$ for third grade fluid is defined as

$$\boldsymbol{\tau} = -p_1\mathbf{I}+\mu\mathbf{A_1}+\alpha_{41}\mathbf{A_2}+\alpha_{42}\mathbf{A_1^2}+\beta_1\mathbf{A_3}\beta_2(\mathbf{A_1A_2}+\mathbf{A_2A_1})+\beta_3(\mathbf{trA_1^2})\mathbf{A_1}, \tag{3.3}$$

where μ is dynamic viscosity, α_{41}, α_{42}, β_1, β_2 and β_3 are constants. It is to be noted that the coefficients μ, α_{41}, α_{42}, β_1, β_2 and β_3 satisfy the following conditions

$$\mu\geq 0,\ \alpha_{41}\geq 0,\ \ |\alpha_{41}+\alpha_{42}|\leq\sqrt{24\mu\beta_3},\ \beta_1=\beta_2=0,\ \beta_3\geq 0. \tag{3.4}$$

The Rivilin -Ericksen tensors $\mathbf{A}_1$, $\mathbf{A}_2$ and $\mathbf{A}_3$ are obtained through following expressions

$$\mathbf{A}_1 = (\boldsymbol{\nabla}\mathbf{V})^{\Upsilon} + \boldsymbol{\nabla}\mathbf{V}, \tag{3.5}$$

$$\mathbf{A}_n = \frac{d\mathbf{A}_n}{dt} + \mathbf{A}_{n-1}\mathbf{L} + \mathbf{L}^{\Upsilon}\mathbf{A}_{n-1},\ n>1, \tag{3.6}$$

$$\mathbf{L} = \boldsymbol{\nabla}\mathbf{V} = \operatorname{grad}\mathbf{V}. \tag{3.7}$$

The Darcy resistance for third grade fluid model is stated as [10]

$$\mathbf{R}_z = -\frac{\phi_1}{\kappa_2}\left(\mu + \Lambda\left(\frac{dv}{dr}\right)^2\right)\mathbf{V}. \tag{3.8}$$

Making use of velocity field defined in chapter one, the required equations of motion and energy are defined as

$$\frac{1}{r}\frac{d}{dr}\left(r\mu\frac{dv}{dr}\right) + \frac{2\beta_3}{r}\frac{d}{dr}\left(r(\frac{dv}{dr})^3\right) - \frac{\phi_1}{\kappa_2}\left(\mu + \Lambda\left(\frac{dv}{dr}\right)^2\right)v = \frac{\partial\hat{p}}{\partial z}, \tag{3.9}$$

$$\mu\left(\frac{dv}{dr}\right)^2 + 2\beta_3\left(\frac{dv}{dr}\right)^4 + \kappa\left[\frac{1}{r}\frac{d}{dr}\left(r\frac{dT}{dr}\right)\right] = 0, \tag{3.10}$$

where

$$\hat{p} = p_1 - \alpha_{42}\left(\frac{dv}{dr}\right)^2. \tag{3.11}$$

We have considered two types of flow problems between coaxial cylinders.

3.2.1 Case 1: Motion of an inner cylinder

In this case, the motion of the fluid is because of a constant pressure gradient and movement of inward cylinder while the outward cylinder is at rest, the boundary conditions are

$$\begin{aligned} v\,(R_0) &= v_0,\, T\ (R_0) = T, \\ v\,(R_1) &= 0,\ T\ (R_1) = T_1. \end{aligned} \tag{3.12}$$

3.2.2 Case 2: Movement of outer cylinder

Here, we consider that the inner cylinder is fixed while the disturbance in the fluid comes because of the constant pressure gradient and the movement of outward cylinder. The boundary conditions for this case are defined as

$$\begin{aligned} v\,(R_0) &= 0,\, T\ (R_0) = T_0, \\ v\,(R_1) &= v_0,\ T\ (R_1) = T_1, \end{aligned} \tag{3.13}$$

The dimensionless forms of equations describing motion and energy are

$$r\frac{d\mu}{dr}\frac{dv}{dr}+\mu(\frac{dv}{dr}+r\frac{d^2v}{dr^2})+\Lambda(\frac{dv}{dr})^2(\frac{dv}{dr}+3r\frac{d^2v}{dr^2})-rP[\mu+\Lambda(\frac{dv}{dr})^2]v=rC, \tag{3.14}$$

$$r\frac{d^2\theta}{dr^2}+\frac{d\theta}{dr}+r\Gamma(\frac{dv}{dr})^2(\mu+\Lambda(\frac{dv}{dr})^2)=0. \tag{3.15}$$

(case 1)

$$v(1)=\theta(1)=1,\ v(b)=\theta(b)=0, \tag{3.16}$$

(case 2)

$$v(1)=\ \theta(b)=0,\ v(b)=\theta(1)=1. \tag{3.17}$$

The nondimensional quantities used in the above equations are defined as

$$\begin{aligned}\bar{r} &= \frac{r}{R_0},\ \Gamma=\frac{v_0\mu_0^2}{(T_0-T_1)\kappa},\ \theta=\frac{(T_1-T)}{(T_1-T_0)},\ b=\frac{R_1}{R_0},\ \Lambda=\frac{2v_0^2\beta_3}{R_0^2\mu_0},\\ C_1 &= \frac{\partial p_1}{\partial z},\ P=\frac{\phi_1}{R_0^2\kappa_2},\ C=\frac{C_1R_0^2}{\mu_0v_0},\ v=\frac{\bar{v}}{v_0},\ \mu=\frac{\bar{\mu}}{\mu_0}.\end{aligned} \tag{3.18}$$

Here μ_0, T_1, v_0, β_3 and Λ are reference viscosity, a reference temperature (the bulk mean fluid temperature), reference velocity, dimensional third grade parameter and the dimensionless non-Newtonian parameter. P is porous medium parameter, ϕ_1 is porosity and k_2 is the permeability [52].

3.3 Solution of the problem

Reynolds and Vogel's models of viscosity are considered for the current analysis, both the models are defined in previous chapter, therefore to avoid repetition the governing equations for third grade fluid for both the viscosity models are directly written as

(For Reynolds model)

$$\begin{aligned}&\frac{1}{C}\frac{dv}{dr}+\frac{r}{C}\frac{d^2v}{dr^2}-\frac{M\theta}{C}\frac{dv}{dr}-\frac{Mr}{C}\frac{d\theta}{dr}\frac{dv}{dr}-\frac{Mr\theta}{C}\frac{d^2v}{dr^2}+\frac{\Lambda}{C}(\frac{dv}{dr})^3\\ &+\frac{3r\Lambda}{C}\frac{d^2v}{dr^2}(\frac{dv}{dr})^2+\frac{MrPv\theta}{C}-\frac{rPv}{C}-\frac{rP\Lambda}{C}(\frac{dv}{dr})^2v=r,\end{aligned} \tag{3.19}$$

$$\frac{r}{\Gamma}\frac{d^2\theta}{dr^2}+\frac{1}{\Gamma}\frac{d\theta}{dr}+r\left(1-M\theta+\Lambda(\frac{dv}{dr})^2\right)(\frac{dv}{dr})^2=0. \tag{3.20}$$

(For Vogel's model)

$$\begin{aligned}&B^2\frac{dv}{dr}+B^2r\frac{d^2v}{dr^2}-A\theta\frac{dv}{dr}+\frac{3rB^2C^*\Lambda}{C}\frac{d^2v}{dr^2}(\frac{dv}{dr})^2\\&-Ar\frac{d\theta}{dr}\frac{dv}{dr}-Ar\theta\frac{d^2v}{dr^2}+\frac{\Lambda rB^2C^*}{Cr}(\frac{dv}{dr})^3-rB^2Pv\\&+ArPv\theta-\frac{rB^2PC^*\Lambda}{C}(\frac{dv}{dr})^2v-rB^2C^*=0,\end{aligned} \tag{3.21}$$

$$rB^2C^*\frac{d^2\theta}{dr^2}+B^2C^*\frac{d\theta}{dr}+rB^2C\Gamma(\frac{dv}{dr})^2-ArC\Gamma\theta(\frac{dv}{dr})^2+rB^2C^*\Lambda\Gamma(\frac{dv}{dr})^4=0. \tag{3.22}$$

The solution of above coupled equations have been found analytically by homotopy analysis method. For HAM solution we require the following initial guesses for both the problems

(for case1)

$$v_0(r)=\theta_0(r)=\frac{(r-b)}{(1-b)}, \tag{3.23}$$

(for case 2)

$$v_0(r)=\theta_0(r)=\frac{(r-1)}{(b-1)}. \tag{3.24}$$

The auxiliary linear operators are

$$\pounds_{vel}(v)=v'',\ \pounds_{temp}(\theta)=\theta'', \tag{3.25}$$

which satisfy

$$\mathcal{L}_{vel}(A_{41}+B_{41}r)=0,\ \mathcal{L}_{temp}(A_{42}+B_{42}r)=0, \tag{3.26}$$

and A_{41}, A_{42}, B_{41}, B_{42} are the constants.

Adopting the technique as discussed earlier, the HAM solution is directly defined as

(For Reynolds' model)

$$v_m(r)=\sum_{n=0}^{4m+1}\varsigma_{m,n}r^n,\ m\geq 0,\ \theta_m(r)=\sum_{n=0}^{4m}\varkappa_{m,n}r^n,\ m\geq 0, \tag{3.27}$$

(For Vogel's model)

$$v_m(r) = \sum_{n=0}^{4m+1} \varsigma'_{m,n} r^n,\ m \geq 0,\ \theta_m(r) = \sum_{n=0}^{4m} \varkappa'_{m,n} r^n,\ m \geq 0, \tag{3.28}$$

where $\varsigma_{m,n}$, $\varkappa_{m,n}$, $\varsigma'_{m,n}$ and $\varkappa'_{m,n}$ are constants and the numerical data of these expression are shown through graphs in the discussion section.

3.4 Numerical solution

In the absence of dissipation, Eq. (3.19) reduces to

$$\begin{aligned}&\frac{1}{M}\frac{dv}{dr} - \frac{r}{b-1}\frac{dv}{dr} - \left(\frac{r-1}{b-1}\right)\frac{dv}{dr} - r\left(\frac{r-1}{b-1}\right)\frac{d^2v}{dr^2} + rPv\left(\frac{r-1}{b-1}\right)\\ &+\frac{r}{M}\frac{d^2v}{dr^2} + \frac{\Lambda}{M}(\frac{dv}{dr})^3 - \frac{rP\Lambda}{M}(\frac{dv}{dr})^2 v - \frac{rPv}{M} + \frac{3r\Lambda}{M}\frac{d^2v}{dr^2}(\frac{dv}{dr})^2 = \frac{rC}{M}.\end{aligned} \tag{3.29}$$

Second order differential Eq. (3.29) subject to the boundary conditions (3.16) is solved numerically by adopting shooting technique. The results are computed in a form of numerical data which is presented and compared with the analytical solution in Table 3.1.

3.5 Graphical results and discussion

The convergence of the achieved series solutions and the influence of pertinent parameters in the present investigation are reported through Figs. 3.1 to 3.14. The convergence regions in the HAM solutions are strongly dependent upon the non-zero auxiliary parameters $\hbar$ which can be adjusted and controlled by means of a proper value of $\hbar$. The convergence region for velocity distribution for Reynold's model is depicted in Fig. 3.1. One has the liberty to choose any value of $\hbar$ in the region between -0.4 and -0.9. Convergence region is sufficient and meets the required criteria for a suitable choice of value of $\hbar$.

Fig. 3.2 exhibits temperature distribution for the Reynolds' model. Increase in values of Λ means particles get momentum. The viscous forces become weak as compared to momentum forces. The velocity and hence average kinetic energy of the fluid is enlarged. The system gains temperature. Fig. 3.3 shows comparison of models for $C = -1$ for velocity profile. It is

evident that graph obtained for Reynolds' model is almost a straight line where as in the case of Vogel's' model, it is a curve.

Fig. 3.4 depicts velocity distribution. The velocity graph for $C = -1$ is almost a straight line where as graphs for $C = -1.5$ and $C = -2.5$ are parabolic curves. We see that velocity decreases form 1 to 0 for pressure gradient $C = -1$ and this graph has 1 as maximum value at $r = 1$. Where as for pressure gradient $C = -2.5$ graph has 1.15 as maximum value at $r = 1.2$. The linear behavior shifts to non-linear for $C = -1.5$ and $C = -2.5$. We observe, reduction in the pressure enhances the motion and causes non-linear behavior. That is what we see in the daily life as well. Fig. 3.5 gives comparison of velocity profile as obtained by shooting method and homotopy analysis method for $b = 2$, $M = 1$, $P = 1$, $\Lambda = 1$. Solutions are in excellent agreement.

Fig. 3.6 reveals temperature distribution. Linear behavior is observed for small values of Γ but graphs become more non-linear for $\Gamma = 3$ and $\Gamma = 5$. Large Γ,enlarges velocity of the fluid particles which in return enhances their kinetic energy. Thus, as a consequence the system gains temperature. Comparison of models for $\Gamma = 3$ for temperature distribution is mentioned in Fig. 3.7. Temperature distribution gets maximum value 1 at $r = 1$ as observed in the case of Reynolds' model. Where as in Vogel's model of viscosity the temperature distribution gets maximum value 1.18 at $r = 1.35$. Reynolds' model shows that temperature varies directly with the radius of the pipe. However, this is not the case as Vogel's model predicts. Vogel's model gives non-linear behavior between temperature and the radius of the pipe.

Fig. 3.8 is plotted to have a look of velocity distribution for pressure gradient C in the case of Vogel's model. Velocity profile decreases as pressure gradient C increases. We can conclude that for $C < 0$, velocity profile decreases as pressure gradient C increases. Temperature distribution for Γ for Vogel's model is given in Fig. 3.9. For $\Gamma = 3$ temperature is maximum at $r = 1.35$ and minimum at $r = 2$ where as for $\Gamma = 1$ temperature is maximum at $r = 1$ and minimum at $r = 2$. The graphs for $\Gamma = 2$ and $\Gamma = 3$ show that temperature variation is non-linear. Temperature variation due to Γ, near the inner cylinder is more sensitive. The temperature of the fluid near the outer cylinder is less non-linear because temperature as well as velocity of the cylinder is zero. Fig. 3.10 is displayed for velocity field for the case Vogel's model. Fig. 3.11 presents velocity distribution for B for the Vogel's model. Fig. 3.12 shows temperature profile for B for

the Vogel's model. Fig. 3.13 is plotted to study velocity profile for P for the Vogel's model. Fig. 3.14 is prepared to see temperature profile for P for the Vogel's model.

Table 3.1: Comparison of solutions for velocity using HAM and Shooting method when $b = 2$, $M = 1$, $P = 1$, $\Lambda = 1$

r(radius)	v(velocity)(HAM)	v(velocity) (Shooting method)	Difference
1	1.000000	1.000000	0.000000000
1.05	0.950000	0.957560512	0.007560512
1.10	0.900000	0.909963285	0.009963285
1.15	0.850000	0.859595377	0.009595377
1.20	0.800000	0.807452390	0.007452390
1.25	0.750000	0.754144495	0.004144495
1.30	0.7000000	0.700103718	0.000103718
1.35	0.650000	0.645663061	0.004336939
1.40	0.600000	0.591094980	0.00890502
1.45	0.550000	0.536633036	0.013366964
1.50	0.500000	0.482485455	0.017514545
1.55	0.450000	0.428844374	0.021155626
1.60	0.400000	0.375892692	0.024107308
1.65	0.350000	0.323809570	0.02619043
1.70	0.300000	0.272775248	0.027224752
1.75	0.250000	0.222975646	0.027024354
1.80	0.200000	0.174607142	0.025392858
1.85	0.150000	0.127881943	0.022118057
1.90	0.100000	0.083034529	0.016965471
1.95	0.050000	0.040329801	0.009670199
2.00	0.000000	0.000073869	0.000073869

3.6 Conclusions

In this chapter, we have investigated numerically and analytically the flow of fluid between coaxial cylinders with temperature dependent viscosity through porous medium. The highly

non-linear problem is solved numerically with the help of shooting method and analytically by powerful technique homotopy analysis method. Effects of the various parameters such as Prandtl number Γ, viscosity parameter M, the dimensionless non-Newtonian parameter Λ and porous medium parameter P on the flow and temperature profiles are examined. From the present analysis, it is noted that:

1. From the present study it is found that by assuming $\mu = 1$ and $\mu = r$, the results for the case of constant as well as space viscosity can be attained.

2. The results for non-porous medium can be achieved by letting $\Phi = 0$ or $\kappa \to \infty$.

3. Results obtained by shooting method and homotopy analysis method are in good agreement.

4. Temperature profiles increase with the increase of Γ and Λ for Reynolds' model.

5. Velocity increases with the increase of B and P for Vogel's model.

6. Velocity decreases with the increase of C and Brinkman number for Vogel's model.

7. The increase of Brinkman number and P leads to the increase of temperature for Vogel's model and the profile decreases with rise of viscosity parameter B.

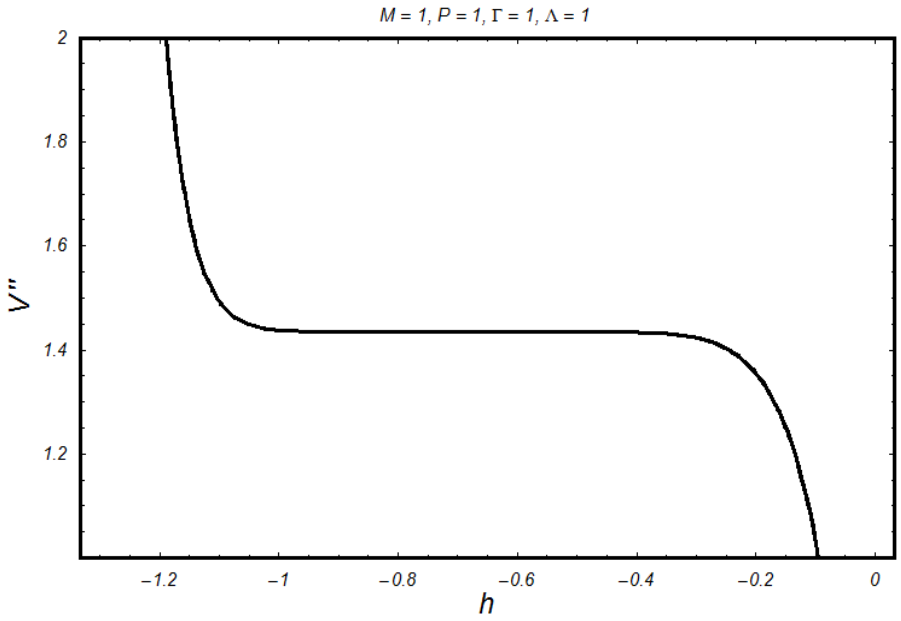

Fig. 3.1: h-curve for velocity distribution for Reynolds' model.

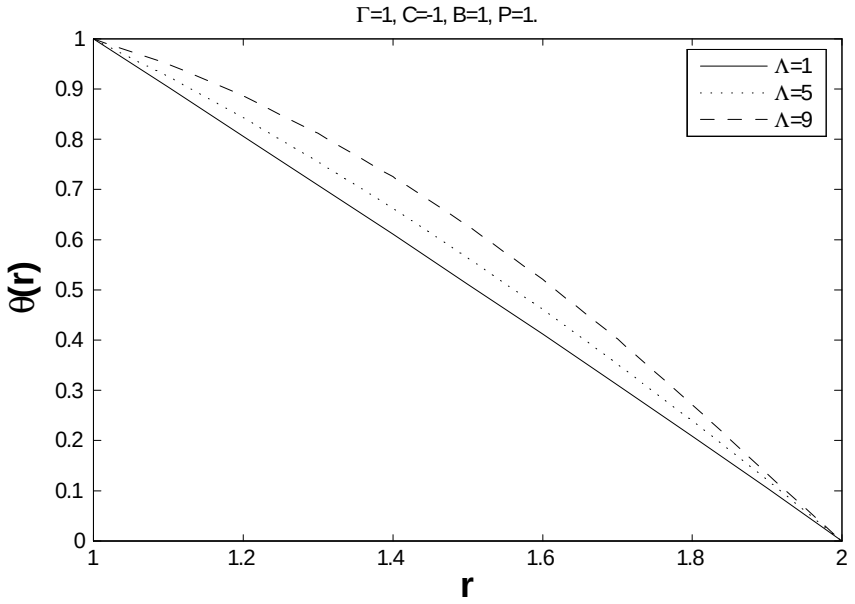

Fig. 3.2: Temperature distribution for Λ for the Reynolds' model.

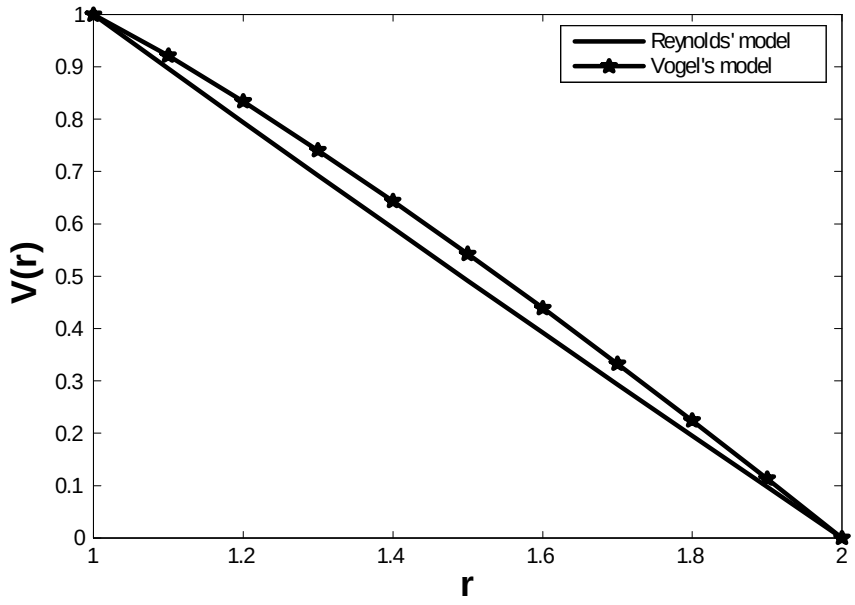

Fig. 3.3: Comparison of models for velocity distribution.

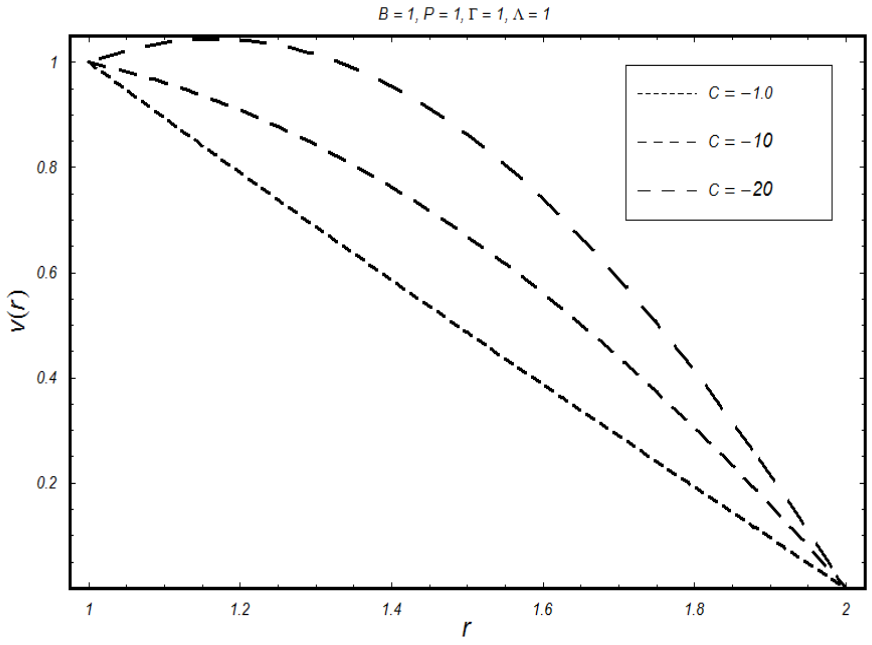

Fig. 3.4: Velocity distribution for C for the Reynolds' model.

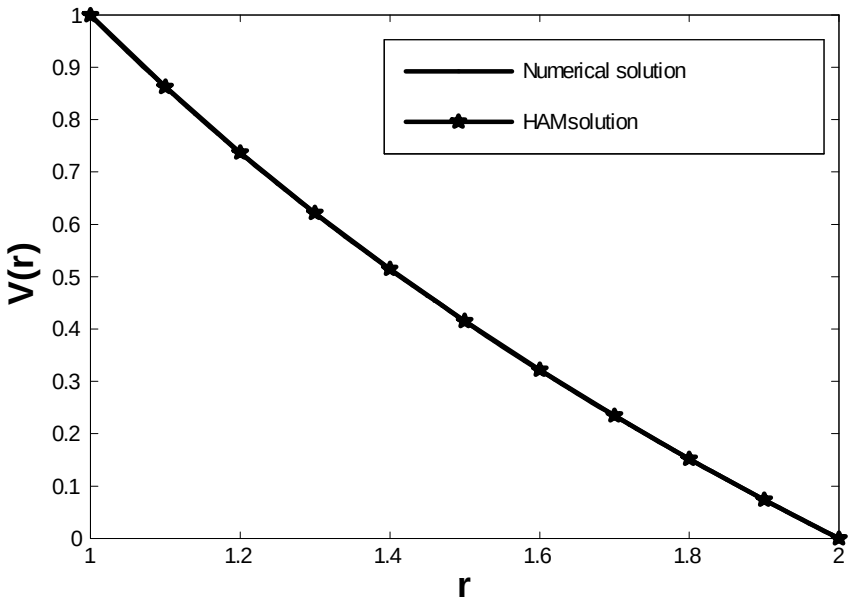

Fig. 3.5: Comparison of methods.

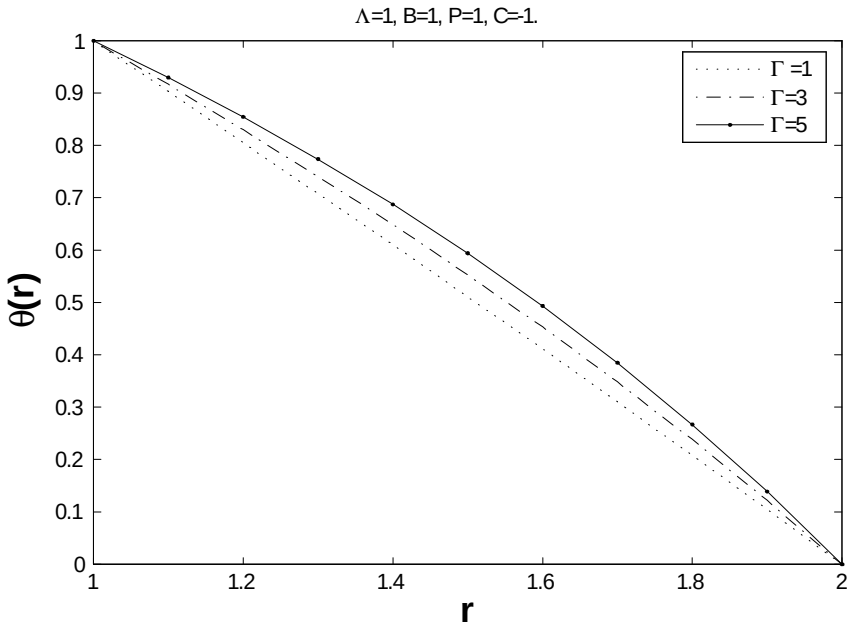

Fig. 3.6: Temperature for Γ for Reynolds' model.

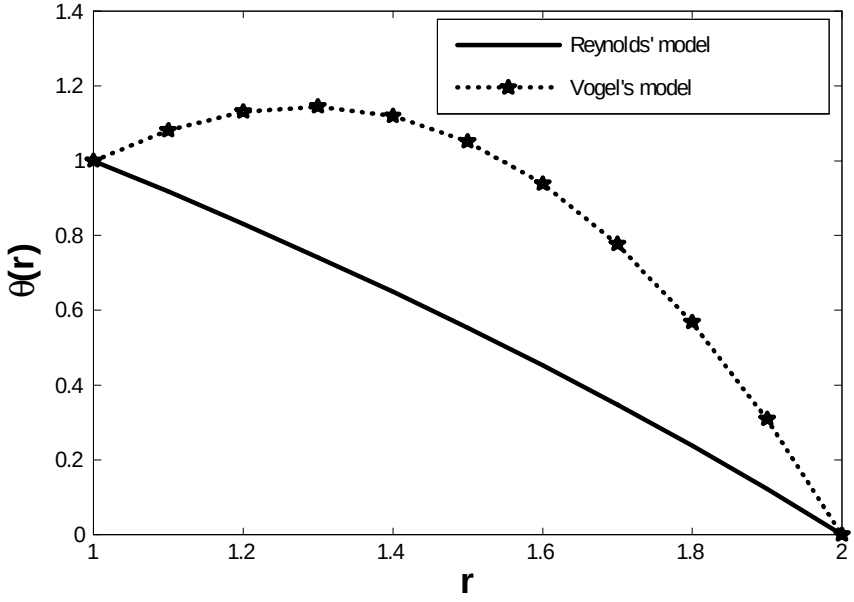

Fig. 3.7: Comparison of models for $\Gamma = 3$ for temperature distribution.

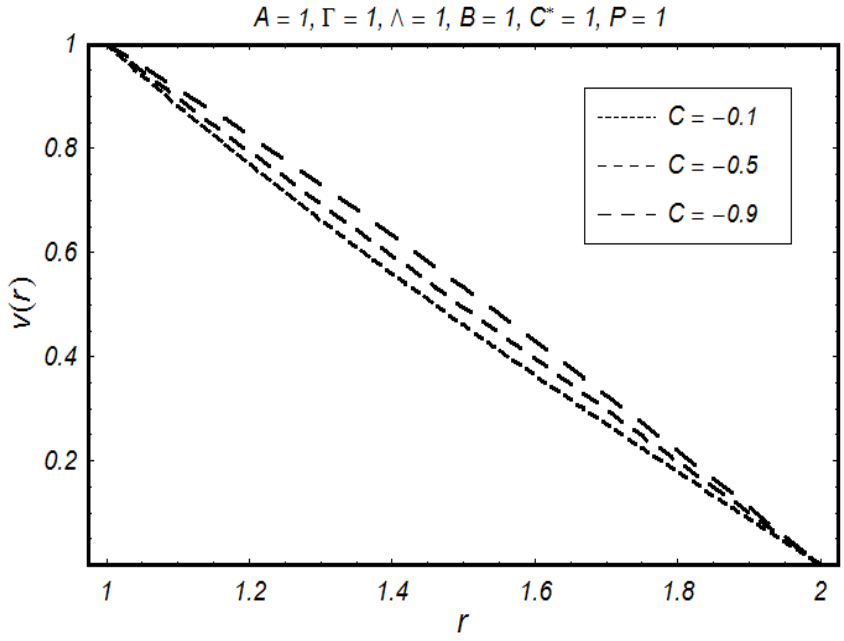

Fig. 3.8: Velocity distribution for C for the Vogel's model.

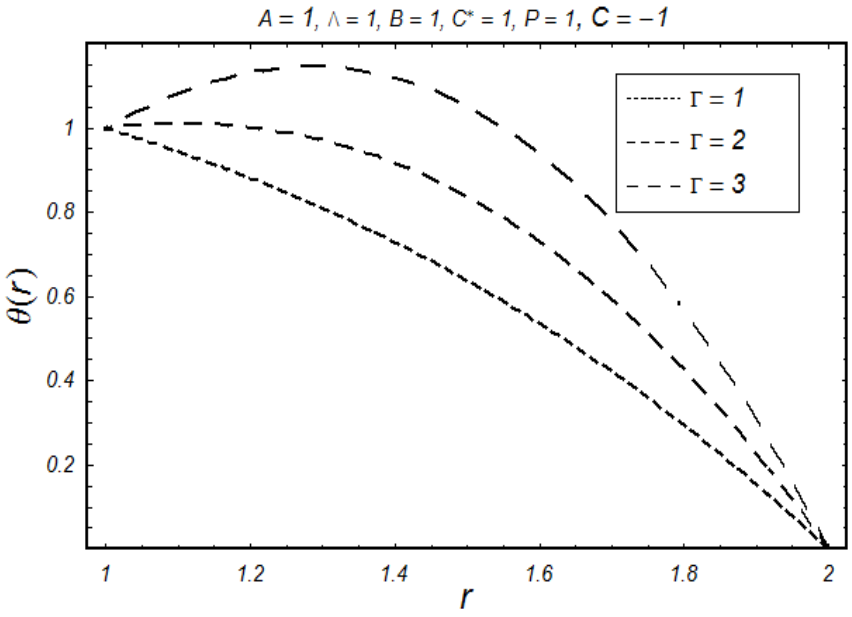

Fig. 3.9 : Temperature distribution for Γ for Vogel's model.

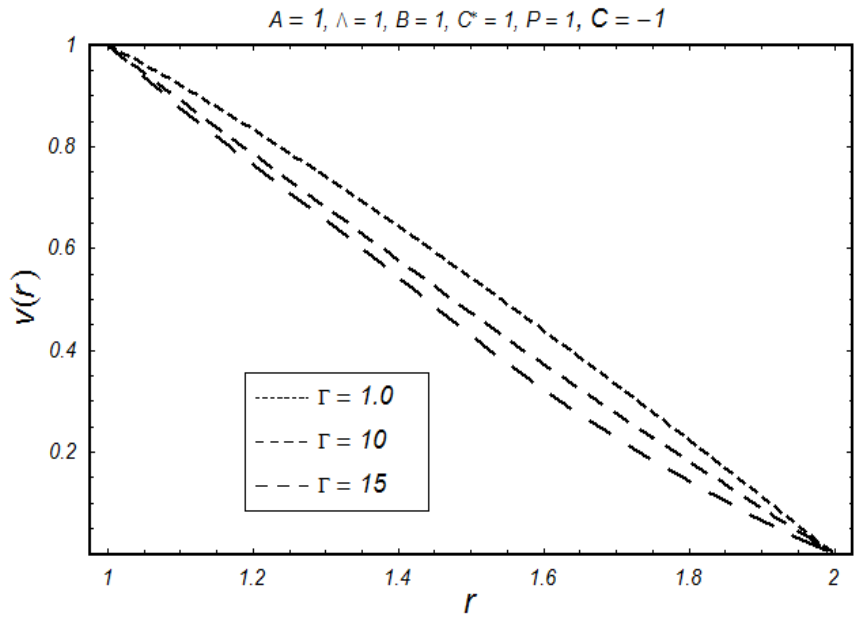

Fig. 3.10: Velocity distribution for Γ for Vogel's model.

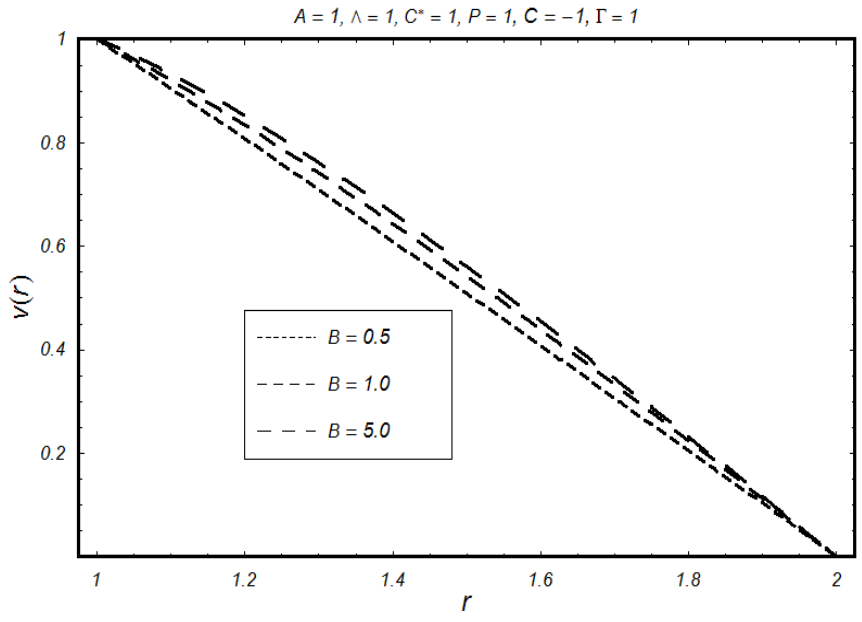

Fig. 3.11: Velocity distribution for B for the Vogel's model.

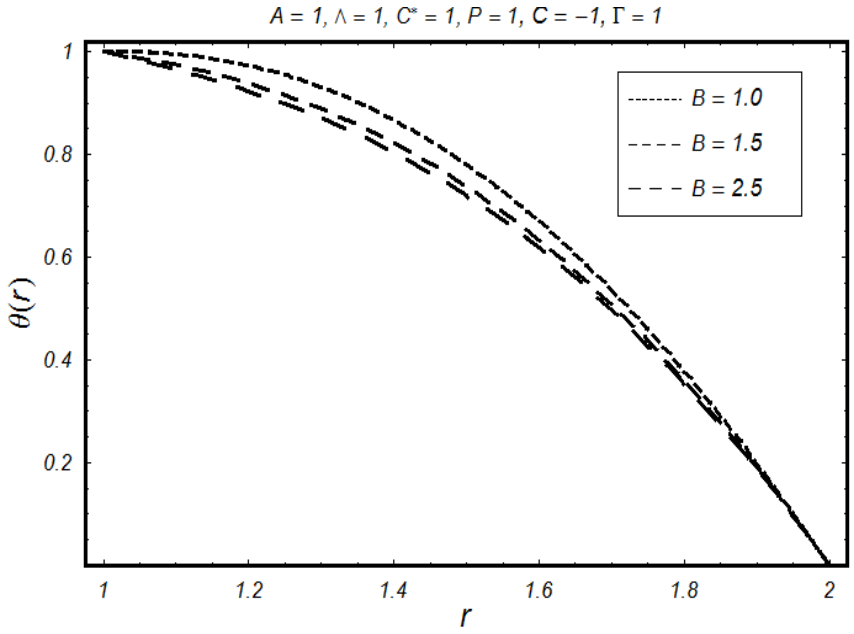

Fig. 3.12: Temperature distribution for B for the Vogel's model.

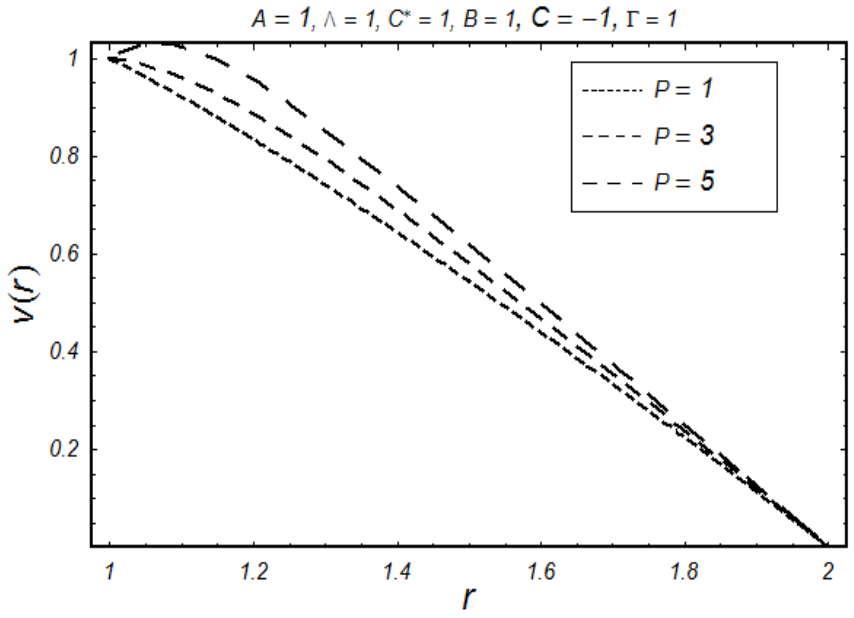

Fig. 3.13: Velocity distribution for P for the Vogel's model.

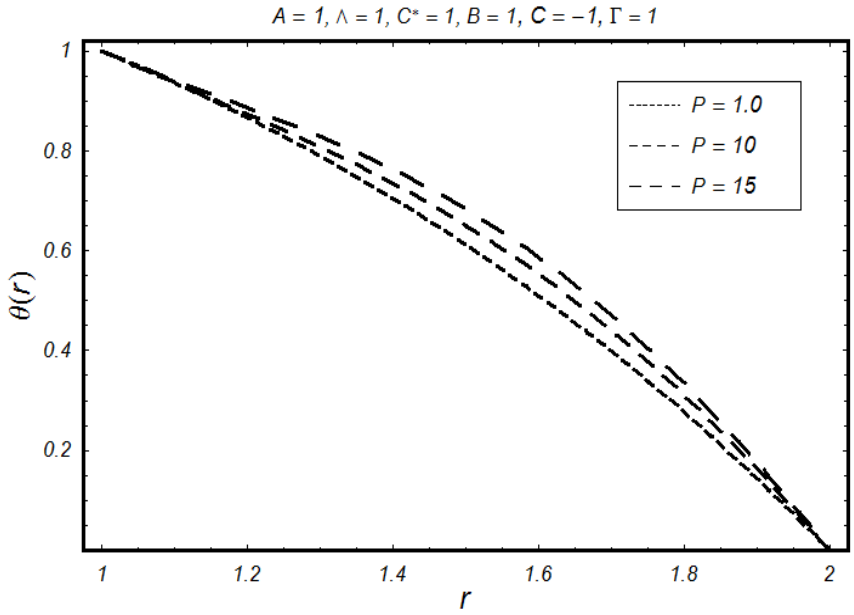

Fig. 3.14: Temperature distribution for P for the Vogel's model.

Chapter 4

An analytical treatment of Generalized Couette non-Newtonian nanofluid flow with variable viscosity

4.1 Introduction

In the present chapter, we have focused our attention to highlight the study of non-Newtonian nanofluid between coaxial cylinders with variable viscosity. The governing equations of non-Newtonian fluid with variable viscosity along with energy and nanoparticles are given. The coupled nonlinear equations have been solved analytically adopting homotopy analysis method. The expressions of velocity, temperature and nanoparticles functions are discussed graphically for emerging physical parameters.

4.2 Problem statement

Considering the same geometry as discussed in chapter 2. The flow is induced by a constant pressure gradient and motion of an inner cylinder. The outer cylinder is kept fixed. The heat transfer analysis is also taken into account. The governing equations for the conservation of

total mass, momentum, thermal energy and nanoparticles respectively are defined as

$$\boldsymbol{\nabla}.\mathbf{V} = 0, \tag{4.1}$$

$$\rho_f \frac{d\mathbf{V}}{dt} = -\boldsymbol{\nabla} p + \boldsymbol{\nabla}.\boldsymbol{\tau} + [\phi\rho_p + (1-\phi)\{\rho_f(1-\beta(T-T_1))\}]g, \tag{4.2}$$

$$(\rho c)_f(\frac{\partial T}{\partial t} + \mathbf{V}.\boldsymbol{\nabla} T) = k\boldsymbol{\nabla}^2 T + (\rho c)p[D_B \bigtriangledown\phi.\boldsymbol{\nabla} T + (D_T/T_1)\boldsymbol{\nabla} T.\boldsymbol{\nabla} T], \tag{4.3}$$

$$\frac{\partial \phi}{\partial t} + \mathbf{V}.\boldsymbol{\nabla}\phi = D_B\boldsymbol{\nabla}^2\phi + (D_T/T_1)\boldsymbol{\nabla}^2 T, \tag{4.4}$$

where ρ_f is the density of the base fluid, ρ_p is the density of the particles, β is volumetric volume expansion coefficient of the nanofluid, $\mathbf{V}$ is the velocity vector, p is the mechanical pressure, ϕ is the nanoparticle fraction, T is the temperature and $\boldsymbol{\tau}$ is the Cauchy stress tensor for third grade fluid defined in previous chapter, $(\rho c)_f$ is heat capacity of fluid, $(\rho c)p$ is heat capacity of the nanoparticle material and κ is thermal conductivity.

We choose

$$\mathbf{V} = [0,\ 0,\ v(r)],\ T = T(r),\ \phi = \phi(r). \tag{4.5}$$

With the help of Eqs. (4.5) equation of continuity (4.1) is identically satisfied, momentum, energy and nanoparticles equations take the form

$$\frac{\partial p}{\partial \theta} = 0, \tag{4.6}$$

$$\frac{1}{r}\frac{\partial}{\partial r}(2r\alpha_1(\frac{\partial v}{\partial r})^2 + \frac{1}{r}\frac{\partial}{\partial r}(r\alpha_2(\frac{\partial v}{\partial r})^2) = \frac{\partial p}{\partial r}, \tag{4.7}$$

$$\frac{1}{r}\frac{\partial}{\partial r}(r\mu(\frac{\partial v}{\partial r})^2 + \frac{1}{r}\frac{\partial}{\partial r}(r^2\beta_3(\frac{\partial v}{\partial r})^3) + [(\rho_p - \rho_{f_1})(\phi-\phi_0) + (1-\phi_1)\rho_{f_1}\beta(T-T_1)]g = \frac{\partial p}{\partial z}, \tag{4.8}$$

$$(\kappa + (\rho c)_p(D_T/T_1))\frac{\partial^2 T}{\partial r^2} + \frac{\kappa}{r}\frac{\partial T}{\partial r} + (\rho c)_p D_B\frac{\partial \phi}{\partial r}\frac{\partial T}{\partial r} = 0, \tag{4.9}$$

$$D_B(\frac{\partial^2\phi}{\partial r^2} + \frac{1}{r}\frac{\partial\phi}{\partial r}) + D_T/T_1(\frac{\partial^2 T}{\partial r^2} + \frac{1}{r}\frac{\partial T}{\partial r}) = 0. \tag{4.10}$$

Using the following nondimensional quantities in the above equations

$$\begin{aligned} r &= \frac{\bar{r}}{R},\ \theta = \frac{(\bar{T}-T_1)}{(T_0-T_1)},\ \phi = \frac{(\bar{\phi}-\phi_1)}{(\phi_0-\phi_1)},\ b = \frac{R_1}{R_0},\ \Lambda = \frac{2\beta_3 v_0^2}{R^2\mu_0}, \\ C_1 &= \frac{\partial p}{\partial z},\ Br = \frac{\left(\rho_p - \rho_{f_1}\right) R^2 \left(\phi_0-\phi_1\right) g}{\mu_0 v_0},\ C = \frac{C_1 R^2}{\mu_0 v_0}, \\ v &= \frac{\bar{v}}{v_0},\ \mu = \frac{\bar{\mu}}{\mu_0},\ G_r = \frac{\left(1-\phi_1\right)\rho_{f_1} R^2 \left(T_0-T_1\right) g}{\mu_0 v_0}, \\ Nt &= \frac{(\rho c)_p D_T \left(T_0-T_1\right)}{(\rho c)_f\ \alpha T_0},\ Nb = \frac{(\rho c)_p D_B \left(\phi_0-\phi_1\right)}{(\rho c)_f\ \alpha}. \end{aligned} \tag{4.11}$$

Making use of Eq. (4.11), Eqs. (4.6) to (4.10) take the following form

$$\frac{r}{G_r\theta}\frac{d\mu}{dr}\frac{dv}{dr} + \frac{\mu}{G_r\theta}\left(\frac{dv}{dr} + r\frac{d^2v}{dr^2}\right) + \frac{\Lambda}{G_r\theta}\left(\frac{dv}{dr}\right)^2\left(\frac{dv}{dr} + 3r\frac{d^2v}{dr^2}\right) + \frac{rB_r\phi}{G_r\theta} - \frac{rC}{G_r\theta} + r = 0, \tag{4.12}$$

$$\frac{d^2\theta}{d^2r}\left(r\alpha + r\alpha_1 N_t\right) + \left(\alpha + rNb\frac{d\phi}{dr}\right)\frac{d\theta}{dr} = 0, \tag{4.13}$$

$$r\left(\frac{Nb}{Nt}\frac{d^2\phi}{d^2r} + \frac{d^2\theta}{d^2r}\right) + \frac{Nb}{Nt}\frac{d\phi}{dr} + \frac{d\theta}{dr} = 0. \tag{4.14}$$

The corresponding boundary conditions are

$$v(1) = \phi(1) = \theta(1) = 1, \tag{4.15}$$

$$v(b) = \phi(b) = \theta(b) = 0. \tag{4.16}$$

4.3 Solution of the problem

The governing equations for both the viscosity models (discussed in previous chapter) are

(For Reynolds model)

$$\left(\frac{1}{r} - \frac{M}{r}\theta - M\frac{d\theta}{dr}\right)\frac{dv}{dr} + \frac{d^2v}{dr^2}\left(1 - M\theta\right) + \left(\frac{\Lambda}{r}\frac{dv}{dr} + 3\Lambda\frac{d^2v}{dr^2}\right)(\frac{dv}{dr})^2 + G_r\theta + B_r\phi = C, \tag{4.17}$$

$$\left(r\alpha + r\alpha_1 N_t - r\alpha_1 M\theta N_t\right)\frac{d^2\theta}{dr^2} + \left(\left(rNb + r\theta MNb\right)\frac{d\phi}{dr} + \alpha\right)\frac{d\theta}{dr} = 0, \tag{4.18}$$

$$(Nb + NbM\theta)\frac{d^2\phi}{dr^2} + (Nt - NtM\theta)\frac{d^2\theta}{dr^2} + \left(\frac{Nb}{r} + \frac{NbM\theta}{r}\right)\frac{d\phi}{dr} - \left(\frac{NtM\theta}{r} - \frac{Nt}{r}\right)\frac{d\theta}{dr} = 0. \tag{4.19}$$

(For Vogel's model)

$$\left(\frac{C}{rC^*} - \frac{AC}{B^2C^*}\frac{d\theta}{dr} - \frac{AC\theta}{B^2C^*}\right)\frac{dv}{dr} + \left(\frac{C}{C^*} - \frac{AC\theta}{B^2C^*} + 3\Lambda(\frac{dv}{dr})^2\right)\frac{d^2v}{dr^2} + \frac{\Lambda}{r}\left(\frac{dv}{dr}\right)^3 + G_r\theta + B_r\phi = C, \tag{4.20}$$

$$\left(r\alpha + \frac{r\alpha_1 N_t C}{C^*} - \frac{r\alpha_1 AC N_t\theta}{B^2C^*}\right)\frac{d^2\theta}{dr^2} + \left(\alpha + \frac{rNbC}{C^*}\frac{d\phi}{dr}\right)\frac{d\theta}{dr} + r\frac{ACNb\theta}{B^2C^*}\frac{d\theta}{dr}\frac{d\phi}{dr} = 0, \tag{4.21}$$

$$\left(\frac{CNb}{C^*} + \frac{ACNb\theta}{B^2C^*}\right)\frac{d^2\phi}{dr^2} + \left(\frac{CNb}{C^*}\frac{1}{r} + \frac{ACNb\theta}{B^2rC^*}\right)\frac{d\phi}{dr} + \frac{NtC}{S}\frac{1}{r}\frac{d\theta}{dr} - \frac{ACNt\theta}{rB^2C^*}\frac{d\theta}{dr} + \left(\frac{NtC}{S} - \frac{ACNt\theta}{B^2C^*}\right)\frac{d^2\theta}{dr^2} = 0. \tag{4.22}$$

The solution of above equations have been found analytically by homotopy analysis method. For HAM solution we require the following initial guesses

$$v_0(r) = \frac{(b-r)}{(b-1)}, \tag{4.23}$$

$$\theta_0(r) = \frac{(b-r)}{(b-1)}, \tag{4.24}$$

$$\phi_0(r) = \frac{(b-r)}{(b-1)}. \tag{4.25}$$

The auxiliary linear operators are

$$\pounds_{vel}(v) = v'', \ \pounds_{temp}(\theta) = \theta'', \ \pounds_{\Phi r}(\theta) = \phi'', \tag{4.26}$$

which satisfy

$$\mathcal{L}_{vr}(A_{51} + B_{51}r) = 0, \tag{4.27}$$

$$\mathcal{L}_{\theta r}(A_{52} + B_{52}r) = 0, \tag{4.28}$$

here A_{51}, A_{52}, A_{53}, B_{51}, B_{52}, B_{53} are the constants.

Adopting the similar procedure as discussed earlier, the HAM solution is straightforward written as

(For Reynolds model)

$$\begin{aligned} v &= \sum v_m(r) = \sum_{n=0}^{3m+1} a_{m,n} r^n,\ m \geq 0, \\ \theta &= \sum \theta_m(r) = \sum_{n=0}^{3m+1} d_{m,n} r^n,\ \phi = \sum \phi_m(r) = \sum_{n=0}^{3m} e_{m,n} r^n, m \geq 0. \end{aligned} \tag{4.29}$$

(For Vogel's model)

$$\begin{aligned} v &= \sum v_m(r) = \sum_{n=0}^{3m+1} a'_{m,n} r^n,\ m \geq 0, \\ \theta &= \sum \theta_m(r) = \sum_{n=0}^{3m+1} d'_{m,n} r^n,\ \phi = \sum \phi_m(r) = \sum_{n=0}^{3m} e'_{m,n} r^n, m \geq 0 \end{aligned} \tag{4.30}$$

where $a_{m,n}$, $d_{m,n}$, $e_{m,n}$, $a'_{m,n}$, $d'_{m,n}$and $e'_{m,n}$ are constants.

4.4 Graphical results and discussion

The convergence of achieved series solutions and influence of pertinent parameters in the present investigation are reported through Figs. 4.1 to 4.13. The effects of Nt, Nb, A and B on velocity, temperature and nanoparticles concentration profiles are observed. Figs. 4.1 to 4.3 have been plotted for Reynolds' model. Fig. 4.1 is prepared to see the convergence region for velocity profile. Fig. 4.2 is prepared to highlight the convergence region for temperature profile. Fig. 4.3 presents the convergence region for the nanoparticles concentration profile. Figs. 4.4 to 4.6 are prepared to check the convergence region for the nanoparticles concentration, temperature and velocity profiles for the Vogel's model.

Fig. 4.7 has been plotted for Reynolds' model. Fig. 4.7 is displayed for the nanoparticles concentration distribution when different values of Nt are used. It can be seen that with an increase in Nt the nanoparticles concentration profile decreases. Figs. 4.8 to 4.13 have been plotted for Vogels' model. Fig. 4.8 is plotted for the temperature for A. The relation (2.49)

explains the fact that viscosity decreases with rise of A. When we increase A, viscous forces become weaker. The fluid particles face less opposition. Ultimately, the velocity of fluid particles increases. This increase in the velocity is responsible for enhancement in average kinetic energy of the particles. As temperature measures the kinetic energy of the system. Consequently, temperature of fluid rises up.

Fig. 4.9 is prepared in order to observe the behavior of the nanoparticles concentration distribution for A. It is noted that nanoparticles concentration distribution decreases with increase in A. As discussed above, when we increase A, viscous forces become weaker. The mutual distance between the particles increases. Mass per unit volume reduces. That is why nanoparticles concentration distribution decreases with increase in A. Fig. 4.10 predicts the nanoparticles concentration profile for B. The nanoparticles concentration profiles increases with rise in B. The relation (2.49) describes the fact that viscosity increases with rise of B. When we increase B, viscous forces become stronger. The fluid particles face more opposition. The mutual distance between the particles decreases. Mass per unit volume increases. That is why nanoparticles concentration distribution increases with increase in B.

Fig. 4.11 predicts temperature distribution for B. It is observed that temperature decreases with rise in B. As explained earlier, the relation (2.49) describes the fact that viscosity increases with rise of B. When we increase B, viscous forces become stronger. The fluid particles face more opposition. The velocity of fluid reduces. Since kinetic energy and velocity are directly proportional. The average kinetic energy of the system reduces. As temperature and kinetic energy of a system are strongly linked i.e. temperature is a measure of average kinetic energy of a system. Consequently, the temperature of the fluid decreases with rise in B. The velocity field is presented in Fig. 4.12 for B. Fig. 4.13 reveals the nanoparticles concentration distribution for Nt.

4.5 Conclusions

In this chapter, we have studied non-Newtonian nanofluid between coaxial cylinders with variable viscosity. The governing equations of non-Newtonian fluid with variable viscosity along with energy and nanoparticles are presented. The coupled nonlinear equations have been solved

analytically with the help of HAM. Effects of the various parameters on the flow and temperature profiles are examined. The following conclusions are drawn.

1. The nanoparticles concentration leads to decrease by increasing thermophorsis parameter for Reynolds model.

2. Temperature field decreases by the increase of viscosity parameter B for Vogel's model.

3. The increase of B and thermophorsis parameter lead to the increase of nanoparticles concentration profile for Vogel's model and the profile decreases with rise of viscosity parameter A.

4. Temperature increases with the increase of A for Vogel's model.

5. The nanoparticles concentration profile decreases with rise of viscosity parameter A for the case of Vogel's model.

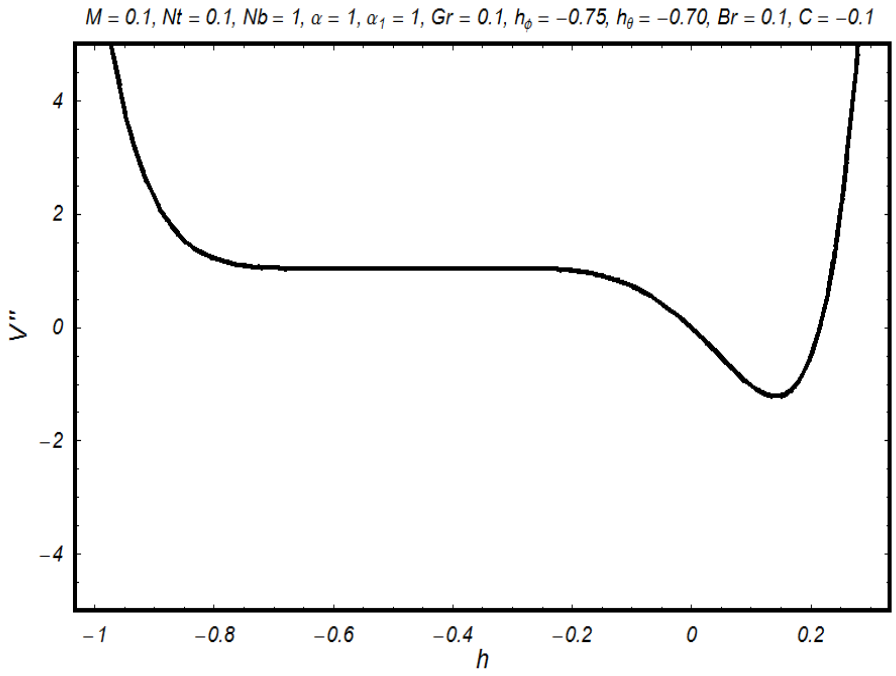

Fig. 4.1: h-curve for velocity distribution for the Reynolds' model.

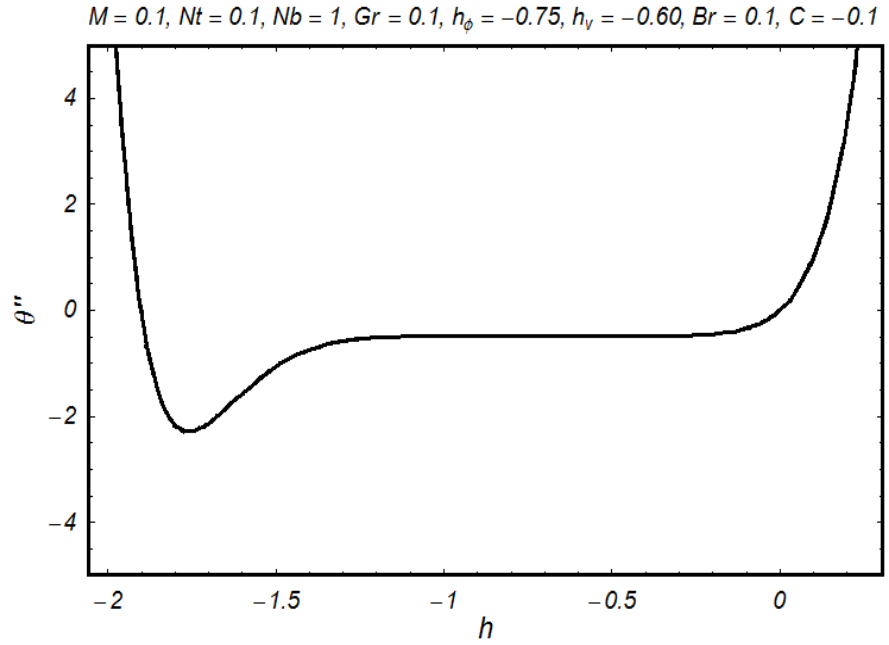

Fig. 4.2: h-curve for temperature distribution for the Reynolds' model.

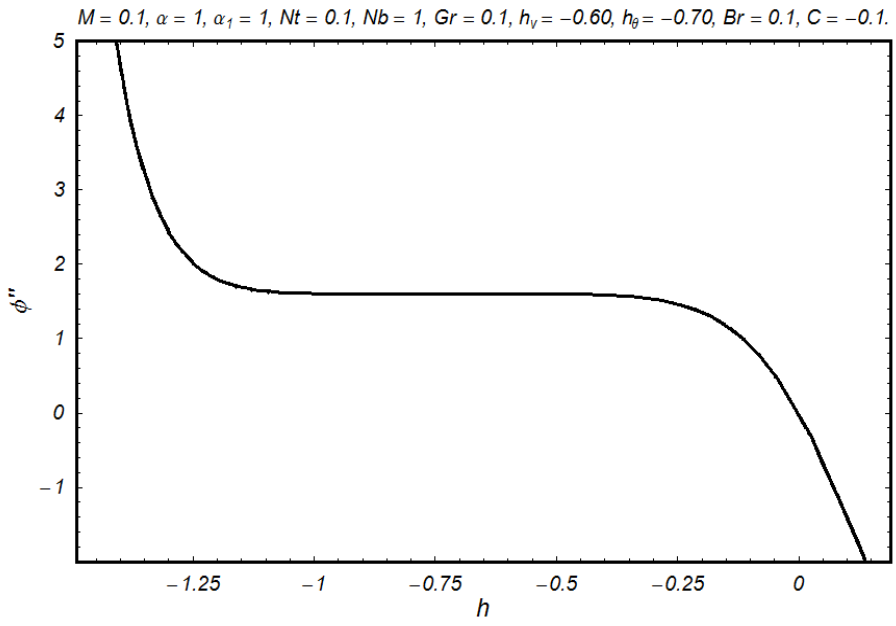

Fig. 4.3: h-curve for the nanoparticles concentration distribution for the Reynolds' model.

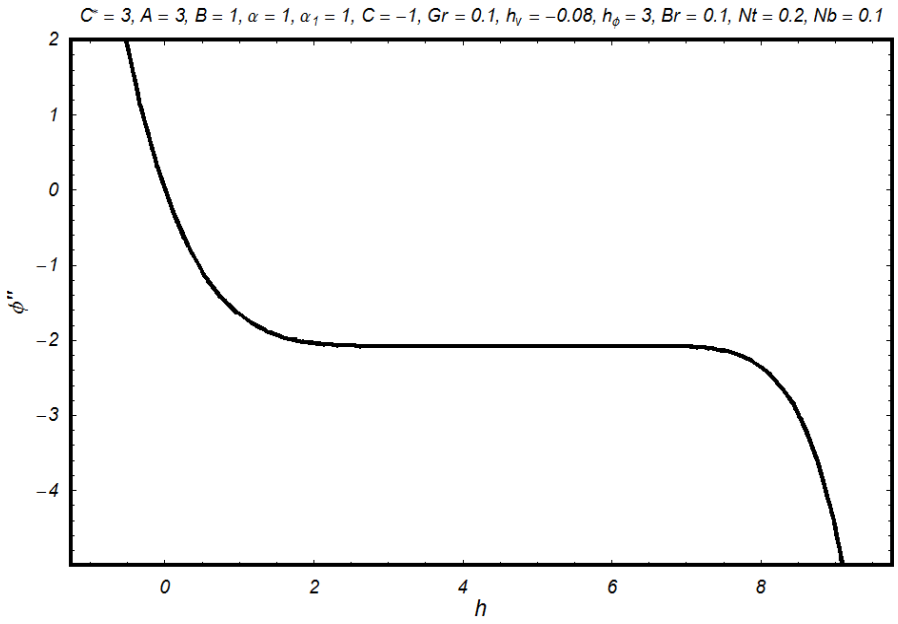

Fig. 4.4: h-curve for the nanoparticles concentration distribution for the Vogel's model.

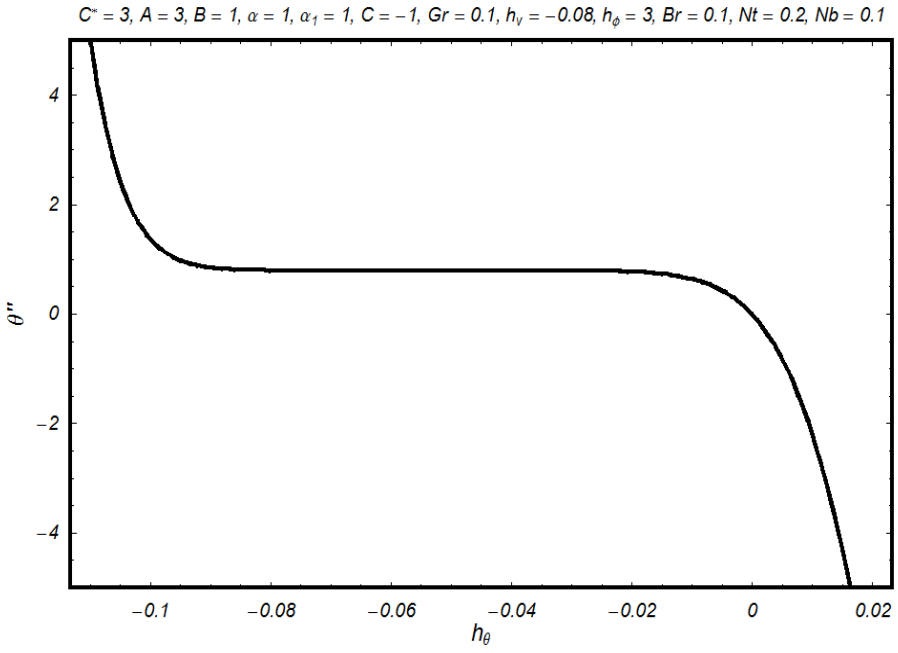

Fig. 4.5: h-curve for temperature distribution for the Vogel's model.

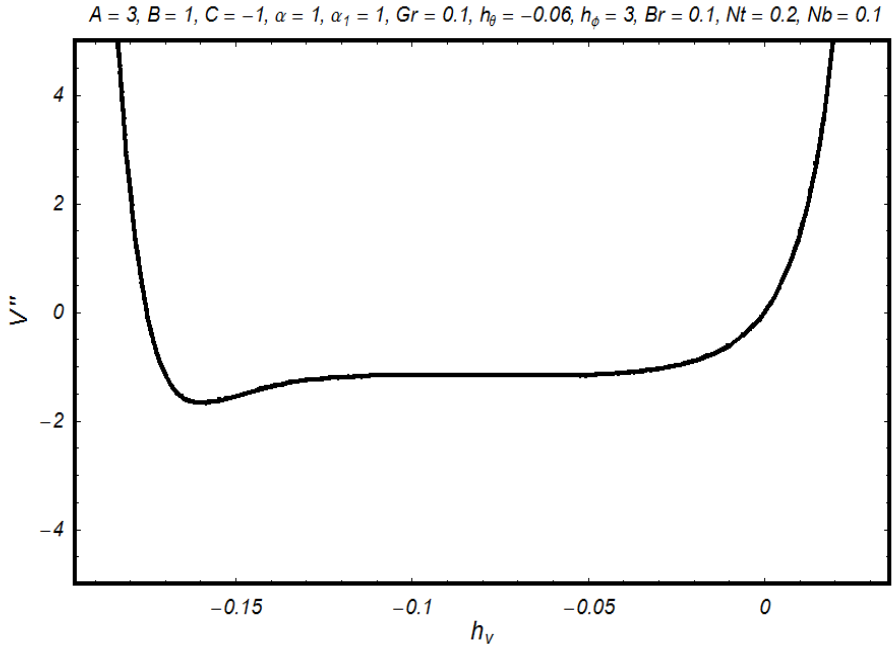

Fig. 4.6: h-curve for velocity distribution for the Vogel's model.

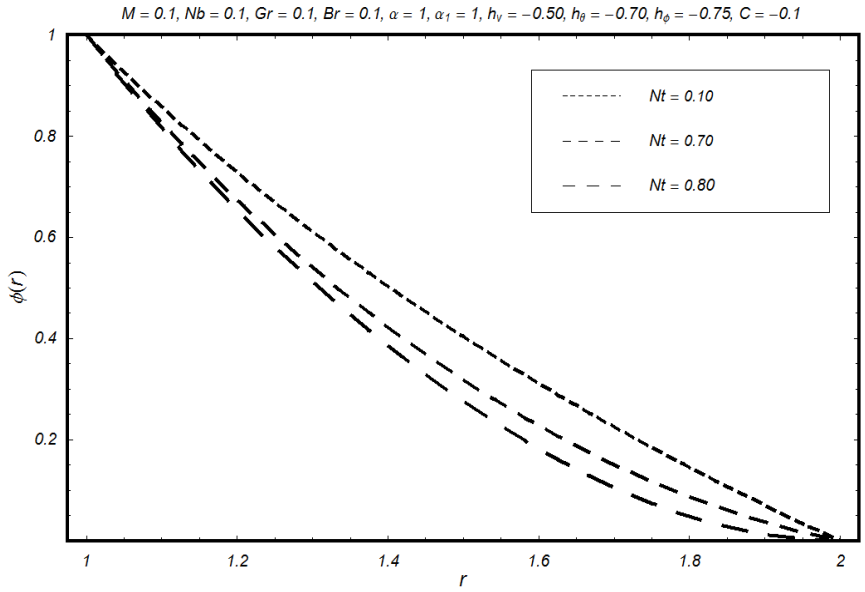

Fig. 4.7. The nanoparticles concentration distribution for Nt for Reynolds' model.

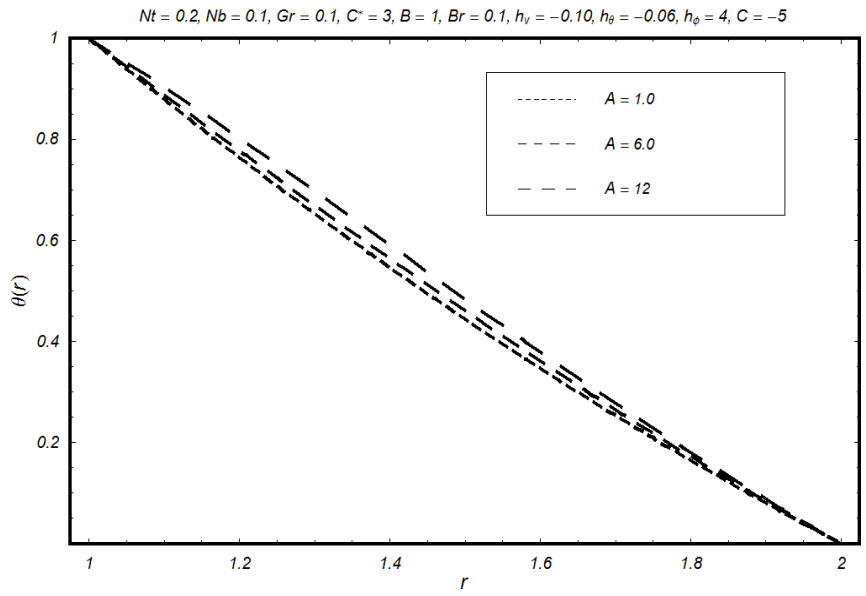

Fig. 4.8. Temperature variation along radial distance for various values of A for Vogel's Model.

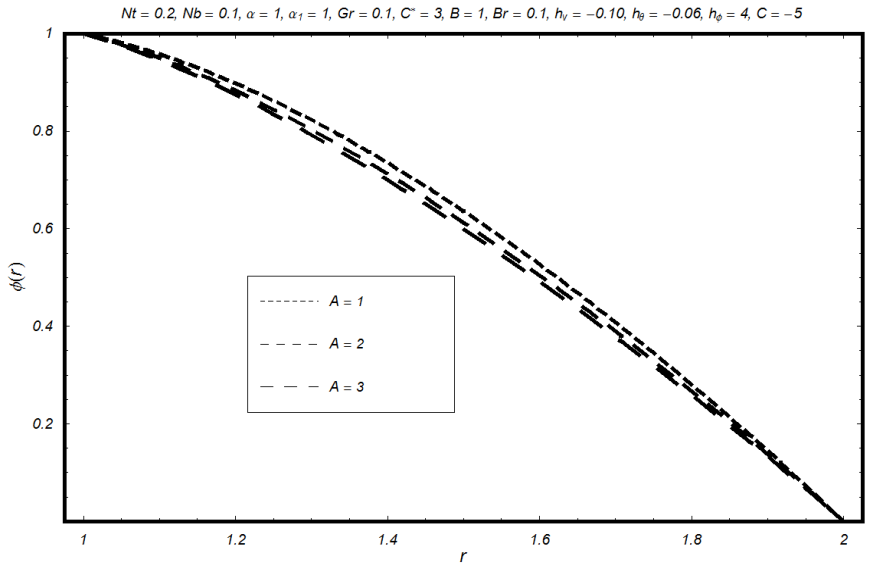

Fig. 4.9. The nanoparticles concentration distribution for A for Vogel's Model.

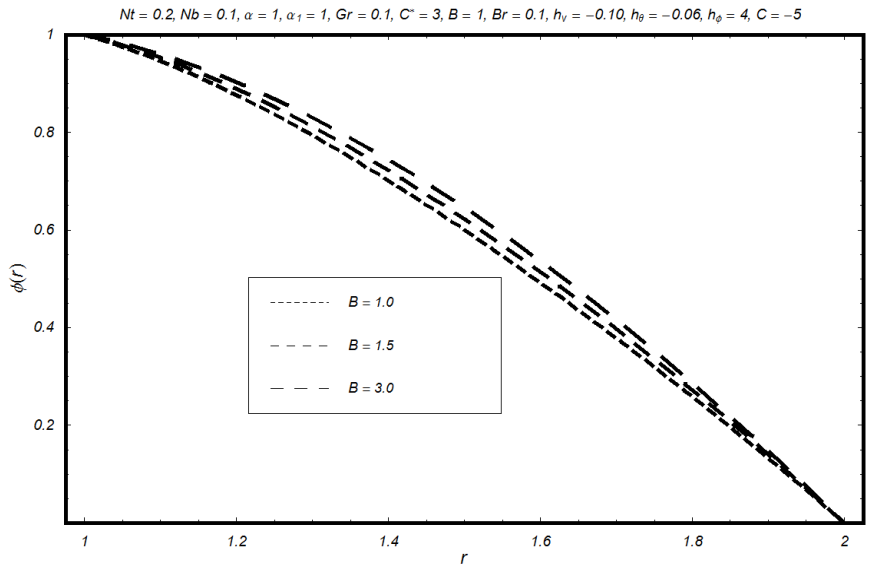

Fig. 4.10. The nanoparticles concentration distribution for B for Vogel's Model.

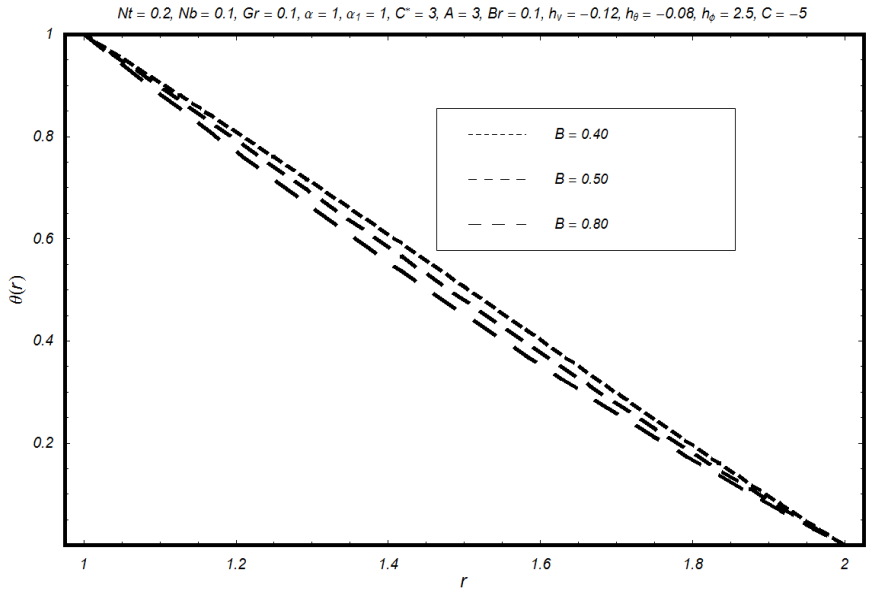

Fig. 4.11. Temperature distribution for B for Vogel's Model.

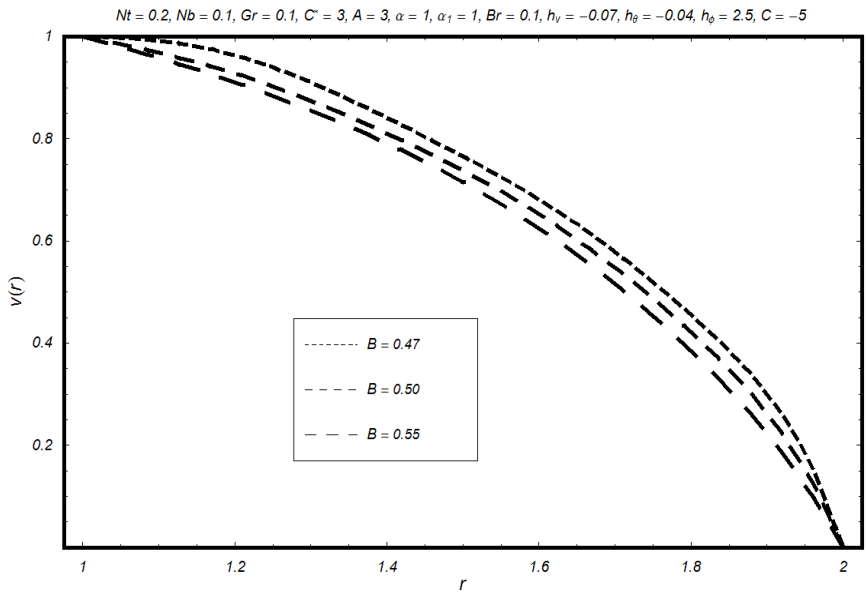

Fig. 4.12. Velocity distribution for B for Vogel's model.

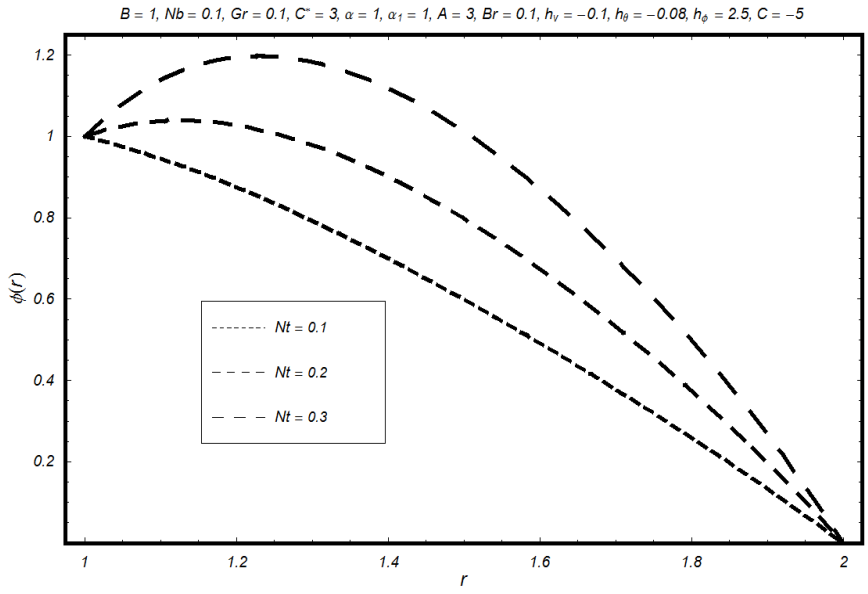

Fig. 4.13. The nanoparticles concentration distribution for Nt for Vogel's Model.

Order of approximation	$\left\|v''(1)\right\|$	$\left\|\theta''(1)\right\|$	$\left\|\phi''(1)\right\|$
5	1.52960	1.42838	0.005
10	1.53939	1.44088	0.006
15	1.53917	1.44093	0.006
20	1.53917	1.44093	0.006
25	1.53917	1.44093	0.006
30	1.53917	1.44093	0.006
35	1.53917	1.44093	0.006

Table : 4.1. Convergence table for Reynolds' model for $M = 0.1$, $\Lambda = 0.001$, $Gr = 0.1$, $\alpha = 1$, $\alpha_1 = 1$, $Br = 0.1, h_\theta = -0.70, h_\phi = -0.75, h_v = -0.65, Nt = 0.1, C = -0.1$.

Chapter 5

Boundary layer flow of an Eyring-Powell model fluid due to a stretching cylinder with variable viscosity

5.1 Introduction

The present investigation consists of an analytical treatment of a steady boundary layer flow of an Eyring-Powell model fluid due to a stretching cylinder with temperature dependent variable viscosity. The governing two dimensional nonlinear partial differential equations of momentum and energy are simplified using usual similarity transformations and are solved by a powerful technique homotopy analysis method. The physical features of various parameters intrinsic to the problem are discussed through graphs.

5.2 Description of the problem

Consider flow of an incompressible Eyring-Powell model fluid through a tube of radius a. The flow is due to stretching of the tube in axial direction. The axis of tube is taken along z-axis. The ambient fluid temperature is T_1 and T_w is temperature at tube surface. The equations

which govern the problem are

$$\frac{\partial(rw)}{\partial z}+\frac{\partial(ru)}{\partial r}=0, \tag{5.1}$$

$$\begin{aligned}\rho(u\tfrac{\partial u}{\partial r}+w\tfrac{\partial u}{\partial z}) &= 2\mu\tfrac{\partial^2 u}{\partial r^2}-\tfrac{4u^3}{3\beta c_1^3 r^4}+\tfrac{2}{\beta c_1}\tfrac{\partial^2 u}{\partial r^2}-\tfrac{2}{3\beta c_1^3}\tfrac{\partial^2 u}{\partial r^2}(\tfrac{\partial u}{\partial z}+\tfrac{\partial w}{\partial r})^2-\tfrac{4}{\beta c_1^3}(\tfrac{\partial u}{\partial r})^2\tfrac{\partial^2 u}{\partial r^2}+\tfrac{2\mu u}{r^2}\\
&-\frac{1}{3r\beta c_1^3}\{4(\frac{\partial u}{\partial r})^3+\left(2\frac{\partial u}{\partial r}+\frac{\partial w}{\partial z}\right)(\frac{\partial u}{\partial z}+\frac{\partial w}{\partial r})^2\}-\frac{1}{3\beta c_1^3}\frac{\partial u}{\partial r}(\frac{\partial u}{\partial z}+\frac{\partial w}{\partial r})\frac{2u}{r}\frac{\partial u}{\partial r}\\
&(\frac{\partial^2 u}{\partial r\partial z}+\frac{\partial^2 w}{\partial r^2})+\frac{2u}{\beta c_1 r^2}-\frac{4}{3\beta c_1^3}\frac{\partial u}{\partial r}(\frac{\partial u}{\partial z}+\frac{\partial w}{\partial r})(\frac{\partial^2 u}{\partial r\partial z}+\frac{\partial^2 w}{\partial r^2})+2\frac{\partial\mu}{\partial r}\frac{\partial u}{\partial r}+\frac{2}{r\beta c_1}\frac{\partial u}{\partial r}\\
&+4\frac{\partial w}{\partial z}(\frac{\partial u}{\partial z}+\frac{\partial w}{\partial r})(\frac{\partial^2 u}{\partial r\partial z}+\frac{\partial^2 w}{\partial r^2})+2\frac{\partial^2 w}{\partial r\partial z}(\frac{\partial u}{\partial z}+\frac{\partial w}{\partial r})^2-\frac{1}{3\beta c_1^3}\frac{\partial^2 u}{\partial r^2}(\frac{\partial u}{\partial z}+\frac{\partial w}{\partial r})^2,\end{aligned} \tag{5.2}$$

$$\begin{aligned}\rho(u\tfrac{\partial w}{\partial r}+w\tfrac{\partial w}{\partial z}) &= \left(\mu+\tfrac{1}{\beta c_1}\right)(\tfrac{\partial^2 u}{\partial r\partial z}+\tfrac{\partial^2 w}{\partial r^2})+\tfrac{2}{\beta c_1}\tfrac{\partial^2 w}{\partial z^2}+\left(\tfrac{\mu}{r}+\tfrac{1}{\beta r c_1}\right)(\tfrac{\partial u}{\partial z}+\tfrac{\partial w}{\partial r})\\
&-\frac{1}{6r^2\beta c_1^3}\{\left(4(\frac{\partial u}{\partial r})^2+(\frac{\partial u}{\partial z}+\frac{\partial w}{\partial r})^2+4\frac{\partial w}{\partial z}\frac{\partial u}{\partial r}+4(\frac{\partial w}{\partial z})^2\right)(\frac{\partial u}{\partial z}+\frac{\partial w}{\partial r})\}+\frac{\partial\mu}{\partial r}\frac{\partial w}{\partial r}\\
&-2\mu\frac{\partial^2 w}{\partial z^2}-\frac{1}{6r\beta c_1^3}\{8\left(\frac{\partial u}{\partial z}+\frac{\partial w}{\partial r}\right)\frac{\partial u}{\partial r}\frac{\partial^2 u}{\partial r^2}\ +(\frac{\partial u}{\partial r})^2(4\frac{\partial^2 u}{\partial r\partial z}+4\frac{\partial^2 w}{\partial r^2})+4\frac{\partial w}{\partial z}\frac{\partial^2 u}{\partial r^2}\frac{\partial u}{\partial z}\\
&+8\frac{\partial w}{\partial z}\frac{\partial^2 w}{\partial r\partial z}\frac{\partial w}{\partial r}+3(\frac{\partial u}{\partial z}+\frac{\partial w}{\partial r})^2(\frac{\partial^2 u}{\partial r\partial z}+\frac{\partial^2 w}{\partial r^2})\ +4(\frac{\partial u}{\partial r}\frac{\partial^2 w}{\partial r\partial z}\frac{\partial u}{\partial z}\ +\frac{\partial u}{\partial r}\frac{\partial^2 w}{\partial r\partial z}\frac{\partial w}{\partial r})\\
&+8\frac{\partial w}{\partial z}\frac{\partial^2 w}{\partial r\partial z}\frac{\partial u}{\partial z}+4\frac{\partial w}{\partial z}\frac{\partial u}{\partial r}(\frac{\partial^2 w}{\partial r^2})+4\frac{\partial w}{\partial z}\frac{\partial^2 u}{\partial r^2}\frac{\partial w}{\partial r}+4\frac{\partial w}{\partial z}\frac{\partial u}{\partial r}\frac{\partial^2 u}{\partial r\partial z}+4(\frac{\partial w}{\partial z})^2\frac{\partial^2 u}{\partial r\partial z}\\
&+4(\frac{\partial w}{\partial z})^2\frac{\partial^2 w}{\partial r^2}\}-\frac{1}{6r\beta c_1^3}\{2\frac{\partial^2 u}{\partial z\partial r}(\frac{\partial u}{\partial z}+\frac{\partial w}{\partial r})^2+4\frac{\partial^2 w}{\partial z^2}((\frac{\partial u}{\partial z})^2+(\frac{\partial w}{\partial r})^2+2\frac{\partial u}{\partial z}\frac{\partial w}{\partial r})\\
&+\left(4\frac{\partial u}{\partial r}\frac{\partial^2 u}{\partial r\partial z}+\frac{\partial^2 w}{\partial r^2}\right)(\frac{\partial u}{\partial z}+\frac{\partial w}{\partial r}))+8\frac{\partial w}{\partial z}(\frac{\partial u}{\partial z}+\frac{\partial w}{\partial r})(\frac{\partial^2 u}{\partial r\partial z}+\frac{\partial^2 w}{\partial r^2}\\
&+12(\frac{\partial w}{\partial z})^2\frac{\partial^2 w}{\partial z^2})\},\end{aligned} \tag{5.3}$$

$$u\frac{\partial T}{\partial r}+w\frac{\partial T}{\partial z}=\alpha_3\left(\frac{\partial^2 T}{\partial r^2}+\frac{1}{r}\frac{\partial T}{\partial r}\right). \tag{5.4}$$

The corresponding boundary conditions are defined as

$$\begin{aligned}u &= 0,\ T=T_w,\ w=w_w,\ \text{at } r=a\\
w &\to 0,\ T\to T_\infty,\ \text{as } r\to\infty,\end{aligned} \tag{5.5}$$

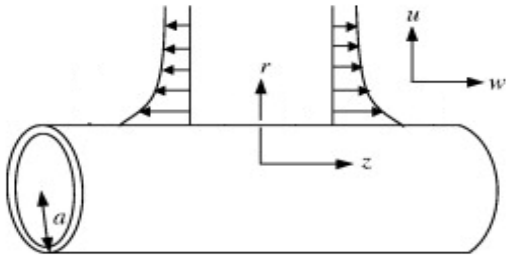

Fig. 5a: Geometry of the problem.

where u is the velocity component along radial direction and w is velocity along axial directions. Here $w_w = 2cz$ in which c is a constant. Further α_3, ν, ρ, T and μ are thermal diffusivity, the kinematic viscosity, fluid density, fluid temperature and viscosity of the fluid. Introducing the following similarity transformations

$$\eta = \left(\frac{r}{a}\right)^2, u = \frac{-caf(\eta)}{\sqrt{\eta}},\ w = 2czf'(\eta),\ \theta = \frac{T - T_\infty}{T_w - T_\infty}. \tag{5.6}$$

Using the boundary layer approach and nondimensional parameters defined in last chapter, we arrive at

$$\begin{aligned}
&4(\mu + E_1)\eta^2 f'' - 16A\eta^2 f\left(f''\right)^2 + \frac{16}{3}A\eta f f' f''' - \frac{304}{3}A\eta^2 f f' f'' - 16A\eta^2 f\left(f''\right)^2 \\
&+\frac{16}{3}A\eta^2\left(f f' f''' - \left(f'\right)^2\right) + 4(\mu + E_1)\eta^3 f''' - \frac{304}{3}A\eta^2 f f' f'' - \frac{352}{3}A\eta^3 f'(f'')^2 \\
&+\frac{176}{3}A\eta^2 f''(f')^2 + 64A\eta f(f'')^2 + 32A\eta(f)^2 f'' - 32A\eta^3\left(f'\right)^2 f''' + 32A\eta^3 f' f'' \\
&+16A\eta f f' f'' + \mu\,\mathrm{Re}\,\eta^2\left(f f'' - f'^2\right) + 8\eta^3\tfrac{\partial\mu}{\partial\eta}f'' - \tfrac{8}{3}Af^2 f'' \quad = \quad 0,
\end{aligned} \tag{5.7}$$

$$\eta\theta'' + (1 + \mathrm{Re}\,\mathrm{Pr}\,f)\,\theta' = 0, \tag{5.8}$$

where

$$\mathrm{Re} = \frac{ca^2}{2\nu},\ \mathrm{Pr} = \frac{\nu}{\alpha_3},\ E_1 = \frac{1}{\mu_*\beta c_1},\ E_2 = \frac{c^3}{\mu_*\beta\,(c_1)^3}. \tag{5.9}$$

The boundary conditions in dimensionless form are

$$f(1)=0,\ f^{'}(1)=1,\ \theta(1)=1,\ f'(\infty)\ \to 0,\ \theta(\infty)\to 0. \tag{5.10}$$

5.3 Series Solutions for Reynolds model

Invoking Eq. (2.28b) into Eqs. (5.7) to (5.8), one has

$$\begin{aligned}
&(1-M\theta)\,\mathrm{Re}\,\eta^2\left(ff''-f'^2\right)+4\left((1-M\theta)+E_1\right)\eta^2 f''-\frac{8}{3}\,E_2 f^2 f''\\
&+4\left((1-M\theta)+E_1\right)\eta^3 f'''-\frac{304}{3}\,E_2\eta^2 f f' f''-\frac{352}{3}\,E_2\eta^3 f'(f'')^2\\
&+16(E_2\eta f f' f''+2\,E_2\eta\,(f)^2 f''+\frac{11}{3}\,E_2\eta^2 f''(f')^2+2\,E_2\eta^3 f' f''))\\
&+\frac{16}{3}\,(\eta^2\left(E_2 f f' f'''-E_2\left(f'\right)^2\right)-6\,E_2\eta^3\left(f'\right)^2 f'''+E_2\eta f f' f''')\\
&-16\,E_2\eta^2 f\left(f''\right)^2-16M\eta^3\frac{d\theta}{d\eta}f''+64\,E_2\eta f(f'')^2=0,
\end{aligned} \tag{5.11}$$

$$\eta\theta''+(1+\mathrm{Re}\,\mathrm{Pr}\,f)\,\theta'=0. \tag{5.12}$$

Since Eqs. (5.11) and (5.12) are highly nonlinear ordinary differential equations, their exact solutions are impossible therefore we are interested to compute their analytical solutions with the help of powerful technique homotopy analysis method.

For HAM solution, we choose the following initial estimate

$$f_0=1-e^{1-\eta} \tag{5.13}$$

$$\theta_0=e^{1-\eta}, \tag{5.14}$$

and the linear operators are chosen as

$$\mathcal{L}(f)=f'''+f'', \tag{5.15}$$

$$\mathcal{L}(\theta)=\theta''+\theta'. \tag{5.16}$$

Zeroth order deformation problem is defined as

$$(1-q)\mathcal{L}_f[\overline{f}(\eta,q)-f_o(\eta)]=q\hbar N_f[\overline{f}(\eta,q),\overline{\theta}(\eta,q)], \tag{5.17}$$

$$(1-q)\mathcal{L}_\theta[\overline{\theta}(\eta,q)-\theta_o(\eta)]=q\hbar N_\theta[\overline{f}(\eta,q),\overline{\theta}(\eta,q)], \tag{5.18}$$

$$\overline{f}(\eta,q)=0,\ \overline{\theta}(\eta,q)=1,\ \overline{f}'(\eta,q)=1,\ \eta=1, \tag{5.19}$$

$$\frac{\partial\overline{f}(\eta,q)}{\partial\eta}=0,\ \overline{\theta}(\eta,q)=0,\quad \eta=\infty, \tag{5.20}$$

$$\begin{aligned}
N_f[\overline{f}(\eta,q),\ \overline{\theta}(\eta,q)] \ &= \ -32\ E_2\eta^3\left(f'\right)^2 f'''+4\eta^3 f'''E_1+\tfrac{16}{3}\ E_2\eta^2 ff'f''' \\
&-\mathrm{Re}\,\eta^2 f'^2-\frac{8}{3}\ E_2 f^2 f''+4\eta^3 f'''+\frac{8}{3}(2E_2\eta^2\left(f'\right)^2-\frac{3}{2}\eta^2 f''M\theta-E_2 f^2 f'') \\
&-\frac{352}{3}\ E_2\eta^3 f'(f'')^2+\frac{16}{3}\ E_2\eta ff'f'''-\mathrm{Re}\,\eta^2 ff''E_2\theta-16\ E_2\eta^2 f\left(f''\right)^2 \\
&-\mathrm{Re}(\eta^2 f'^2E_2\theta+\eta^2 ff'')+\frac{176}{3}\ E_2\eta^2 f''(f')^2-16M\eta^3\frac{d\theta}{d\eta}f''+4\eta^2 f''E_1 \\
&+32\eta(E_2\eta^2 f'f''+E_2\left(f\right)^2 f''+E_2 ff'f'')-\frac{304}{3}\ E_2\eta^2 ff'f''-4\eta^3 f'''M\theta \\
&+4\eta^2 f'',
\end{aligned} \tag{5.21}$$

$$N_\theta[\overline{f}(\eta,q),\ \overline{\theta}(\eta,q)]=\eta\theta''+(1+\mathrm{Re}\,\mathrm{Pr}\,f)\,\theta'. \tag{5.22}$$

The mth order deformation equations are defined as

$$\mathcal{L}_f[f_m(\eta)-\chi_m f_{m-1}(\eta)]=\hbar R_f(\eta), \tag{5.23}$$

$$\mathcal{L}_\theta[\theta_m(\eta)-\chi_m\theta_{m-1}(\eta)]=\hbar R_\theta(\eta), \tag{5.24}$$

where

$$\chi_m=\begin{cases}0, & m\le 1,\\ 1, & m>1.\end{cases}, \tag{5.25}$$

$$
\begin{aligned}
R_f(\eta) &= 32E_2\eta^3\sum_{k=0}^{m-1} f_{m-1-k}f_k^{''} - 4M\eta^2\sum_{k=0}^{m-1} f_{m-1-k}^{''}\theta_k - 8E_2\sum_{k=0}^{m-1}\sum_{l=0}^{k} f_{m-1-k}f_{k-l}f_l^{''} + 4E_1\eta^3 f_{m-1}^{'''} \\
&-M\sum_{k=0}^{m-1}\sum_{l=0}^{k} f_{m-1-k}^{'}f_{k-l}^{'}\theta_l + 4\left(1+E_1\right)\eta^2 f_{m-1}^{''} - 4M\eta^3\sum_{k=0}^{m-1} f_{m-1-k}^{'''}\theta_k - \sum_{k=0}^{m-1} f_{m-1-k}^{'}f_k^{'}) \\
&+\frac{16}{3}\ E_2\eta^2(\sum_{k=0}^{m-1}\sum_{l=0}^{k} f_{m-1-k}f_{k-l}^{'}f_l^{'''} - \frac{304}{3}\ E_2\eta^2\sum_{k=0}^{m-1}\sum_{l=0}^{k} f_{m-1-k}f_{k-l}^{'}f_l^{''} - \sum_{k=0}^{m-1} f_{m-1-k}^{'}f_k^{'}) \\
&-\frac{8\ E_2}{3}(44\ \eta^3\sum_{k=0}^{m-1}\sum_{l=0}^{k} f_{m-1-k}^{'}f_{k-l}^{''}f_l^{''} + 2\eta\sum_{k=0}^{m-1}\sum_{l=0}^{k} f_{m-1-k}f_{k-l}^{'}f_l^{'''}) + \mathrm{Re}\,\eta^2\sum_{k=0}^{m-1} f_{m-1-k}f_k^{''} \\
&+16E_2\eta^2(\frac{11}{3}\sum_{k=0}^{m-1}\sum_{l=0}^{k} f_{m-1-k}^{''}f_{k-l}^{'}f_l^{'} + 2\sum_{k=0}^{m-1}\sum_{l=0}^{k} f_{m-1-k}f_{k-l}f_l^{''}) - 16M\eta^3\sum_{k=0}^{m-1} f_{m-1-k}^{''}\theta_k^{'} \\
&+4\eta^3 f_{m-1}^{'''} - M\sum_{k=0}^{m-1}\sum_{l=0}^{k} f_{m-1-k}f_{k-l}^{''}\theta + 16\ E_2\eta\sum_{k=0}^{m-1}\sum_{l=0}^{k} f_{m-1-k}f_l^{''}(4f_{k-l}^{''} - \eta f_{k-l}^{''} + 4f_{k-l}^{'}) \\
&-32\ E_2\eta^3\sum_{k=0}^{m-1}\sum_{l=0}^{k} f_{m-1-k}^{'}f_{k-l}^{'}ff_l^{'''}, \qquad (5.26)
\end{aligned}
$$

$$
R_\theta(\eta) = \eta\theta_{m-1}^{''} + \theta_{m-1}^{'} + \mathrm{Re}\,\mathrm{Pr}\sum_{k=0}^{m-1} f_{m-1-k}\theta_k^{'}. \qquad (5.27)
$$

It is found that $f_m(\eta)$ and $\theta_m(\eta)$ can be written as

$$
\begin{aligned}
f_m(\eta) &= \sum_{n=0}^{m}\sum_{l=0}^{m} b_{m,n}^{'}\eta^{3n}e^{(2l+1)-(3n+1)\eta}, \\
\theta_m(\eta) &= \sum_{n=1}^{m}\sum_{l=0}^{m} c_{m,n}^{'}\eta^{3n}e^{2l+3n\eta}, \quad m \geq 0. \qquad (5.28)
\end{aligned}
$$

The solution thus can be defined as

$$
f(\eta) = \lim_{Q\to\infty}\left[\sum_{m=0}^{Q}\left(\sum_{n=0}^{m}\sum_{l=0}^{m} b_{m,n}^{'}\eta^{3n}e^{(2l+1)-(3n+1)\eta}\right)\right], \qquad (5.29)
$$

$$
\theta(\eta) = \lim_{Q\to\infty}\left[\sum_{m=0}^{Q}\left(\sum_{n=1}^{m}\sum_{l=0}^{m} c_{m,n}^{'}\eta^{3n}e^{2l+3n\eta}\right)\right]. \qquad (5.30)
$$

5.4 Series solutions for Vogel's model

Invoking Eq. (2.49), Eqs. (5.7) and (5.8) become

$$\begin{aligned}
&\frac{16}{3}\ E_2(\eta^2 f f' f''' - \eta^2 \left(f'\right)^2) + \frac{16}{3}\ E\eta_2(f f' f''' - 3\eta f \left(f''\right)^3 + 6\eta^2 f' f'') \\
&+ \left(4\eta^2(\frac{C}{C^*}(1 - \frac{A\theta}{B^2}) + E_1)) + 32\ E_2\eta \left(f\right)^2\right) f'' - 32\ E_2\eta^3 \left(f'\right)^2 f''' \\
&+4\eta^3 f'''(\frac{C}{C^*}(1 - \frac{A\theta}{B^2}) + E_1) + \frac{176}{3}\ E_2\eta^2 f''(f')^2 + 64\ E_2\eta f(f'')^2 \\
&+\frac{\mathrm{Re}\, C}{C^*}(\eta^2 - \frac{A\theta\eta^2}{B^2}) \left(f f'' - f'^2\right) - \frac{306}{3}\ E_2\eta^2 f f' f'' + 32\ E_2\eta f f' f'' \\
&-\frac{8}{3}\ E_2 f^2 f''\ - \frac{8AC}{B^2C^*}\eta^3 \frac{d\theta}{d\eta} f'' - \frac{352}{3}\ E_2\eta^3 f'(f'')^2 = 0, \qquad (5.31)
\end{aligned}$$

$$\eta\theta'' + (1 + \mathrm{Re}\,\mathrm{Pr}\, f)\,\theta' = 0. \qquad (5.32)$$

The solution of this case is straightforward written as.

$$\begin{aligned}
f_m(\eta) &= \sum_{n=0}^{m}\sum_{l=0}^{m} b''_{m,n}\eta^{3n} e^{(2l+1)-(3n+1)\eta}, \qquad (5.33) \\
\theta_m(\eta) &= \sum_{n=1}^{m}\sum_{l=0}^{m} c''_{m,n}\eta^{3n} e^{2l-3n\eta}, \quad m \geq 0,
\end{aligned}$$

where $b''_{m,n}$ and $c''_{m,n}$ are constants.

5.5 Graphical results and discussion

In order to report the effects of sundry parameters in the present investigation we plotted Figs. 5.3 to 5.11. Fig. 5.1 is prepared to see the convergence region for velocity for Reynolds' model. Fig. 5.2 is prepared to highlight the convergence region for temperature for Reynolds' model. Fig. 5.3 exhibits velocity profile for Re for Reynolds' model. It can be seen that velocity decreases as Re increases. Fig. 5.4 gives temperature profile for Pr for Reynolds' model. The temperature profiles for air ($\mathrm{Pr} = 0.7$) and for water ($\mathrm{Pr} = 7$) can be observed here. The temperature profile decreases from 1 to zero as η increases from 1 to ∞. The fluid temperature depends upon the distance from surface of the tube. The fluid temperature attains maximum value at the surface of the tube. It is to note that temperature profile decreases with increase

in Pr. In Fig. 5.5 temperature profile for Re for Reynolds' model can be seen.

Fig. 5.6 presents velocity profile for C for Vogel's model. With the increase of pressure gradient the fluid particles are accelerated in axial direction. Since particles are forced in the same direction as that of motion of fluid and movement of inner cylinder, ultimately the velocity of the fluid rises. That is what we are observing in Fig. 5.6. Effects of Re on velocity profile for Vogel's model are displayed in Fig. 5.7. The velocity decreases as we increase the values of Re .

Fig. 5.8 reveals velocity profile for E_1 for Vogel's model. The velocity field decreases as we increase the values of E_1. Temperature distribution for E_2 is displayed in Fig. 5.9. It is noted that temperature decreases with increase in E_2. The temperature decreases from 1 to zero as the fluid gets away from outer surface of cylinder. Maximum temperature is attained at the surface of the tube. Temperature distribution for Pr is shown in Fig. 5.10. It is observed that the temperature decreases with increase in Pr . As we have seen in case of E_2, temperature decreases from 1 to zero as the fluid gets away from outer surface of cylinder. Maximum temperature is attained at the surface of the tube. Fig. 5.11 gives temperature profile for Re for Vogel's model. It can be seen that temperature decreases with increase in Re.

5.6 Conclusions

In this chapter, we have investigated analytically the heat transfer flow of an Eyring-Powell model fluid due to a stretching cylinder. Effects of the various parameters such as Re, E_2, M, C, A, E_1 and Pr are examined. It is concluded that:

1. The velocity decreases from 1 to zero as η increases from 1 to ∞.
2. Temperature decreases from 1 to zero as η increases from 1 to ∞.
3. The similarity profile $f(\eta)$ increases from zero.
4. The similarity profile $f'(\eta)$ decreases from unity.
5. The thermal boundary layer decreases with increased Prandtl number and Reynolds number.

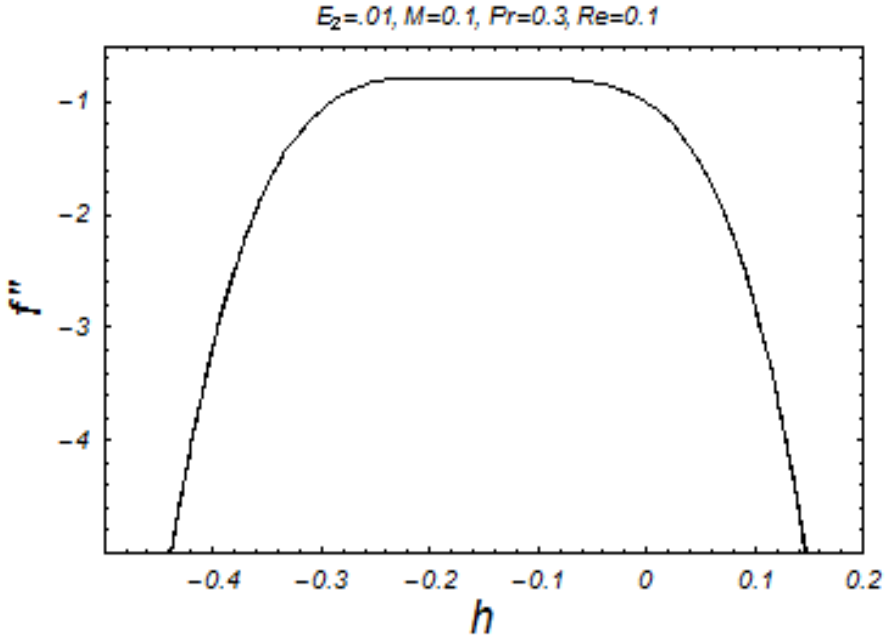

Fig. 5.1: h-curve for velocity for Reynolds' model.

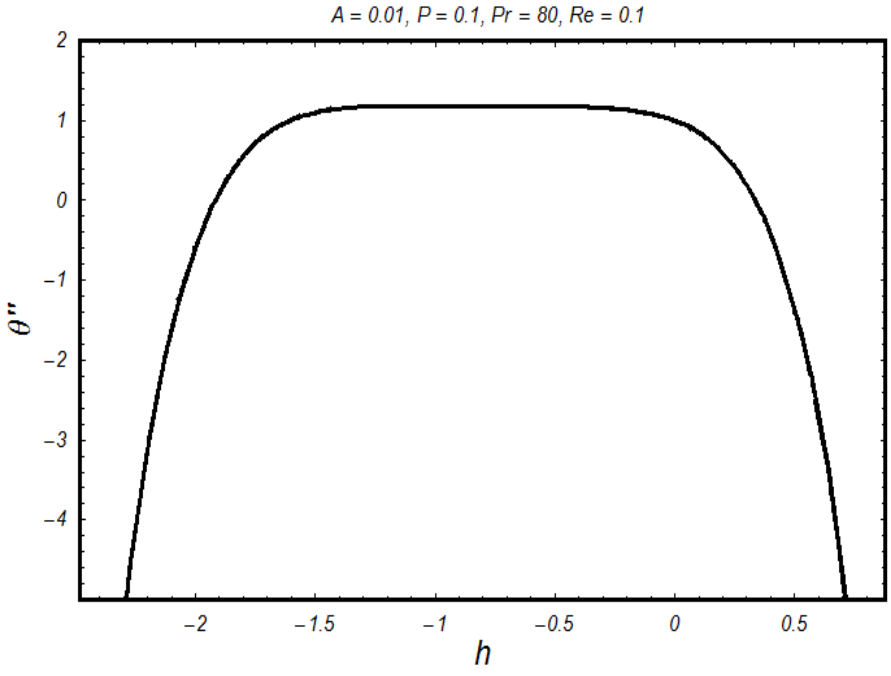

Fig. 5.2: h-curve for temperature for Reynolds' model.

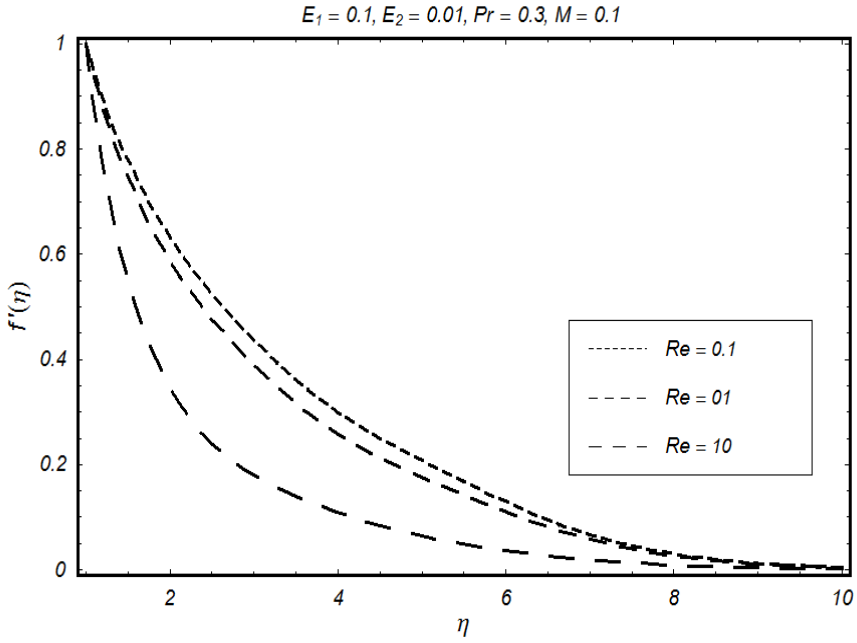

Fig. 5.3: Velocity distribution for Re for Reynolds' model.

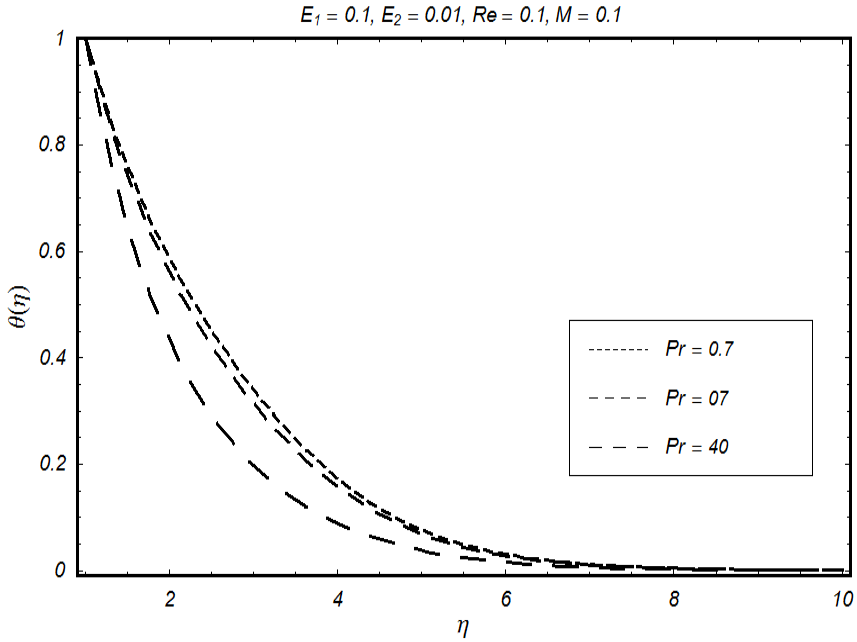

Fig. 5.4: Temperature distribution for Pr for Reynolds' model.

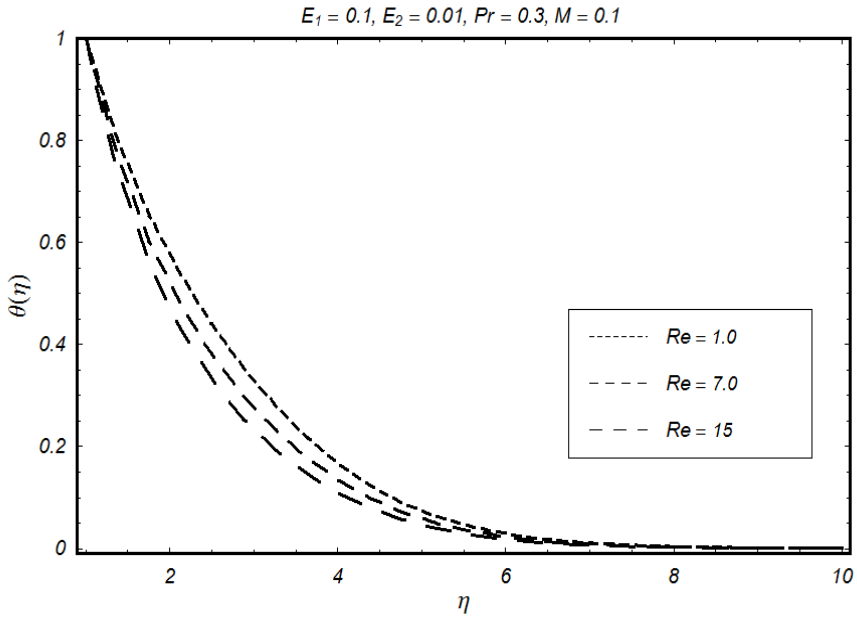

Fig. 5.5: Temperature distribution for Re for Reynolds' model

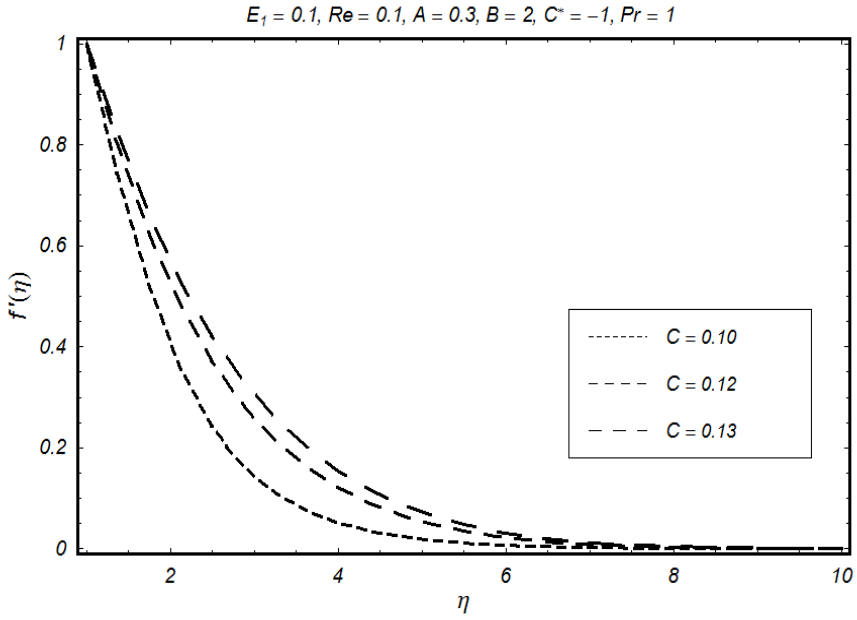

Fig. 5.6: Velocity distribution for C for Vogel's model.

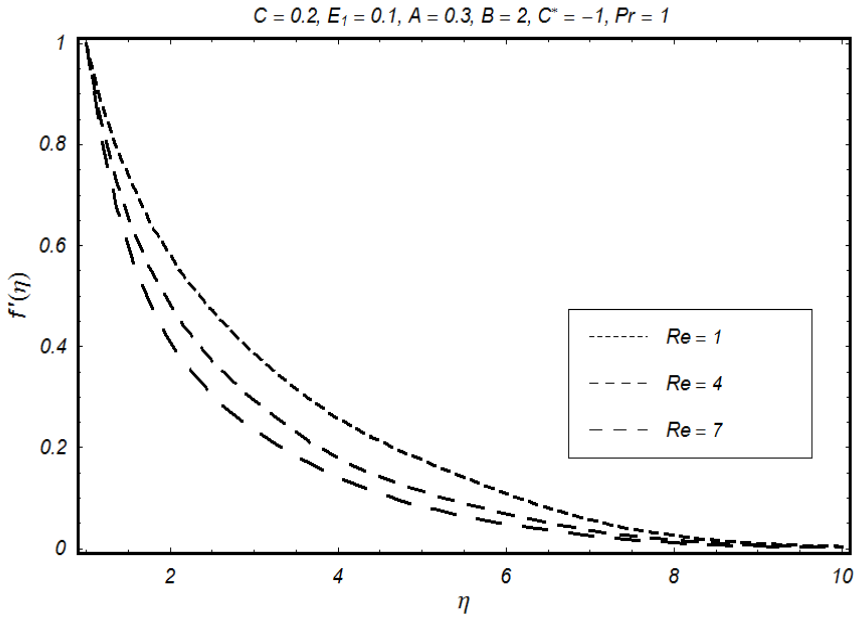

Fig. 5.7: Velocity distribution for Re for Vogel's model.

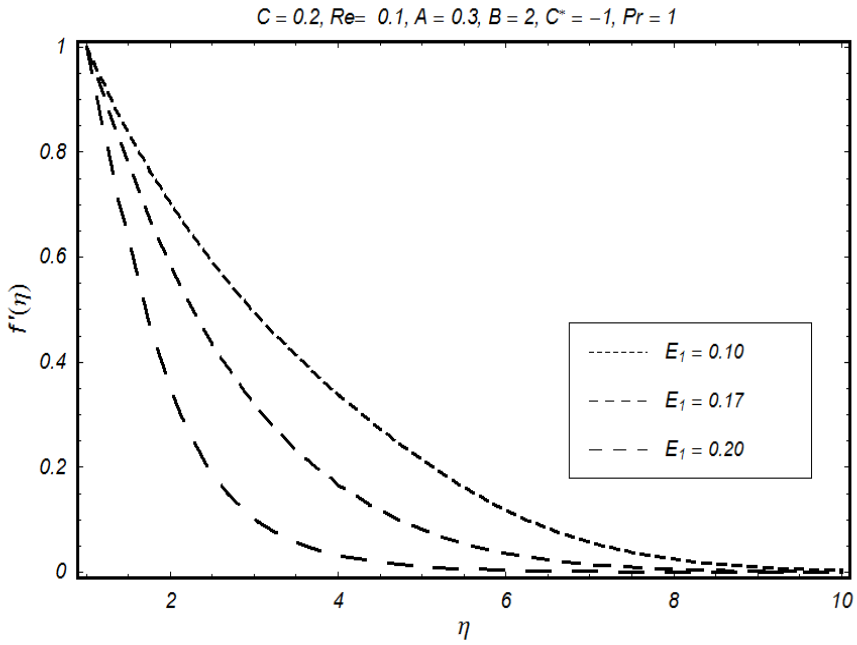

Fig. 5.8: Velocity distribution for E_1 for Vogel's model.

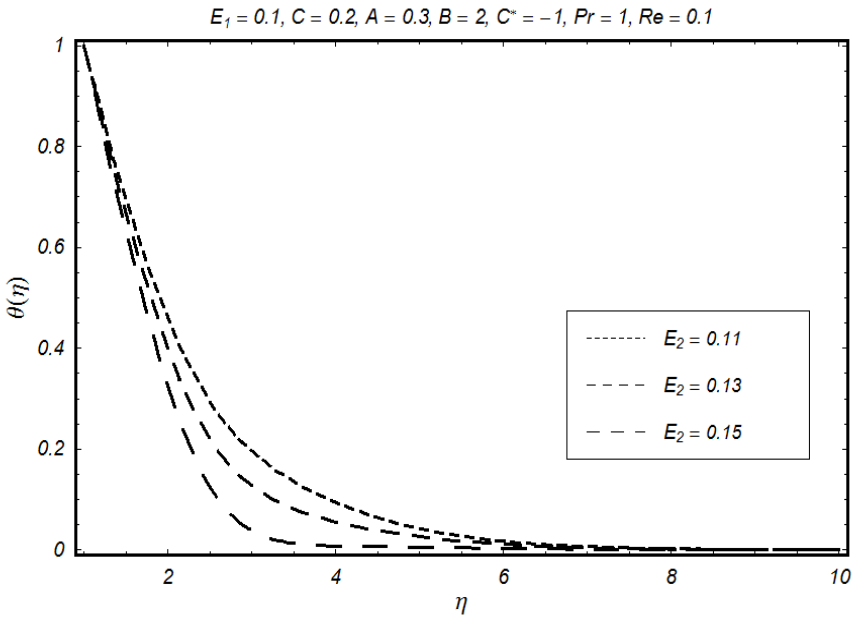

Fig. 5.9: Temperature distribution for E_2 for Vogel's model.

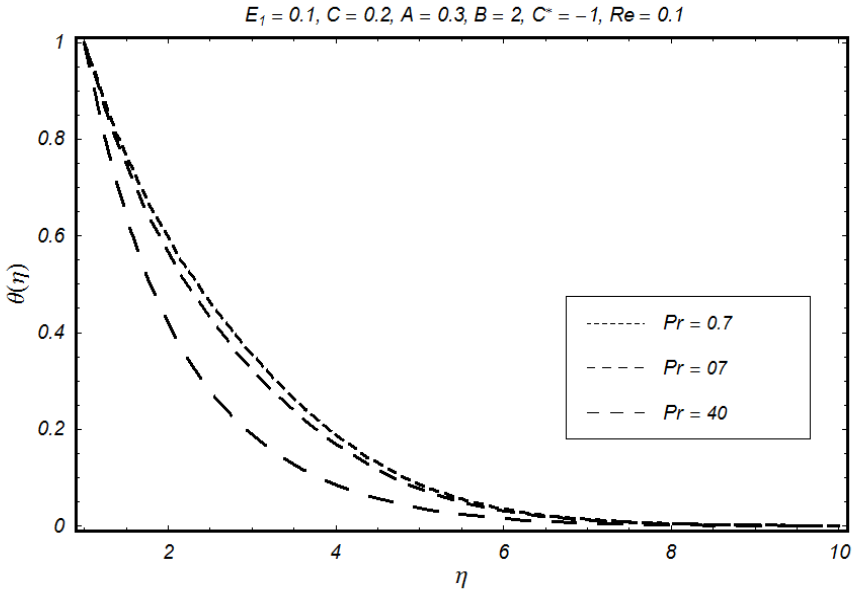

Fig. 5.10: Temperature distribution for Pr for Vogel's model.

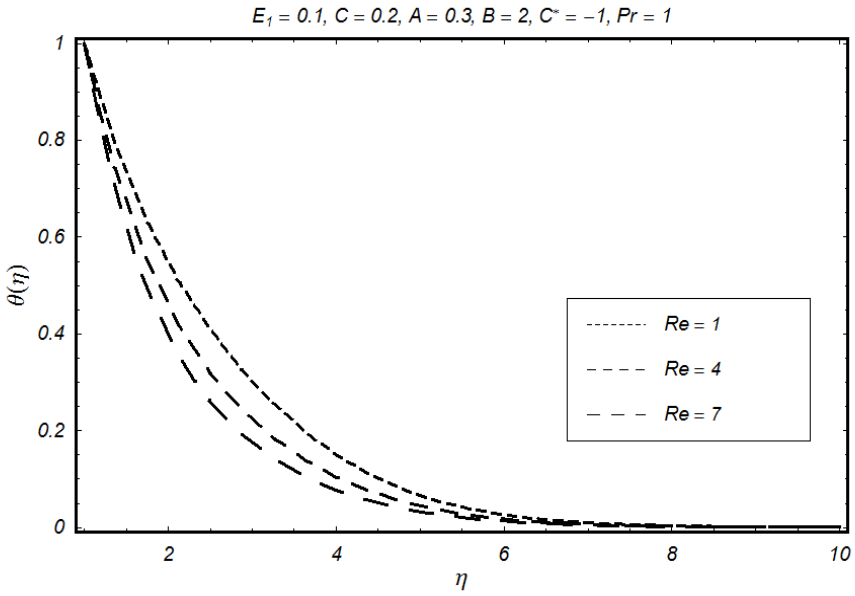

Fig. 5.11: Temperature distribution for Re for Vogel's model.

Chapter 6

Boundary layer flow of a Walter's B fluid due to a stretching cylinder with temperature dependent viscosity

6.1 Introduction

This chapter presents study of boundary layer flow of a Walter's B fluid due to a stretching cylinder with temperature dependent variable viscosity. The effects of heat transfer are also discussed. The governing equations have been transformed into non-linear ordinary differential equations with the help of a suitable similarity transformation and then the reduced nonlinear boundary value problem is solved analytically by a powerful technique homotopy analysis method. Two models are considered to analyze effects of variable viscosity on two dimensional steady boundary layer flow. For the validity of homotopy analysis method solution h-curves are plotted. The graphical results are obtained to gauge the effects of various parameters intrinsic to the problem.

6.2 Description of the problem

The governing equations are

$$\frac{\partial(rw)}{\partial z}+\frac{\partial(ru)}{\partial r}=0, \tag{6.1}$$

$$\begin{aligned}\rho(u\tfrac{\partial u}{\partial r}+w\tfrac{\partial u}{\partial z}) &= \tfrac{2\eta_0}{r}\tfrac{\partial u}{\partial r}-\tfrac{\partial}{\partial z}(u(k_0\tfrac{\partial^2 u}{\partial r\partial z}+k_0\tfrac{\partial^2 w}{\partial r^2})-wk_0(\tfrac{\partial^2 u}{\partial z^2}+\tfrac{\partial^2 w}{\partial z\partial r}))\\ &+\frac{\partial}{\partial r}(2\eta_0\frac{\partial u}{\partial r}-2k_0u\frac{\partial^2 u}{\partial r^2}-2k_0w\frac{\partial^2 u}{\partial z\partial r})-2k_0\frac{u^2}{r^3}-\eta_0\frac{\partial^2 w}{\partial z\partial r}\frac{2k_0}{r^2}\frac{\partial u}{\partial z}\\ &-\frac{2wk_0}{r}\frac{\partial^2 u}{\partial z\partial r}-\eta_0\frac{\partial^2 u}{\partial z^2}-\frac{2k_0}{r}u\frac{\partial^2 u}{\partial r^2}-2\eta_0\frac{u}{r^2},\end{aligned} \tag{6.2}$$

$$\begin{aligned}\rho(u\tfrac{\partial w}{\partial r}+w\tfrac{\partial w}{\partial z}) &= -\tfrac{k_0u}{r}(\tfrac{\partial^2 u}{\partial r\partial z}+\tfrac{\partial^2 w}{\partial r^2})-\tfrac{k_0w}{r}\tfrac{\partial^2 u}{\partial z^2}+\tfrac{k_0w}{r}\tfrac{\partial^2 w}{\partial z\partial r}\\ &-k_0\frac{\partial}{\partial r}(u(\frac{\partial^2 u}{\partial r\partial z}+\frac{\partial^2 w}{\partial r^2})-(w\frac{\partial^2 u}{\partial z^2}+w\frac{\partial^2 w}{\partial z\partial r}))+\eta_0\frac{\partial^2 u}{\partial r\partial z}\\ &+\eta_0(\frac{\partial^2 u}{\partial z^2}+\frac{\partial^2 w}{\partial z\partial r})+\eta_0\frac{\partial w^2}{\partial r^2}-2k_0\frac{\partial}{\partial z}(u\frac{\partial^2 w}{\partial r\partial z}-w\frac{\partial^2 w}{\partial z^2})\\ &+\frac{\eta_0}{r}(\frac{\partial u}{\partial z}+\frac{\partial w}{\partial r}),\end{aligned} \tag{6.3}$$

$$u\frac{\partial T}{\partial r}+w\frac{\partial T}{\partial z}=\alpha_3(\frac{\partial^2 T}{\partial r^2}+\frac{1}{r}\frac{\partial T}{\partial r}). \tag{6.4}$$

The boundary conditions are defined through Eq. 5.5.Introducing the following similarity transformations

$$\eta=\left(\frac{r}{a}\right)^2, u=\frac{-caf(\eta)}{\sqrt{\eta}},\ w=2czf'(\eta),\ \theta=\frac{T-T_\infty}{T_w-T_\infty}. \tag{6.4a}$$

The dimensionless problem which can describe the boundary flow is given by

$$\begin{aligned}&\eta_0\,\mathrm{Re}\,\eta^2\left(ff''-f'^2\right)+2\eta_0\eta\left(f''+f'''\right)+4\zeta_5\eta ff'''+2\zeta_5\eta f''f'''\\ &-2\zeta_5\eta f'f''+8\eta\tfrac{\partial\mu}{\partial\eta}f''+2\zeta_5(f'')^2+4\zeta_5\eta^2 ff''''-\zeta_5\eta ff'' = 0,\end{aligned} \tag{6.5}$$

$$\eta\theta''+(1+\mathrm{Re}\,\mathrm{Pr}\,f)\,\theta'=0, \tag{6.6}$$

where

$$\mathrm{Re}=\frac{ca^2}{\nu}\ ,\ \mathrm{Pr}=\frac{\nu}{\alpha_3},\ \zeta_5=\frac{k_0c}{\eta_0^*},\ Ec=\frac{z^2c^2}{c_p\,(T_w-T_\infty)}. \tag{6.7}$$

The boundary conditions in dimensionless form are

$$f(1)=0,\ f'(1)=1,\ \theta(1)=1,\ f'(\infty)\ \to 0,\ \theta(\infty)\to 0. \tag{6.8}$$

6.3 Solution of the problem

Reynolds and Vogel's models of viscosity are considered for the current analysis, both the models are defined in previous chapters, therefore to avoid repetition the governing equations for Walter's B fluid for both the viscosity models are directly written as

(For Reynolds model)

$$\begin{aligned}
&-\zeta_5\eta f f''+2\eta f''+2\eta f'''+2\zeta_5\eta f''f'''+4\zeta_5\eta f f'''+4\zeta_5\eta^2 f f''''-8\eta M\frac{d\theta}{d\eta}f''\\
&+\mathrm{Re}\,\eta^2 f f''+\mathrm{Re}\,\eta^2 f'^2-\mathrm{Re}\,\eta^2 M\theta f f''-\mathrm{Re}\,\eta^2 M\theta f'^2+2A(f'')^2-2M\theta\eta f''\\
&-2\zeta_5\eta f' f''-2M\theta\eta f''' \;=\; 0,
\end{aligned} \tag{6.9}$$

$$\eta\theta''+(1+\mathrm{Re}\,\mathrm{Pr}\,f)\,\theta'=0, \tag{6.10}$$

(For Vogel's model)

$$\begin{aligned}
&\frac{2\eta C}{C^*}f''+\frac{2\eta C}{C^*}f'''-\frac{2\eta AC\theta}{C^*B^2}f''-\zeta_5\eta f f''+\frac{\mathrm{Re}\,\eta^2 C}{C^*}f f''-\frac{2\eta AC\theta}{C^*B^2}f'''\\
&-2\zeta_5\eta f' f''+2\zeta_5\eta f''f'''-\frac{AC\,\mathrm{Re}\,\eta^2\theta}{C^*B^2}f'^2-\frac{\mathrm{Re}\,\eta^2 C}{C^*}f'^2-\frac{8A\eta C}{C^*B^2}\frac{d\theta}{d\eta}f''\\
&+4\zeta_5\eta^2 f f''''-\tfrac{AC\,\mathrm{Re}\,\eta^2\theta}{C^*B^2}f f''+2\zeta_5(f'')^2+4\zeta_5\eta f f''' \;=\; 0,
\end{aligned} \tag{6.11}$$

Using the initial guesses and linear operators defined in Eqs. (5.13) to (5.16), HAM solution for both models can be written as

$$\begin{aligned}
f_m(\eta) &= \sum_{n=0}^{2m}\sum_{l=0}^{m} b'''_{m,n}\eta^n e^{l-n\eta},\\
\theta_m(\eta) &= \sum_{n=1}^{m}\sum_{l=0}^{m} c'''_{m,n}\eta^{2(n-1)}e^{l-(2n+1)\eta},\quad m\geq 0,
\end{aligned} \tag{6.12}$$

$$
\begin{aligned}
f_m(\eta) &= \sum_{n=0}^{2m}\sum_{l=0}^{m} b'''_{m,n}\eta^n e^{l-n\eta}, \\
\theta_m(\eta) &= \sum_{n=1}^{m}\sum_{l=0}^{m} c'''_{m,n}\eta^{2(n-1)} e^{l-(2n+1)\eta}, \quad m \geq 0,
\end{aligned} \tag{6.13}
$$

where $b'''_{m,n}, b''''_{m,n}, c'''_{m,n}$ and $c''''_{m,n}$ are constants.

6.4 Graphical results and discussion

In order to report the convergence of the obtained series solutions and the effects of sundry parameters in the present investigation we plotted Figs. 6.1 to 6.16. Figs. 6.1 to 6.2 are prepared to see the convergence region. Fig. 6.1 is plotted to see the convergence region for velocity for Reynolds' model. Fig. 6.2 is prepared to highlight the convergence region for temperature for Reynolds' model. Fig. 6.3 shows the velocity variation for Ec for Reynolds' model. It can be seen that velocity increases as Ec increases. Fig. 6.4 is displayed to see the velocity variation for Reynolds' model for M, it is depicted that velocity decreases as M increases. Fig. 6.5 presents velocity distribution for Pr for Reynolds' model. The velocity increases with increase in Pr .

Fig. 6.6 reveals velocity profile for Re for Vogel's model. The velocity decreases with increase in Re . Fig. 6.7 shows the temperature variation for ζ_5 for Reynolds' model. It can be seen that velocity decreases as ζ_5 increases. Fig. 6.8 gives the temperature variation for M for Reynolds' model. It can be seen that temperature decreases as M increases. Fig. 6.9 is displayed to see the velocity variation for Vogel's model for Ec. It can be seen that velocity decreases with increase in Ec. Fig. 6.10 exhibits the velocity variation for Vogel's model for Pr. It is observed that velocity decreases with increase in Pr . Fig. 6.11 depicts velocity profile for Re for Vogel's model. It is noted that velocity increases with increase in Re .

Fig. 6.12 presents temperature profile for ζ_5 for Vogel's model. The temperature decreases with increase in ζ_5. Fig. 6.13 reveals temperature profile for Ec for Vogel's model. It is depicted that temperature decreases as Ec increases. Fig. 6.14 is plotted to see the temperature profile variation for C for Vogel's model. Fig. 6.15 reveals temperature profile for A for Vogel's model. It is seen that temperature increases as A increases. The relation (2.49) explains the fact that

viscosity decreases with rise of A. When we increase A, viscous forces become weaker. The fluid particles face less opposition. Ultimately, the velocity of fluid particles increases. This increase in the velocity is responsible for enhancement in average kinetic energy of the particles. As temperature measures the kinetic energy of the system. Consequently, temperature of fluid rises up.

Fig. 6.16 reveals temperature profile for Pr for Vogel's model. It is seen that temperature decreases as Pr increases. The temperature decreases from 1 to zero as the fluid gets away from outer surface of cylinder. Maximum temperature is attained at the surface of the tube.

6.5 Conclusions

In this chapter, we have investigated analytically the heat transfer flow of a Walter's B fluid due to a stretching cylinder. The highly non-linear problem is then solved by homotopy analysis method. Effects of the various parameters are examined. It is concluded :

1. The velocity profile decreases with increase in Re, ζ_5 and M in case of Reynolds' model and it decreases with increase in Ec and Pr.

2. In Reynolds' model the temperature profile decreases with increase in ζ_5 and M.

3. Reynold number Re, ζ_5 and A lead to increase the velocity profile in Vogel's model where as this profile decreases with increase in Ec and Pr. It means effects of Ec and prandtl number on velocity are almost similar in both viscosity models.

4. The temperature profile increases with increase in A. This profile decreases with rise in Ec, ζ_5 and prandtl number in Vogel's model.

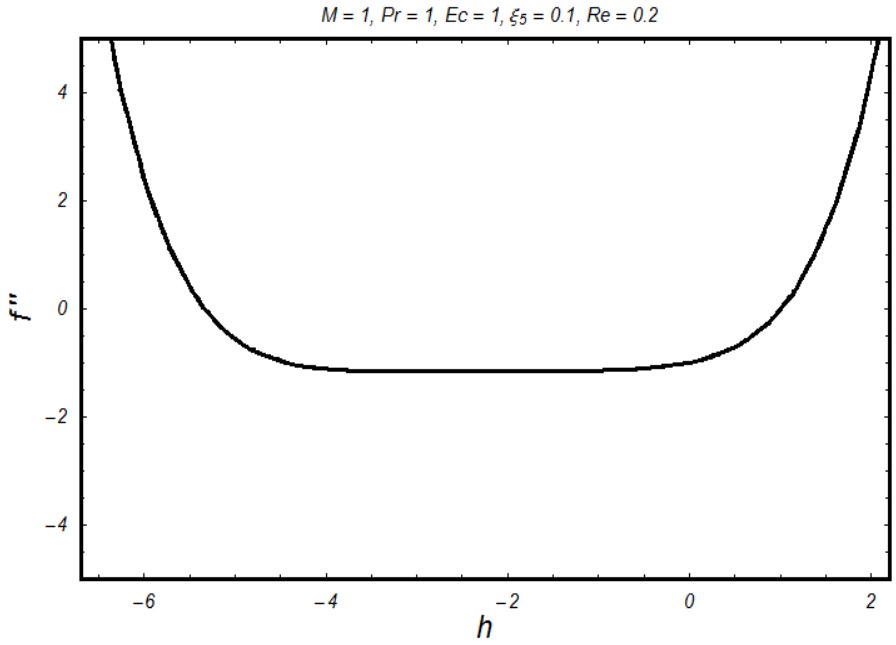

Fig. 6.1: h-curve for velocity profile for Reynolds' model.

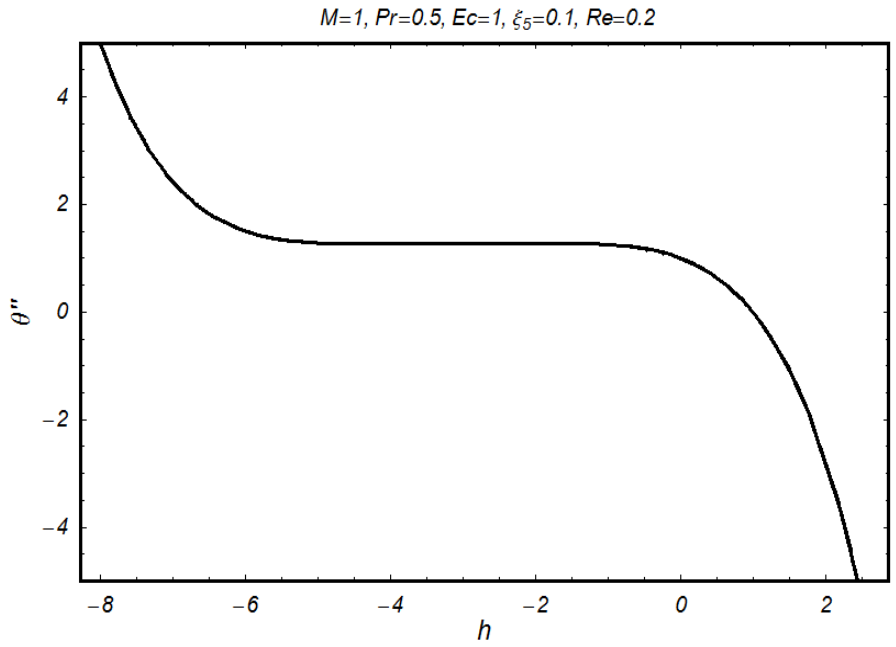

Fig. 6.2: h-curve for temperature profile for Reynolds' model.

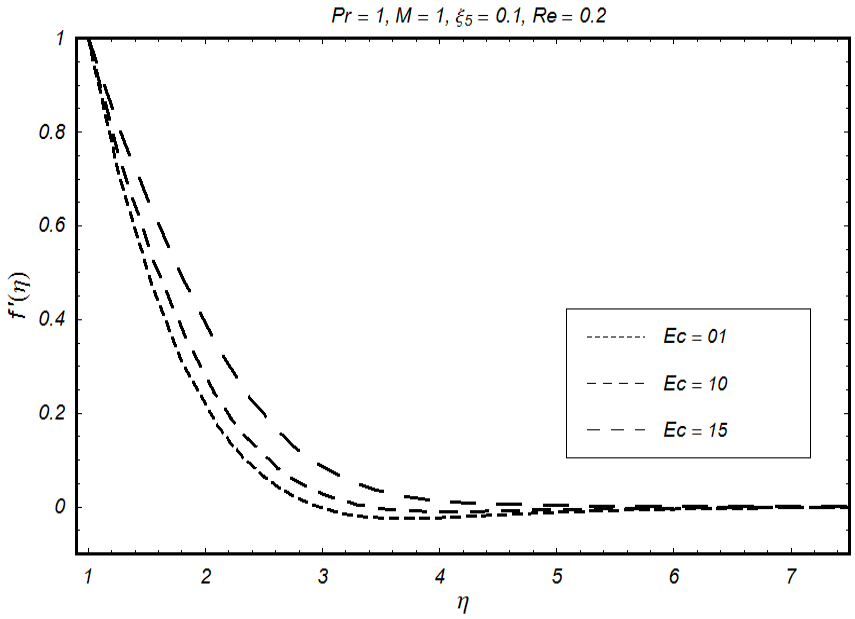

Fig. 6.3: Velocity distribution for Ec for Reynolds' model.

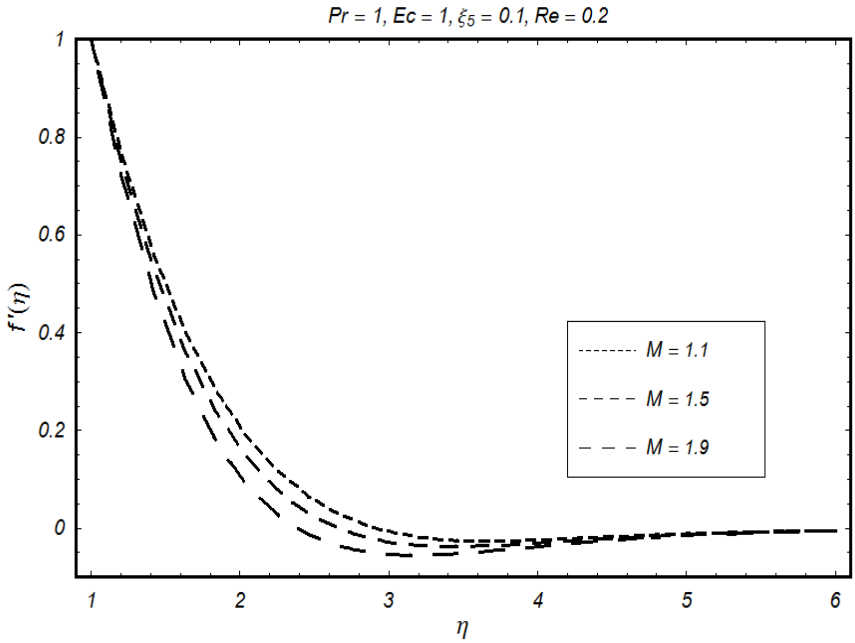

Fig. 6.4: Velocity distribution for M for Reynolds' model.

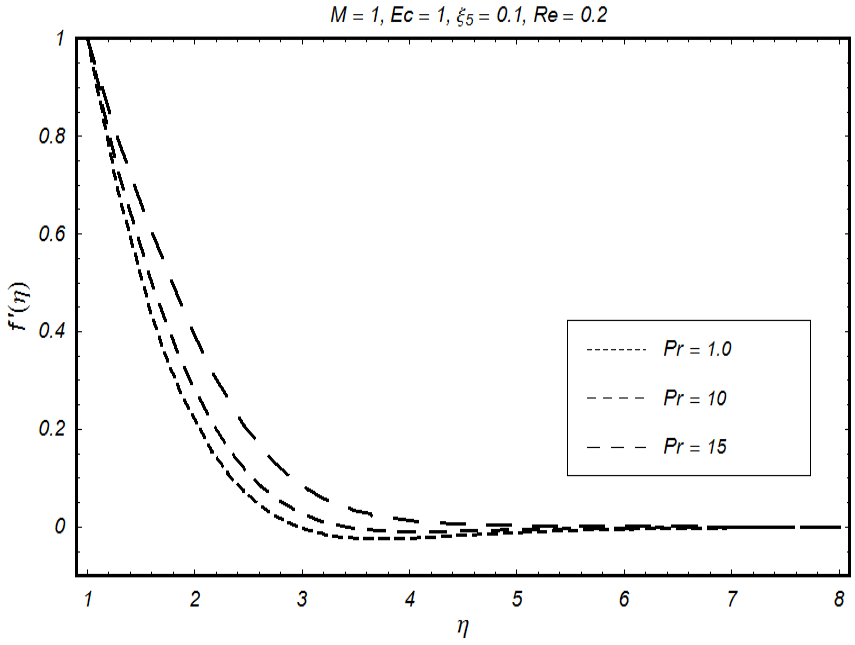

Fig. 6.5: Velocity distribution for Pr for Reynolds' model.

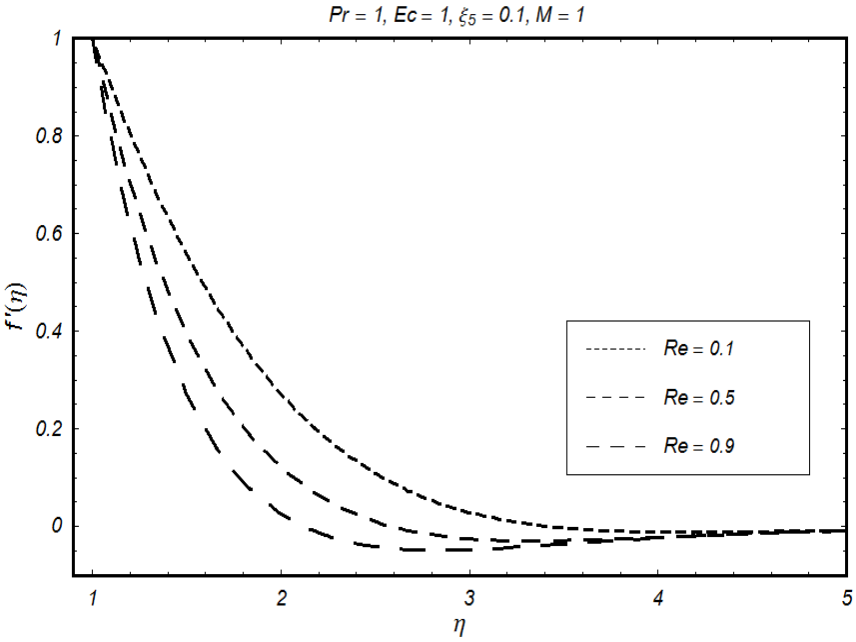

Fig. 6.6: Velocity distribution for Re for Reynolds' model.

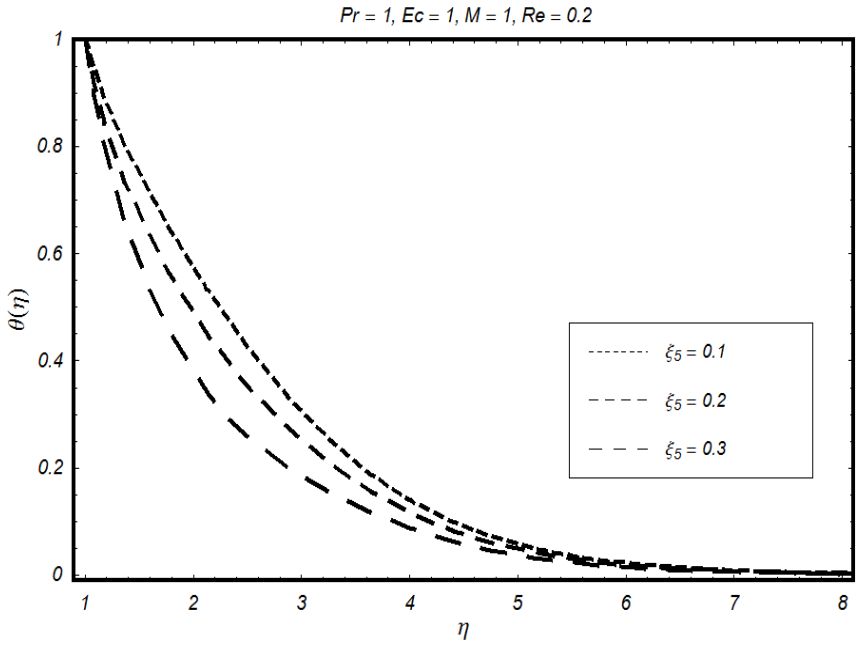

Fig. 6.7: Temperature distribution for ζ_5 for Reynolds' model.

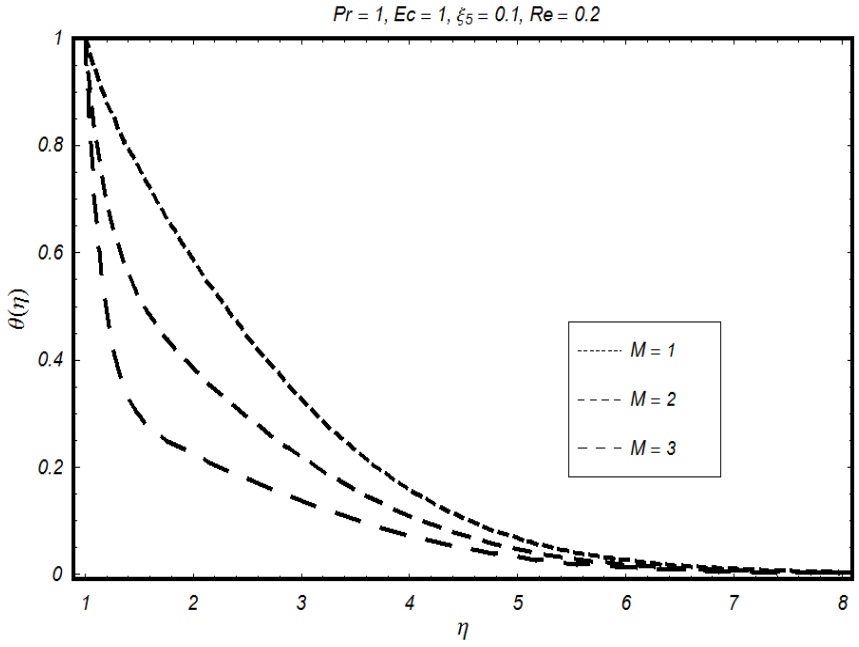

Fig. 6.8: Temperature distribution for M for Reynolds' model.

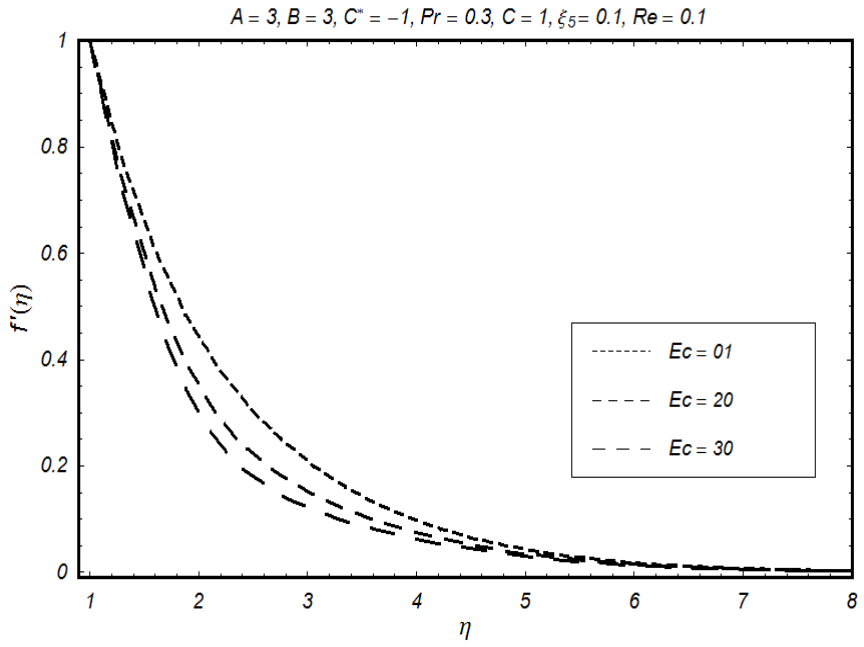

Fig. 6.9: Velocity distribution for Ec for Vogel's model.

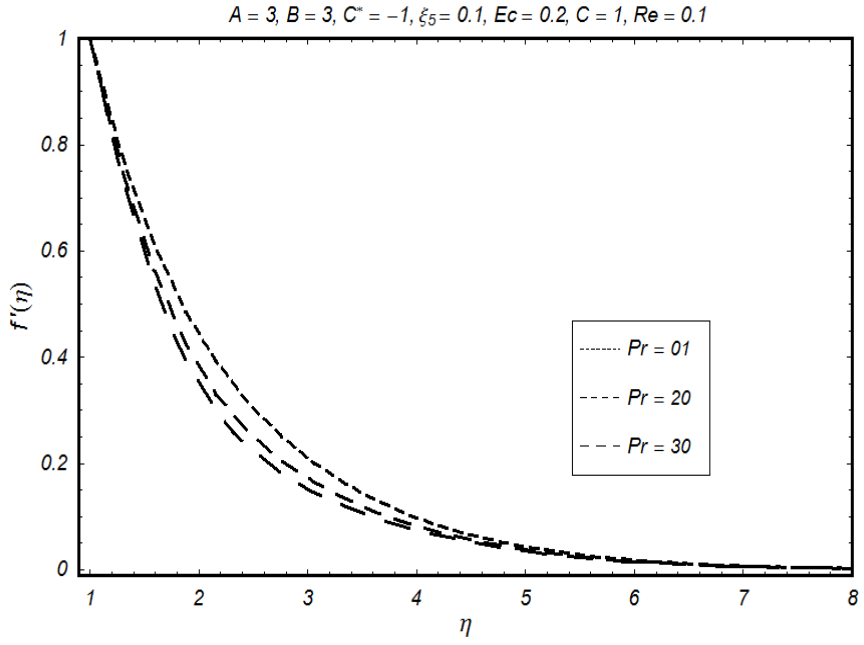

Fig. 6.10: Velocity distribution for Pr for Vogel's model.

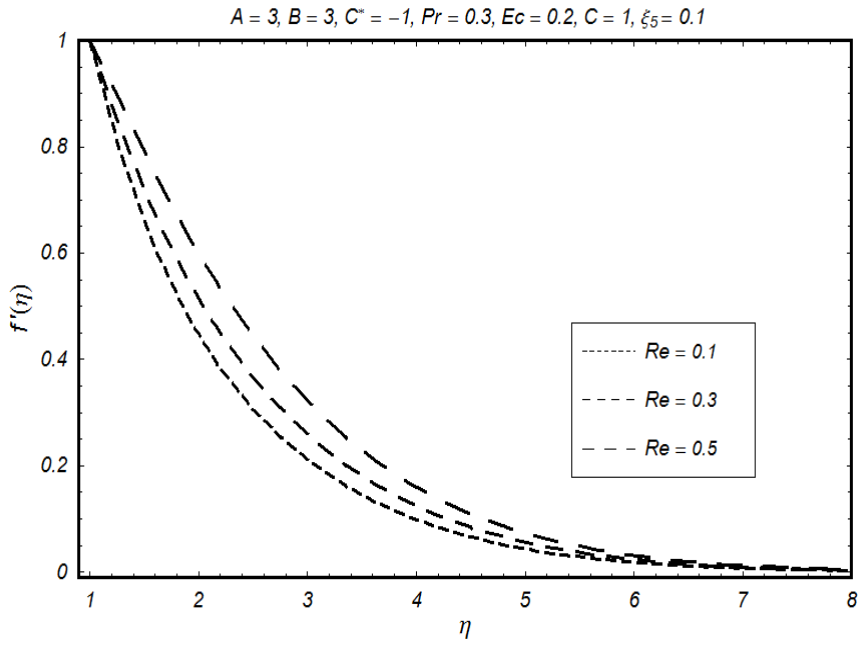

Fig. 6.11: Velocity distribution for Re for Vogel's model.

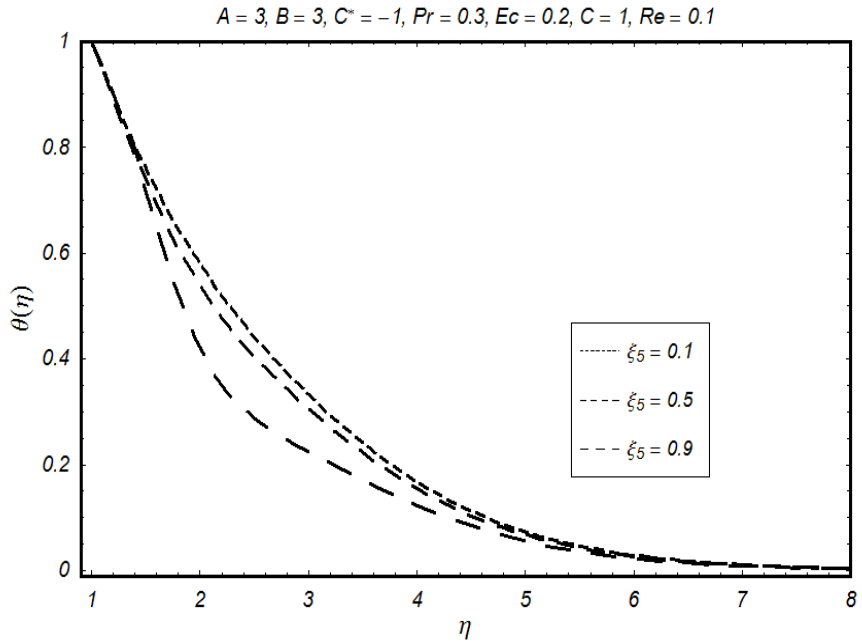

Fig. 6.12: Temperature distribution for ζ_5 for Vogel's model.

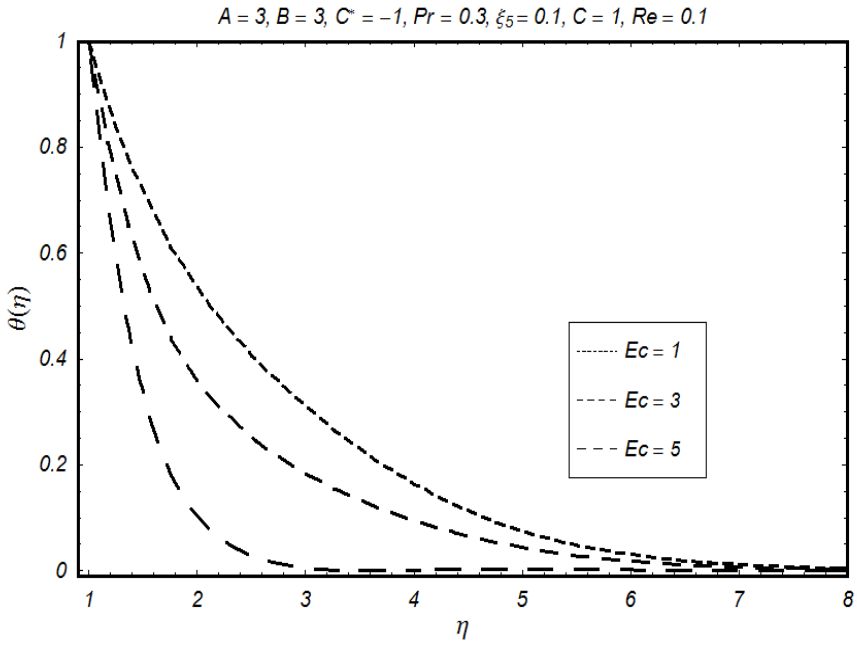

Fig. 6.13: Temperature distribution for Ec for Vogel's model.

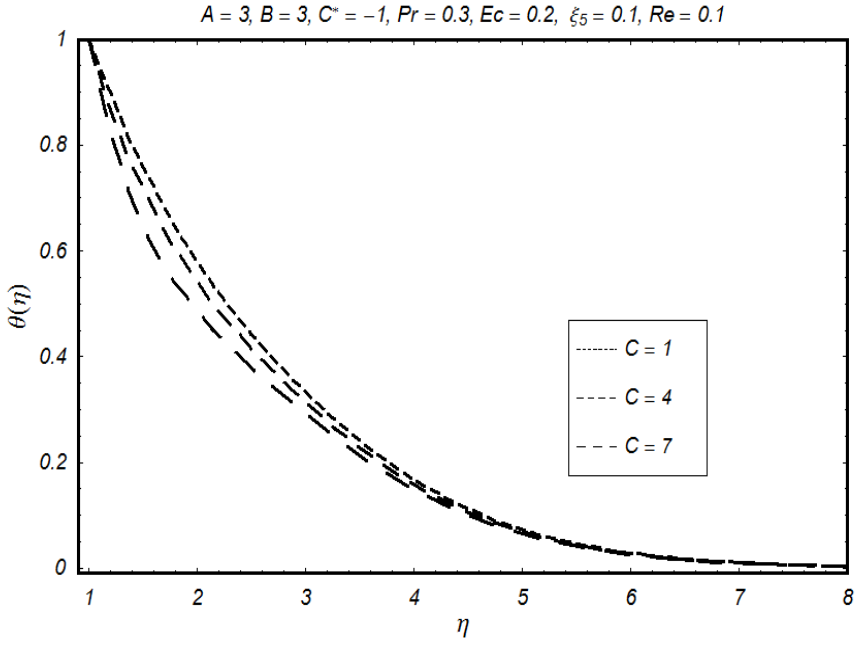

Fig. 6.14: Temperature distribution for C for Vogel's model.

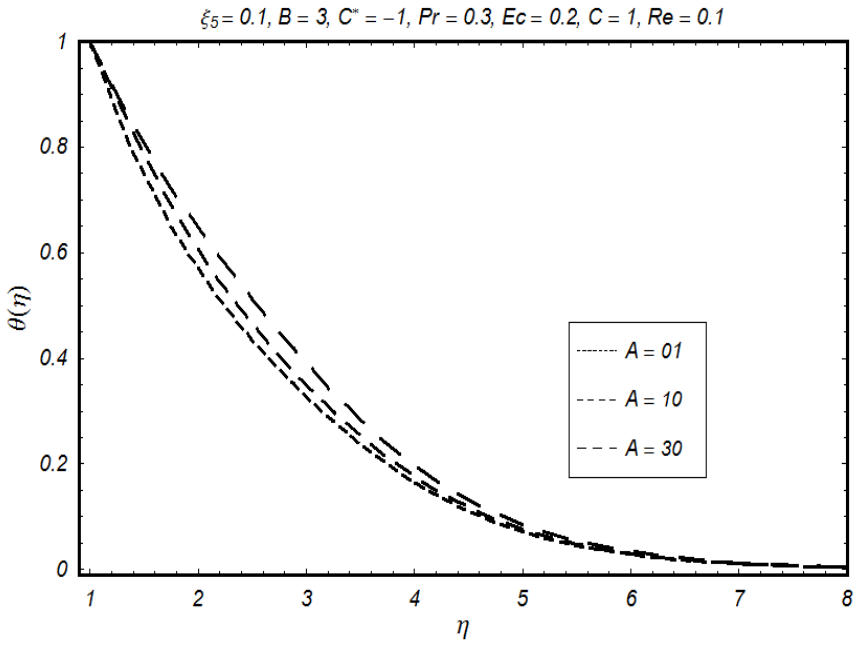

Fig. 6.15: Temperature distribution for A for Vogel's model.

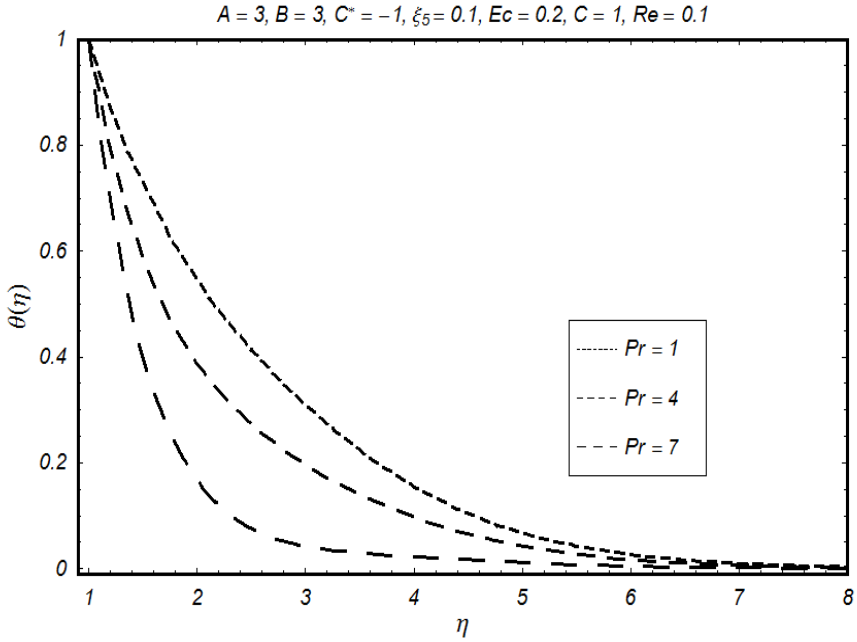

Fig. 6.16: Temperature distribution for Pr for Vogel's model.

Chapter 7

Boundary layer flow of a hyperbolic tangent fluid due to a stretching cylinder with temperature dependent viscosity

7.1 Introduction

The objective of this chapter is to present investigation consisting of an analytical solution of a steady boundary layer flow of a hyperbolic tangent fluid due to a stretching cylinder with temperature dependent variable viscosity. The two dimensional boundary layer equations of hyperbolic tangent fluid are modelled in cylindrical coordinates. The governing partial differential equations have been transformed into non-linear ordinary differential equations with help of usual similarity transformations. Non-linear ordinary differential equations attained in this way are then solved by a powerful technique homotopy analysis method. To highlight effects of variable viscous properties on boundary layer flow two models of variable viscosity, namely, Reynolds' and Vogel's model are taken into account. The h-curves are drawn in order to check convergence. The effects of emerging parameters intrinsic to the problem are studied by plotting graphs.

7.2 Description of the problem

The governing equations are

$$\frac{\partial(rw)}{\partial z}+\frac{\partial(ru)}{\partial r}=0, \tag{7.1}$$

$$\begin{aligned}\rho(u\tfrac{\partial u}{\partial r}+w\tfrac{\partial u}{\partial z}) &= -\tfrac{2\eta_0}{r}\tfrac{\partial u}{\partial r}\left[1+n_2(\Gamma\bar{\dot{\gamma}}-1)\right]-2\eta_0\tfrac{\partial^2 u}{\partial r^2}\left[1+n_2(\Gamma\bar{\dot{\gamma}}-1)\right]\\ -\eta_0\left[1+n_2(\Gamma\bar{\dot{\gamma}}-1)\right](&\frac{\partial^2 w}{\partial z\partial r}+\frac{\partial^2 u}{\partial z^2}+\frac{2u}{r}),\end{aligned} \tag{7.2}$$

$$\text{where}\quad \bar{\dot{\gamma}}=\frac{1}{\sqrt{2}}\sqrt{2\left((\frac{\partial u}{\partial r})^2+\frac{u^2}{r^2}+(\frac{\partial w}{\partial z})^2\right)+\left(\frac{\partial u}{\partial z}+\frac{\partial w}{\partial r}\right)^2} \tag{7.3}$$

$$u\frac{\partial T}{\partial r}+w\frac{\partial T}{\partial z}=\alpha_3(\frac{\partial^2 T}{\partial r^2}+\frac{1}{r}\frac{\partial T}{\partial r}). \tag{7.4}$$

The boundary conditions are defined through Eq. 5.5. Introducing the following similarity transformations

$$\eta=\left(\frac{r}{a}\right)^2, u=\frac{-caf(\eta)}{\sqrt{\eta}},\ w=2czf'(\eta),\ \theta=\frac{T-T_\infty}{T_w-T_\infty}. \tag{7.4a}$$

The dimensionless problem which can describe the boundary flow is given by

$$2\eta\mu(1-n_2)\left(\eta f'''+f''\right)+\mathrm{Re}\,\eta\left(ff''-f'^2\right)+4\sqrt{2}n_2We\mu\eta f''\left(2f'''+f''\right)=0, \tag{7.5}$$

$$\eta\theta''+(1+\mathrm{Re}\,\mathrm{Pr}\,f)\,\theta'=0, \tag{7.6}$$

where

$$We=\frac{\Gamma c}{a},\ \mathrm{Re}=\frac{ca^2}{2\nu}\ ,\ \mathrm{Pr}=\frac{\nu}{\alpha_3}. \tag{7.7}$$

The boundary conditions in dimensionless form are

$$f(1)=0,\ f'(1)=1,\ \theta(1)=1,\ f'(\infty)\ \to 0,\ \theta(\infty)\to 0. \tag{7.8}$$

7.3 Solution of the problem

The governing equations for hyperbolic tangent fluid for Reynolds' and Vogel's models of viscosity are directly written as

(For Reynolds' model)

$$2\eta\left(1-n_2\right)\left(\eta f'''+f''\right)-2M\theta\eta\left(1-n_2\right)\left(\eta f'''+f''\right)+\mathrm{Re}\,\eta\left(ff''-f'^2\right)$$
$$+4\sqrt{2}n_2\eta We f''\left(2f'''+f''\right)-4\sqrt{2}n_2\eta WeM\theta\left(2f'''f''+(f'')^2\right)=0, \tag{7.9}$$

(For Vogel's model)

$$\frac{2C\left(1-n_2\right)\eta}{C^*}\left(\eta f'''+f''\right)-\frac{2A\theta C\left(1-n_2\right)\eta}{B^2C^*}\left(\eta f'''+f''\right)+\mathrm{Re}\,\eta\left(ff''-f'^2\right)$$
$$+\frac{4\sqrt{2}n_2\eta CWe}{C^*}f''\left(2f'''+f''\right)-\frac{4\sqrt{2}An_2\eta C\theta We}{B^2C^*}\left(2f'''f''+(f'')^2\right)=0, \tag{7.10}$$

$$\eta\theta''+\left(1+\mathrm{Re}\,\mathrm{Pr}\,f\right)\theta'=0, \tag{7.11}$$

Using the initial guesses and linear operators defined in Eqs. 5.13 to 5.16, HAM solution for above mentioned models can be written as

$$\begin{aligned} f_m(\eta) &= \sum_{n=0}^{m}\sum_{l=0}^{m}\gamma_{m,n}\eta^n e^{(2l+1)-(3n+1)\eta}, \\ \theta_m(\eta) &= \sum_{n=1}^{m}\sum_{l=0}^{m}\delta_{m,n}\eta^n e^{2l-3n\eta}, \quad m\geq 0. \end{aligned} \tag{7.12}$$

$$\begin{aligned} f_m(\eta) &= \sum_{n=0}^{m}\sum_{l=0}^{m}\Gamma'_{m,n}\eta^n e^{(2l+1)-(3n+1)\eta}, \\ \theta_m(\eta) &= \sum_{n=1}^{m}\sum_{l=0}^{m}\Omega'_{m,n}\eta^n e^{2l-3n\eta}, \quad m\geq 0, \end{aligned} \tag{7.13}$$

where $\gamma_{m,n}$, $\delta_{m,n}$, $\Gamma'_{m,n}$ and $\Omega'_{m,n}$are constants.

7.4 Graphical results and discussion

To report the convergence of the obtained series solutions and the effects of sundry parameters in the present investigation we plotted Figs. 7.1 to 7.10. The convergence regions in the HAM solutions are strongly dependent upon the non-zero auxiliary parameters $\hbar$ which can be adjusted and controlled by means of a proper value of $\hbar$. To see the range of admissible value of $\hbar$, $\hbar-$curves are displayed in Figs. 7.1 to 7.3. Figs. 7.1 and 7.2 correspond to Reynolds' model. The horizontal line in Fig. 7.1 shows the convergence region for velocity and Fig. 7.2 depicts the convergence region for temperature. Fig. 7.3 is prepared for h-curve for temperature profile for Vogel's model.

Fig. 7.4 predicts velocity profile for Re for Reynolds' model. It is observed that velocity decreases as Re increases. Fig. 7.5 presents temperature profile for Pr for Reynolds' model. It is noted that temperature decreases as Pr increases. The temperature profile decreases from 1 to zero as η increases from 1 to ∞. The fluid temperature depends upon the distance from surface of the tube. The fluid temperature attains maximum value at the surface of the tube.

Fig. 7.6 shows temperature profile for Re . As we have seen in case of Pr, the temperature profile decreases from 1 to zero as η increases from 1 to ∞. The fluid temperature depends upon the distance from surface of the tube. The fluid temperature attains maximum value at the surface of the tube. Fig. 7.7 is displayed to examine velocity profile for C for Vogel's model. In this case velocity decreases with increase in C. Fig. 7.8 gives velocity profile for Re for Vogel's model. Velocity profile decreases as Re increases. The velocity profile decreases from 1 to zero as η increases from 1 to ∞. The fluid velocity depends upon the distance from surface of the tube. The fluid velocity attains maximum value at the surface of the tube.

Fig. 7.9 studies temperature profile for Pr for Vogel's model. It is noted that temperature decreases as Pr increases. Fig. 7.10 exhibits temperature profile for Re for Vogel's model. It is seen that temperature decreases as Re increases.

7.5 Conclusions

In this chapter, we have investigated analytically the heat transfer flow of a hyperbolic tangent fluid due to a stretching cylinder with variable viscosity. The governing equations have been

transformed into non-linear ordinary differential equations using similarity transformations. The homotopy analysis method is employed to get the series solution of thus obtained highly non-linear problem. Effects of the involved parameters are examined with the help of graphs. It is concluded that:

1. The velocity and f(η) profiles decrease with increase in Re and We.
2. Temperature profile increases with rise in B, C^* and We.

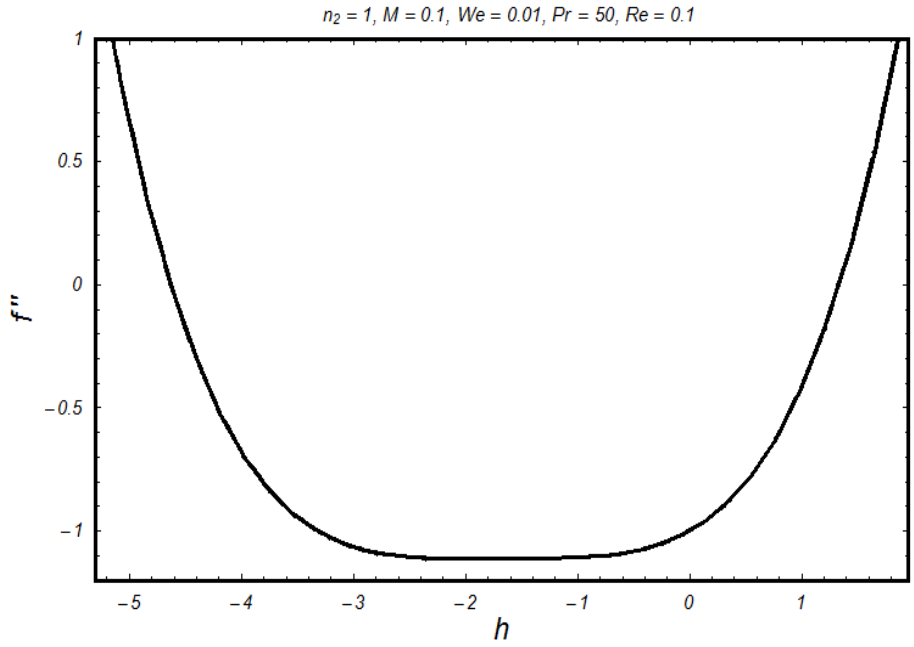

Fig. 7.1: h-curve for velocity profile for Reynolds' model.

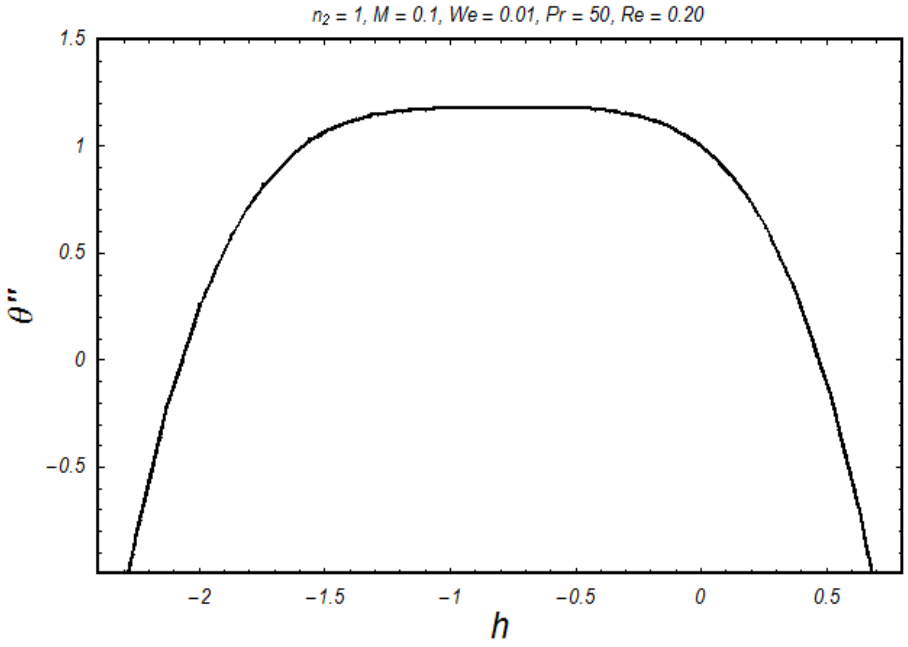

Fig. 7.2: h-curve for temperature profile for Reynolds' model.

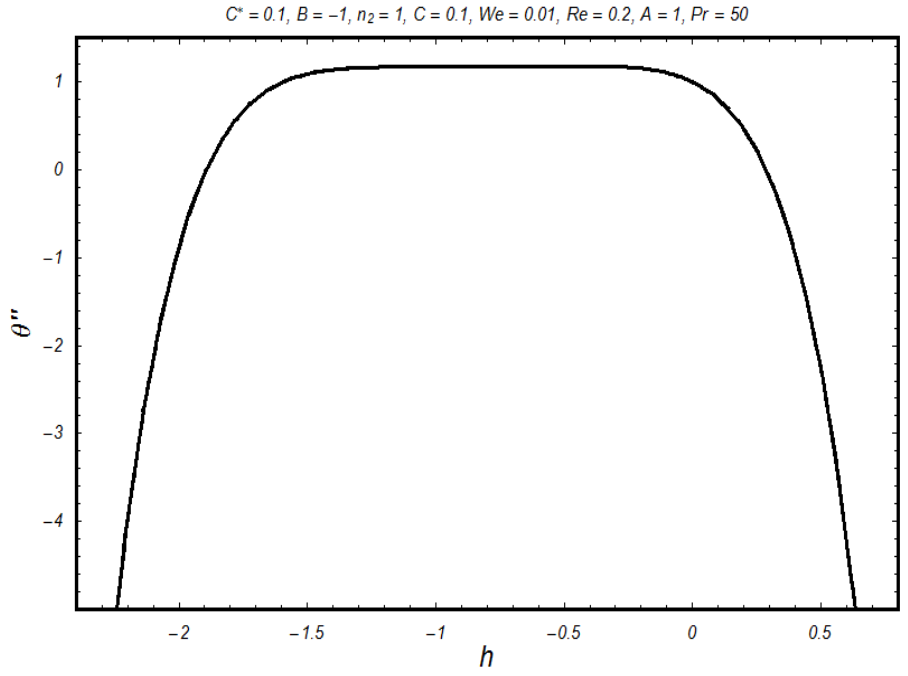

Fig. 7.3: h-curve for temperature profile for Vogel's model.

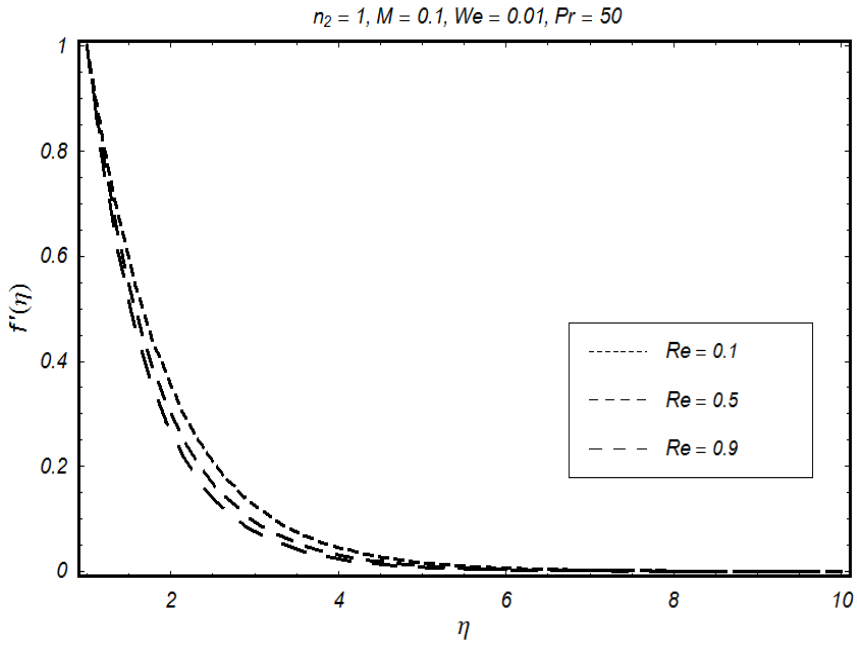

Fig. 7.4: Velocity profile for different values of Re for Reynolds' model.

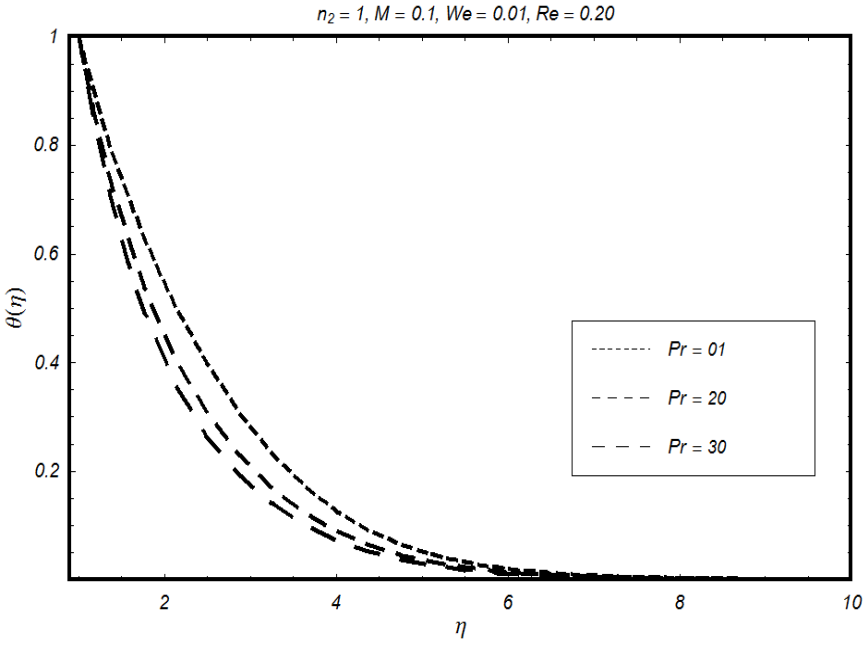

Fig. 7.5: Temperature profile for Pr for Reynolds' model.

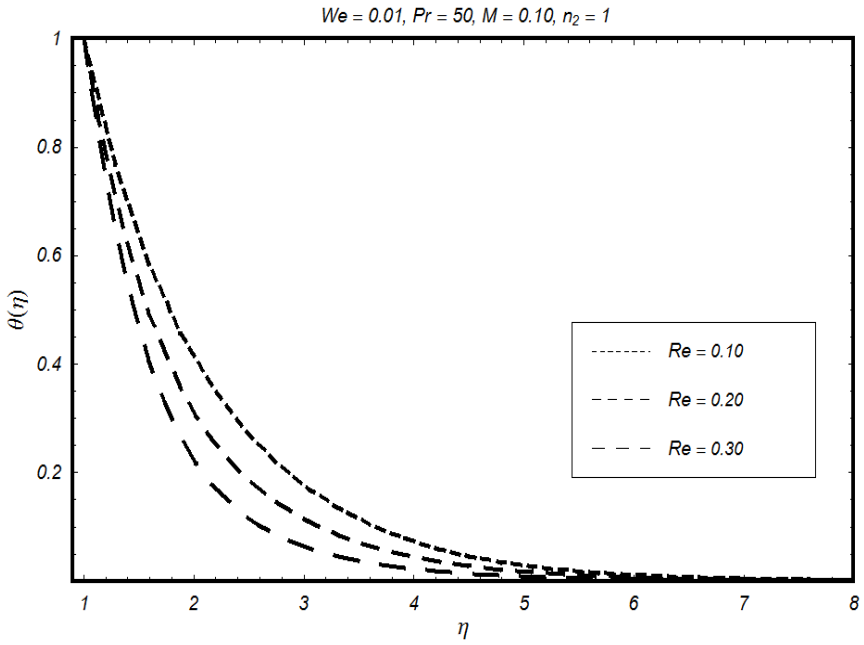

Fig. 7.6: Temperature profile for Re for Reynolds' model.

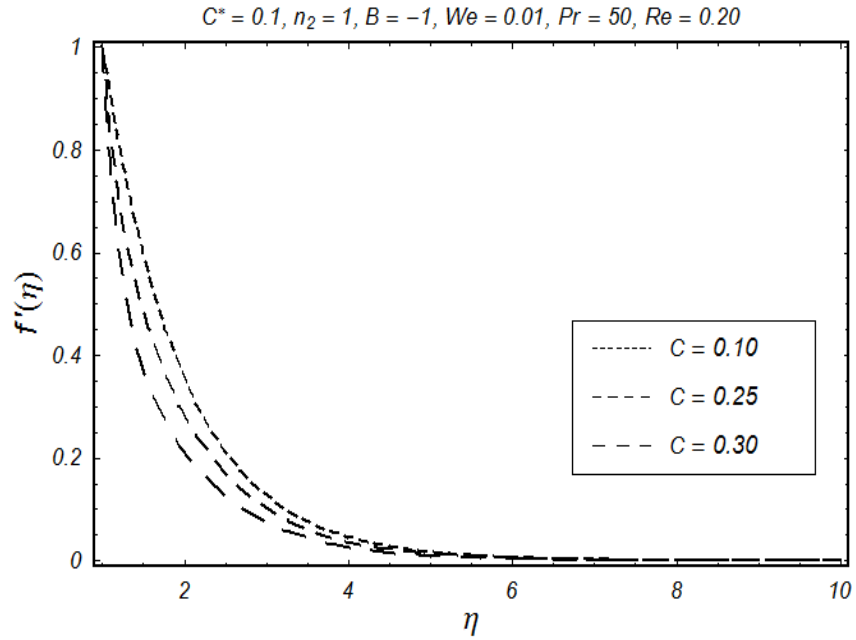

Fig. 7.7: Velocity distribution for C for Vogel's model.

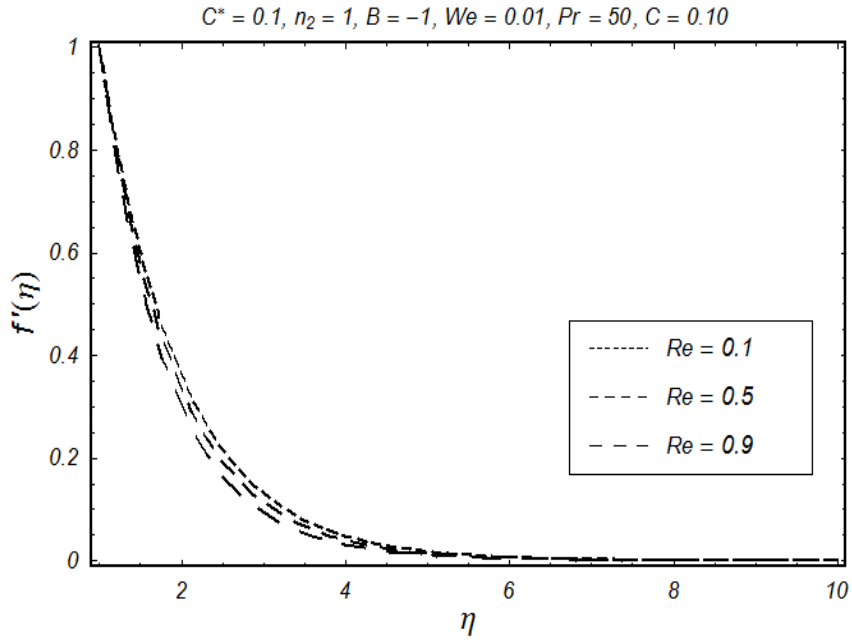

Fig. 7.8: Velocity distribution for Re for Vogel's model.

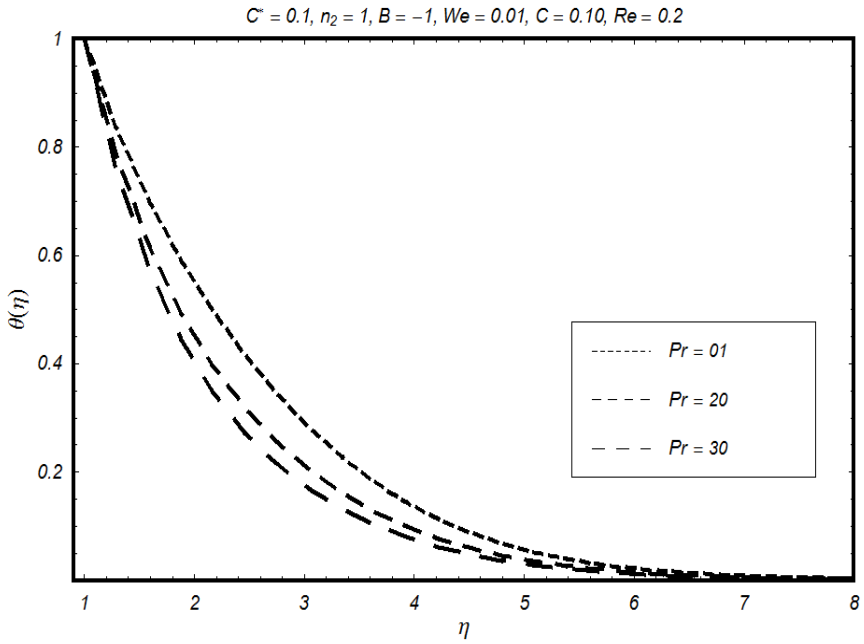

Fig. 7.9: Temperature profile for Pr for Vogel's model.

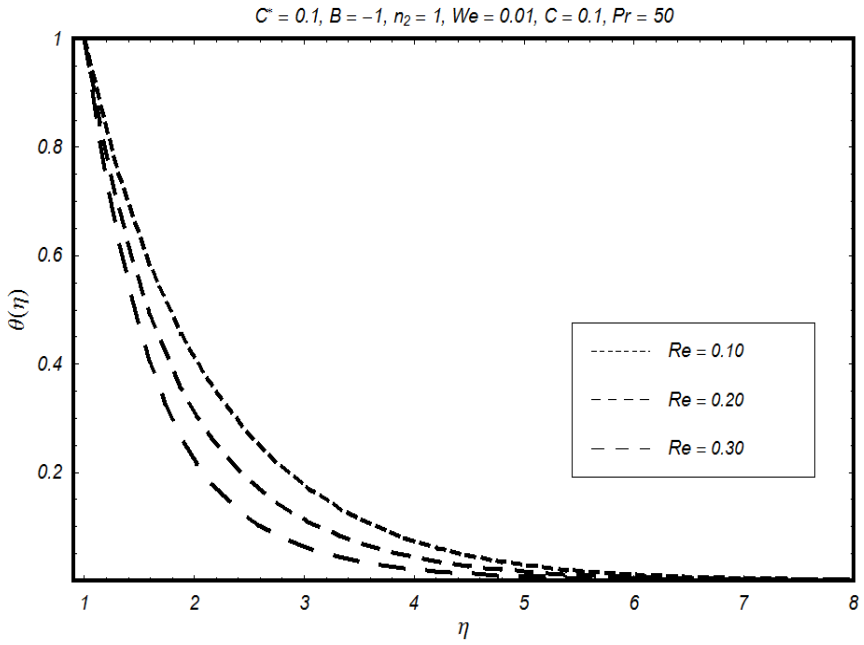

Fig. 7.10: Temperature profile for Re for Vogel's model.

Chapter 8

Conclusions

The main points of this thesis can be summarized as follows:

1. Results obtained by shooting method and homotopy analysis method are in good agreement.

2. Velocity field increases with rise of pressure gradient for Generalized Couette flow for Jeffery-six constant fluid.

3. Velocity field decreases with rise of viscosity parameter for Vogel's model for an Oldroyd 8-constant fluid.

4. Temperature profile decreases with rise of viscosity parameter for Vogel's model for an Oldroyd 8-constant fluid.

5. It is found that by assuming $\mu = 1$ and $\mu = r$, the results for the case of constant as well as space viscosity can be attained for third grade fluid flow with variable viscous properties.

6. Velocity increases with the increase of porous medium parameter for Vogel's model for third grade fluid.

7. Velocity increases with the increase of Brinkman number for Vogel's model for third grade fluid.

8. Temperature increases with the increase of Brinkman number for Vogel's model for third grade fluid.

9. Velocity increases with the increase of viscosity parameter for Reynolds' model for an Oldroyd 8-constant fluid.

10. Temperature increases with the increase of Brinkman number for Reynolds' model for

third grade fluid.

11. Temperature increases with the increase of porous medium parameter for Vogel's model for third grade fluid.

12. It is obsreved that velocity increases with the increase of brownian motion parameter for Reynolds' model for non-Newtonian nano fluid flow.

13. Nanoparticle concentration profile increases with the increase of thermophoresis parameter for Vogel's model for non-Newtonian nano fluid flow.

14. Nanoparticle concentration profile increases with the increase of brownian motion parameter for Reynolds' model for non-Newtonian nano fluid flow.

15. Nanoparticle concentration profile decreases with the increase of thermophoresis parameter for Reynolds' model for non-Newtonian nano fluid flow.

16. The thermal boundary layer decreases with increased Prandtl number and Reynolds number in case of Eyring-Powell model fluid flow due to stretching cylinder.

17. Effects of prandtl number and Reynolds number on velocity profile are opposite in case of Reynolds' model for Walter's B fluid flow.

18. Effects of viscosity parameter on velocity and temperature profiles are similar in case of Reynolds' model for Walter's B fluid flow.

Bibliography

[1] M. Kempegowda, P. M. Balagondar, Exact Solutions of non-Newtonian Fluid Flow between Two Moving Parallel Disks and Stability Analysis, Applied Mathematical Sciences, 6(2012)1827 – 1835.

[2] G. H. Tang, Y. B. Lu, S. X. Zhang, F. F. Wang, W. Q. Tao, Experimental investigation of non-Newtonian liquid flow in microchannels, Journal of Non-Newtonian Fluid Mechanics, 173 – 174(2012)21 – 29.

[3] L. L. Melton, W. T. Malone, Halliburton Co, Fluid Mechanics Research and Engineering Application in Non-Newtonian Fluid Systems, SPE Journal, 4(1964)56 – 66.

[4] S. Nahar, B. H. Birkhofer, S. A. K. Jeelani and E. J. Windhab, Non-Newtonian fluid flow in elastic tubes, 6th International Symposium on Ultrasonic Doppler Methods for Fluid Mechanics and Fluid Engineering.

[5] K. R. Rajagopal and A. S. Gupta, An exact solution for the flow of a non-Newtonian fluid past an infinite plate, Meccanica, 19(1984)158 – 160.

[6] K. R. Rajagopal, A. Z. Szeri and W. Troy, An existence theorem for the flow of a non-Newtonian fluid past an infinite porous plate, Int. J. Non-linear Mech. 21(1986)279 – 289.

[7] C. Fetecau, T. Hayat, Corina Fetecau and N. Ali, Unsteady flow of a second grade fluid between two side walls perpendicular to a plate,Nonlinear Analysis: Real World Applications, 9(2008)1236 – 1252.

[8] D. Vieru, M. Nazar, Corina Fetecau and C. Fetecau, New exact solutions corresponding to the first problem of Stokes for Oldroyd-B fluids,Computers & Mathematics with Applications, 55(2008)1644 − 1652.

[9] D. Vieru, T. Hayat, Corina Fetecau and C. Fetecau,On the first problem of Stokes for Burgers' fluids, Applied Mathematics and Computation, 197(2008)76 − 86.

[10] W. C. Tan and T. Masuoka, Stokes first problem for an Oldroyd-B fluid in a porous half space, Phys. fluids, 17(2005)023101 − 023107.

[11] C. I. Chen, C. K. Chen and Y. T. Yang, Unsteady unidirectional flow of an Oldroyd-B Fluid in a circular duct with different given volume flow rate conditions, Heat Mass Transfer, 40(2004)203 − 209.

[12] P. D. Ariel, Flow of a third grade fluid through a porous flat channel,Int. J. Eng. Sci., 41 (2003) 1267 − 1285.

[13] A. M. Siddiqui, T. Hayat and S. Asghar, Some unsteady unidirectional flows of a non-Newtonian fluid, International Journal of Engineering Science, 38(2000)337 − 345.

[14] S. Asghar, T. Hayat and A. M. Siddiqui, Moving boundary in a non-Newtonian fluid,International Journal of Non-Linear Mechanics, 37(2002)75 − 80.

[15] T. Hayat, S. Nadeem, A. M. Siddiqui and S. Asghar,An oscillating hydromagnetic non-Newtonian flow in a rotating system,Applied Mathematics Letters, 17(2004)609 − 614.

[16] T. Hayat, R. Naz and S. Asghar, Hall effects on unsteady duct flow of a non-Newtonian fluid in a porous medium, Applied Mathematics and Computation, 157(2004)103 − 114.

[17] S. Nadeem, N. S. Akbar, Numerical solutions of peristaltic flow of a Jeffrey-six constant fluid with variable MHD, Zeitschrift fur Naturforschung, 2010 in press.

[18] Massoudi, M. and Christie, I., Effect of variable viscosity and viscous dissipation on the flow of a third grade fluid in a pipe, Int. J. Non-Linear Mech. 30(1995)687 − 699.

[19] M. Pakdermirli, B. S. Yilbas, Entropy generation for pipe flow of a third grade fluid with Vogel model of viscosity, Int. J. Non-Lin. Mech. 41 (2006) 432 − 437.

[20] A. Pantokratoras, The Falkner-Skan flow with constant wall temperature and variable viscosity, Int.J.Thermal.Sci., 45 (2006) 378 − 389.

[21] S. N. Aristov, O. I. Skul'skii, On a Six-constant Jeffreys model of fluid in a plane channel, 43(2002)817 − 822.

[22] S. Nadeem,T. Hayat, S. Abbasbandy, M. Ali, Effects of partial slip on a fourth grade fluid with variable viscosity : An analytical solution, Nonlinear Analysis: Real World Applications, 11(2010)856.

[23] N. S. Akbar. S. Nadeem, Simulation of heat transfer on the peristaltic flow of a Jeffrey-six constant fluid in a diverging tube International Communication in Heat and Mass transfer 2010 in press.

[24] S. Baris, Flow of an Oldroyd 8-constant fluid in a convergent channel, Acta Mech. 148(2001)117 − 127.

[25] T. Hayat, A. M. Siddiqui, S. Asghar, Some simple flows of an Oldryd-B fluid, Internat. j. Engrg. Sci. 39(2001)135 − 147.

[26] R. Ellahi, T. Hayat, T. javed, S. Asghar, On the analytic solution of nonlinear flow problem involving Oldroyd 8-constant fluid, Mathematical and Computer Modelling, 48(2008)1191 − 1200.

[27] R. Ellahi, T. Hayat, F. M. Mahomed, A. Zeeshan, Exact solutions for flows of an Oldroyd 8-constant fluid with nonlinear slip conditions, Commun Nonlinear Sci Numer Simulat, 15(2010)322 − 330.

[28] R. E. Powell, H. Eyring, Mechanism for the relaxation theory of viscosity, Nature. 154(1944)427 − 428.

[29] T. Y. Na and I. Pop, Boundary-layer flow of a micropolar fluid due to a stretching wall, Archive of Applied Mechanics, Volume 67, Number 4, 229-236, DOI: 10.1007/s004190050113.

[30] S. P. Anjalidevi and M. Thiyagarajan, Nonlinear hydromagnetic flow and heat transfer over a surface stretching with a power-law velocity, Heat and Mass Transfer, 38(2002)723 − 726.

[31] Mohamed E. Ali, The effect of variable viscosity on mixed convection heat transfer along a vertical moving surface, International Journal of Thermal Sciences, 45(2006)60 – 69.

[32] T. Altan, S. Oh, H. Gegel, Metal Forming Fundamentals and Applications, American Society of Metal, Metals Park, Ohio, USA, 1979.

[33] E. G. Fisher, Extrusion of Plastics, Wiley, New York (1976).

[34] Z. Tadmor, I. Klein, Engineering Principles of Plasticating Extrusion, Polymer Science and Engineering Series, Van Nostrand Reinhold, New York (1970).

[35] L. J. Crane, Flow past a stretching plate, Z. Angew. Math. Phys. 21(1970)645 – 647.

[36] F. K. Tsou, E.M. Sparrow, R.J. Goldstein, Flow and heat transfer in the boundary layer on a continuous moving surface, Int. J. Heat Mass Transf. 10(1967)219 – 235.

[37] L. E. Erickson, L.T. Fan, V.G. Fox, Heat and mass transfer on a moving continuous flat plate with suction or injection, Ind. Eng. Chem. Fundam. 5(1966)19 – 25.

[38] A. Mucoglu, T. S. Chen, Mixed convection on inclined surfaces, ASME J. Heat Transf., 101(1979)422 – 426.

[39] L. G. Grubka, K.M. Bobba, Heat transfer characteristics of a continuous stretching surface with variable temperature, ASME J. Heat Transf. 107(1985)248 – 250.

[40] M. V. Karwe, Y. Jaluria, Fluid flow and mixed convection transport from a moving plate in rolling and extrusion processes, ASME J. Heat Transf. 110(1988)655 – 661.

[41] C. H. Chen, Laminar mixed convection adjacent to vertical, continuously stretching sheets, Heat Mass Transf. 33(1988)471 – 476.

[42] E. M. Abo-Eldahab, M. Abd El-Aziz, Blowing/suction effect on hydromagnetic heat transfer by mixed convection from an inclined continuously stretching surface with internal heat generation/absorption, Int. J. Therm. Sci. 43(2004)709 – 719.

[43] A. M. Salem, M. Abd El-Aziz, Effect of Hall currents and chemical reaction on hydromagnetic flow of a stretching vertical surface with internal heat generation/absorption, Appl. Math. Model. 32(2008)1236 – 1254.

[44] M. Abd El-Aziz, Thermal-diffusion and diffusion-thermo effects on combined heat and mass transfer by hydromagnetic three-dimensional free convection over apermeable stretching surface with radiation, Phys. Lett. A, 372(3)(2007)263 − 272.

[45] I. Vleggaar, Laminar boundary-layer behavior on continuous accelerating surfaces, Chem. Eng. Sci. 32(1977)1517 − 1525.

[46] C.Y.Wang, Fluid flow due to a stretching cylinder. Phys Fluids, 31(1988)466 − 8.

[47] N. Putra, Wilfried Roetzel, Sarit K. Das, Natural convection of nanofluids, Heat and Mass Transfer, 39(2003)775 − 784.

[48] A. V. Kuznetsov, D. A. Nield. Natural convective boundary-layer flow of a nanofluid past a vertical plate, Int. J. Thermal Sci. 49(2010)243 − 247.

[49] D. A. Nield, A. V. Kuznetsov, The Cheng-Minkowycz problem for natural convective boundary-layer flow in a porous medium saturated by nanofluid, Int. J. Heat Mass Transfer 52(2009)5792 − 5795.

[50] W. A. Khan, I. Pop, Boundary-layer flow of a nanofluid past a stretching sheet, Int. J. Heat Mass Transfer (2010) doi,10.1016/j, ijheatmasstransfer.2010.01,032.

[51] S. J. Liao, Beyond perturbation: Introduction to homotopy analysis method. Boca Raton: Chapman & Hall/CRC Press; 2003.

[52] R. Ellahi, S. Afzal, Effects of variable viscosity in a third grade fluid with porous medium; An analytic solution, Comm. Nonlinear Sci. Numer. Simulation, 14 (2009) 2056 − 2072.

[53] M. Turkyilmazoglu, I. Pop, Exact analytical solutions for the flow and heat transfer near the stagnation point on a stretching/shrinking sheet in a jeffrey fluid, Int. J. Heat Mass Transfer, 57(2013)82 − 88.